6-8-2018 4:00 PM

The Effect of Implant Girth and Implant Collar on the Degree of Bone to Implant Contact and Bone Stresses in the Proximal Humerus

Stephanie Synnott, *The University of Western Ontario*

Supervisor: Johnson, James A, *The University of Western Ontario*
Co-Supervisor: Athwal, George S, *The University of Western Ontario*
Co-Supervisor: Langohr, G Daniel G, *The University of Western Ontario*
A thesis submitted in partial fulfillment of the requirements for the Master of Engineering Science degree in Biomedical Engineering

Abstract

Stem design is a crucial element for the success of shoulder prostheses. Various components of stem design have been investigated; however, little research has been conducted on the effects of (1) implant girth and (2) an implant collar on load transfer. A generic implant model was designed and employed in a (FE) model to determine 3 outcome measures: changes in the degree of bone to implant contact (BIC), changes in cortical and trabecular bone stresses from the intact state, and changes in cortical and trabecular strain energy densities (SED). The variables examined were (1) implant girth (small, medium [generic base model], and large sizes), and (2) the implant collar and collarless. The small implant produced the overall greatest amount of BIC when compared to the other two sizes. The small implant also produced the lowest change in stress from the intact state in both cortical and trabecular bone, as well as the lowest amount of bone volume expected to resorb. Removing the implant collar caused an increase in the degree of BIC, when compared to the collared state. In terms of the changes in stress, removing the implant collar resulted in an increase in both the change in cortical and trabecular bone stresses, and resulted in an increased risk in the amount of cortical bone expected to resorb. Collectively, these findings suggest that a smaller sized implant may be beneficial, while the collar may be beneficial if less stress changes in bone relative to the native state are desired.

Keywords

total shoulder arthroplasty, proximal humerus, implant girth, collared implant, collarless implant, Finite Element modeling, change in bone stress, change in strain energy density (SED), bone to implant contact (BIC)

Co-Authorship Statement

Without my collaborators, the completion of this thesis would not be possible. I would like to acknowledge the following:

Chapter 1: ***Sole Author:*** Stephanie Synnott
Manuscript Revisions: Jim Johnson

Chapter 2: ***Study Design:*** Stephanie Synnott, Jim Johnson, Dan Langohr, George Athwal
Data Collection: Stephanie Synnott, Dan Langohr, Jacob Reeves
Data Analysis: Stephanie Synnott, Dan Langohr
Statistical Analysis: Stephanie Synnott
Manuscript Preparations: Stephanie Synnott
Manuscript Revisions: Jim Johnson

Chapter 3: ***Study Design:*** Stephanie Synnott, Jim Johnson, Dan Langohr, George Athwal
Data Collection: Stephanie Synnott, Dan Langohr, Jacob Reeves
Data Analysis: Stephanie Synnott, Dan Langohr
Statistical Analysis: Stephanie Synnott
Manuscript Preparations: Stephanie Synnott
Manuscript Revisions: Jim Johnson

Chapter 4: ***Sole Author:*** Stephanie Synnott
Manuscript Revisions: Jim Johnson

Appendix: ***Sole Author:*** Stephanie Synnott
Manuscript Revisions: Jim Johnson

Acknowledgments

The work completed for this dissertation would not have been achieved without the contributions and guidance of my advisors and colleagues. First and foremost, I would like to thank my supervisor, Dr. Jim Johnson. It was an immense honor to have worked alongside you and to be a part of the HULC bioengineering team. I have learnt so much about orthopaedics under your guidance and your passion for this industry has greatly inspired me. Dr. Dan Langohr and Jacob Reeves, thank you both so much for all your help with data collection and analysis; this work would not have been possible without your intellectual efforts. I would also like to thank Dr. Athwal for being a part of my advisory committee and providing me with support and guidance for my future career goals. Finally, to all the members of the HULC team, I am so happy to have met you all; your support and friendship has made this journey about so much more than the 166-page thesis I have just completed.

Table of Contents

List of Tables

List of Figures

List of Appendices

Chapter 1

1 Introduction

Total shoulder arthroplasty is a common treatment option for patients suffering from severe arthritis of the glenohumeral joint and proximal humeral fractures. The humeral stem is an important feature of the shoulder implant and has been widely research. However, little is known about the effect of implant girth, or what is commonly referred to in the literature as implant stem diameter, and the presence or absence of an implant collar on the proximal humerus. For this dissertation, a finite element (FE) analysis was conducted to determine the effects of implant girth and implant type (collar versus collarless), on interface contact, proximal bone stresses, and the prediction of proximal bone resorption. This primary chapter provides an overview of shoulder anatomy, material properties of bone, shoulder arthroplasties, and FE modeling. The motivation for this study, as well as the hypotheses regarding these investigations, is also outlined herein.

1.1 Shoulder Anatomy

The shoulder is a complex musculoskeletal structure, which functions as an integrated unit comprised of various components[1]. The shoulder complex consists of three bones, three joints, one pseudojoint, several muscles, ligaments, and tendons that act to both stabilize and create motion about the joint (Figure 1-1). The combined articulations and musculature of the upper limb allow the shoulder to have the greatest range of motion in all three planes when compared to other joints in the body. The spherical shaped head of the humerus articulates within the concave cavity of the scapula allowing for an impressive range of motion with little constraint by surrounding osseous structures (Culham, Peat, & Culham, 1993; Dutton, 2012; Jobe, Phipatanakul, & Coen, 2009; Moore, Agur, & Dalley, 2011). The degree of motility and stability of the shoulder joint is dependent on a healthy articular surface, and intact muscle-tendon units and capsuloligamentous structures; thus, optimal performance of the shoulder joint strictly relies on the cooperative function of these aforementioned anatomic structures (Dutton, 2012).

To better understand the biomechanical aspects of shoulder motion, the contribution of each component of the shoulder must be well understood. These structures can be divided into two main categories: (i) osseous anatomy: bony structures and articulations and (ii) soft tissue constructs: passive soft tissue and active musculature.

1.1.1 Osseous Anatomy

The desired motion of the shoulder is achieved with four articulations: the glenohumeral joint, acromioclavicular (AC) joint, sternoclavicular (SC) joint, and scapulothoracic pseudojoint. The three main bones of the shoulder are the humerus, scapular, and clavicle (Figure 1-1). These three bones, along with the ribs and sternum create the four articulations at the shoulder (Dutton, 2012).

---

[1] Appendix A provides a glossary of medical terminology used throughout this dissertation

1.1.1.1 Bony Structures

The humerus is the most proximal and largest bone in the upper limb. The proximal end of the humerus is largely spherical, containing the humeral head and greater and lesser tubercles (Grey, 1995). Relative to the long axis of the humerus, the head is oriented in the superior-medial-posterior direction. The head of the humerus, which roughly resembles one-third of a sphere, articulates with the scapular glenoid cavity to provide motion of the shoulder (Figure 1-2). A hyaline cartilage that is centrally thicker, envelopes the articular surface and is essentially constructed to resist and dissipate compressive forces generated during movement or upon impact (Grey, 1995). The distal end of the humerus forms the elbow and is transversely wider than the shaft containing both articular and non-articular surfaces. The capitulum and trochlea are the humeral structures that articulate with the radius and ulna respectively, while the non-articular structures of the distal humerus are the medial and lateral epicondyles.

The greater and lesser tubercles serve as the location sites for important muscles involved in the movement and stabilization of the shoulder. The greater tuberosity is located on the most lateral edge of the humeral head and is positioned posteriorly beyond the acromion of the scapula. The lesser tuberosity is located laterally from the articular margin of the humeral head and is positioned anteriorly just beyond the anatomical neck (Grey, 1995). Near the anatomical neck, on the most posterosuperior aspect of the greater tuberosity, the tendons from three of the four rotator cuff muscles attach (supraspinatus, infraspinatus, and teres minor). The tendon of the fourth rotator cuff muscle, subscapularis, attaches to the lesser tubercle. Due to its distance from the center of rotation, the greater tuberosity lengthens the moment arm of the supraspinatus and deltoid muscles for abduction angles greater than 30 degrees and less than 60 degrees correspondingly. Separating the greater and lesser tubercles, the bicipital groove acts as a guide for the long head biceps tendon, wrapping it around the glenohumeral joint where it attaches to the scapula. Along the anterolateral shaft of the humerus, the distal deltoid tendon attaches at the deltoid tuberosity.

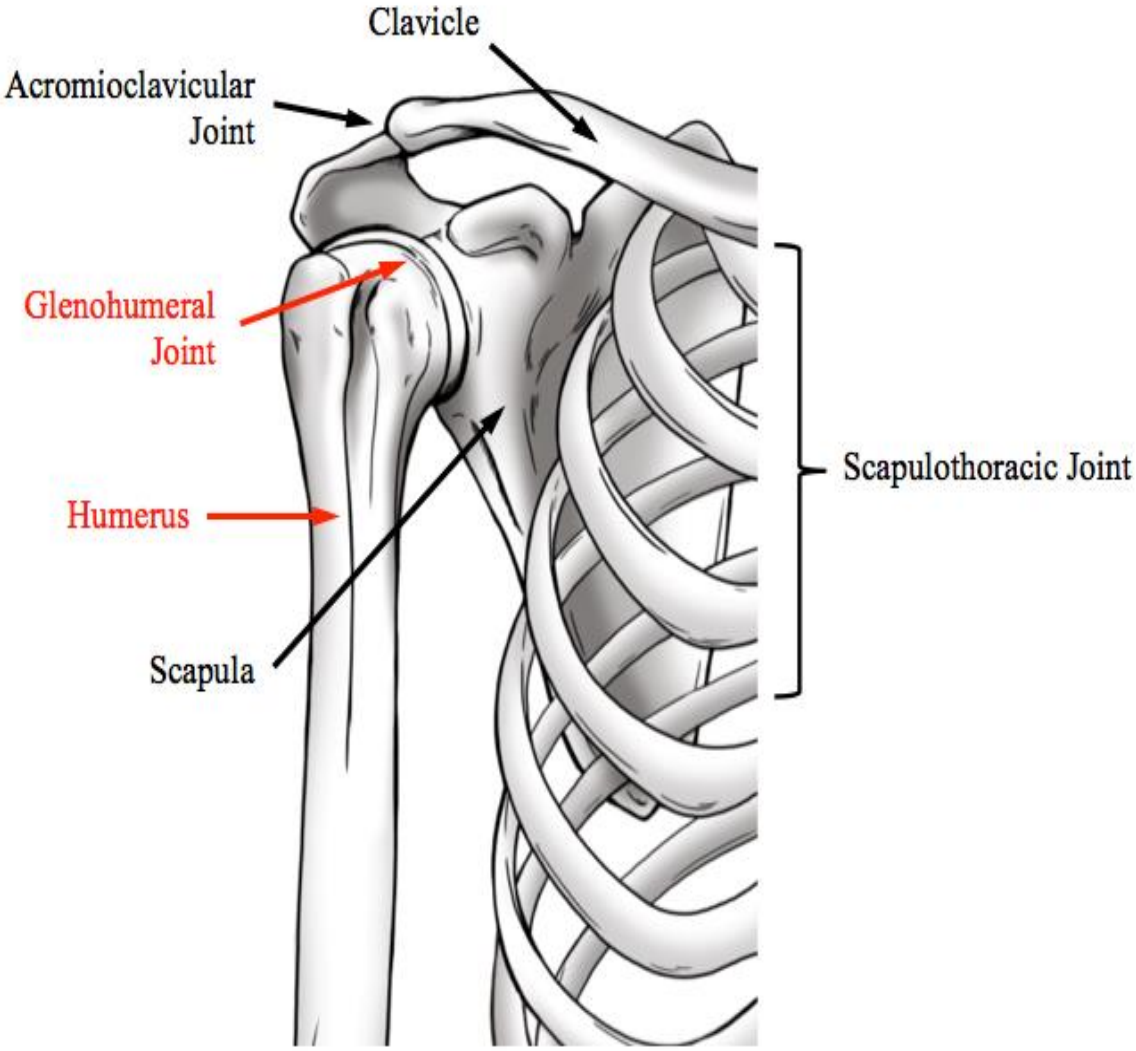

Figure 1-1: Bony Structures and Articulations of the Right Shoulder Joint

The bone and joint of interest, the humerus and glenohumeral joint respectively, are highlighted alongside the primary bony structures of the shoulder.

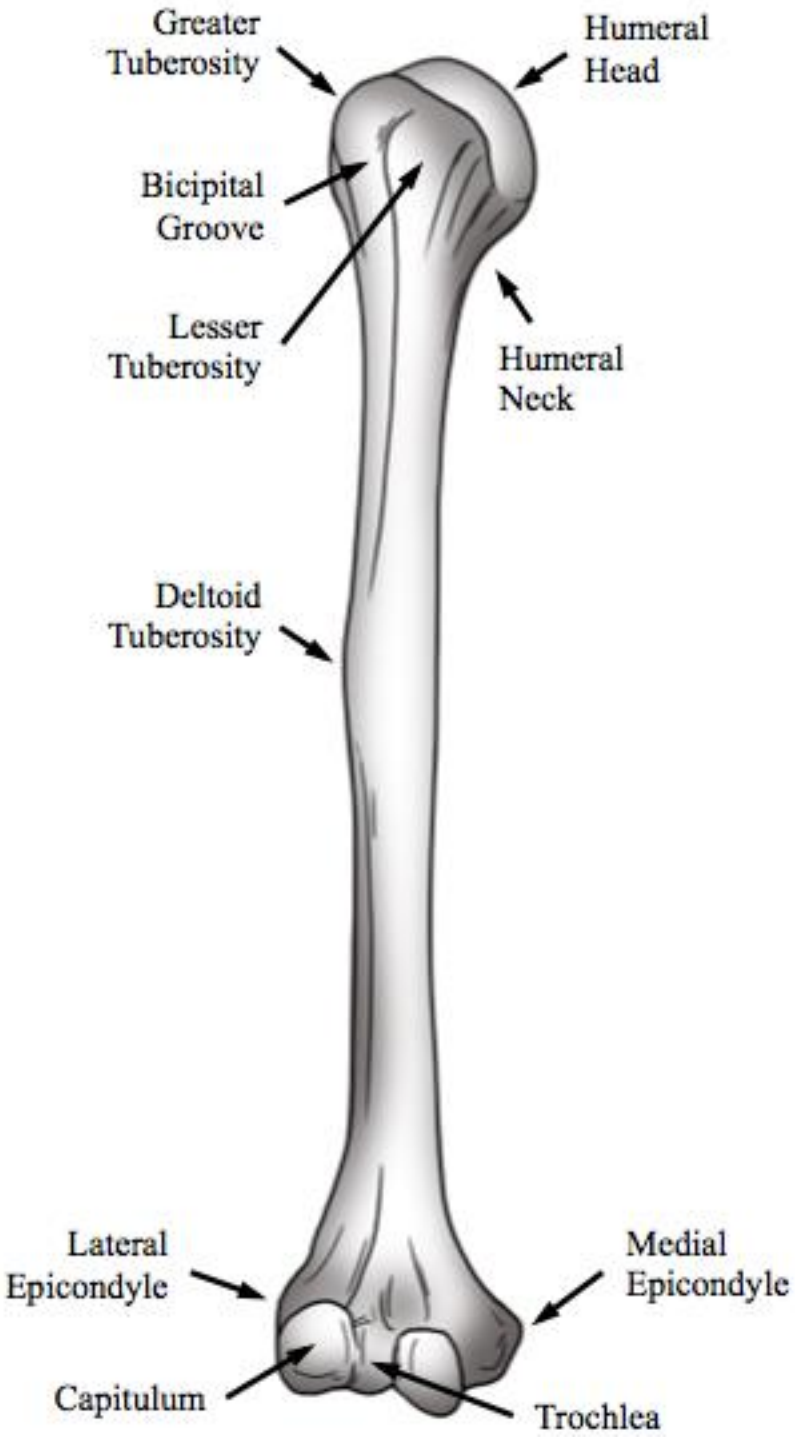

Figure 1-2: Landmarks of a Right Humerus

Important landmarks of the humerus which are assocated with several muscles and articulations that allow movement about the shoulder joint.

The scapula is a thin, flat, triangular bone, located on the posterolateral aspect of the thorax, overlying the second to seventh ribs (Figure 1-3) (Culham et al., 1993; Moore et al., 2011). The strut configuration, formed by the scapula's attachment to the axial skeleton via the clavicle, provides a degree of stabilization against applied forces, as well as the transmission of forces from the upper limb to the axial skeleton and vice versa. Additionally, the scapula functions as a stable base for which the humerus articulates within the concave-shaped glenoid cavity. This articulation, known as the glenohumeral joint, gives rise to the large degree of motion at the shoulder. The scapula has three notable bony projections: the spine, acromion, and coracoid process. These projections serve as the origin and insertion sites for several muscles that allow for the rotation of the shoulder at the glenohumeral joint (Dutton, 2012; Matsen III, Clinton, Rockwood Jr, Wirth, & Lippitt, 2009; Moore et al., 2011).

The clavicle or collarbone serves as a strut for the shoulder to allow the upper limb to swing clear of the body. It extends laterally from the sternum to the acromion of the scapula, which acts to stabilize shoulder motion. The two articulations of the clavicle, the SC joint and the AC joint, assist in the rotation of the scapula guiding shoulder motion and rotation about the scapulothoracic joint (Grey, 1995; Matsumura et al., 2013).

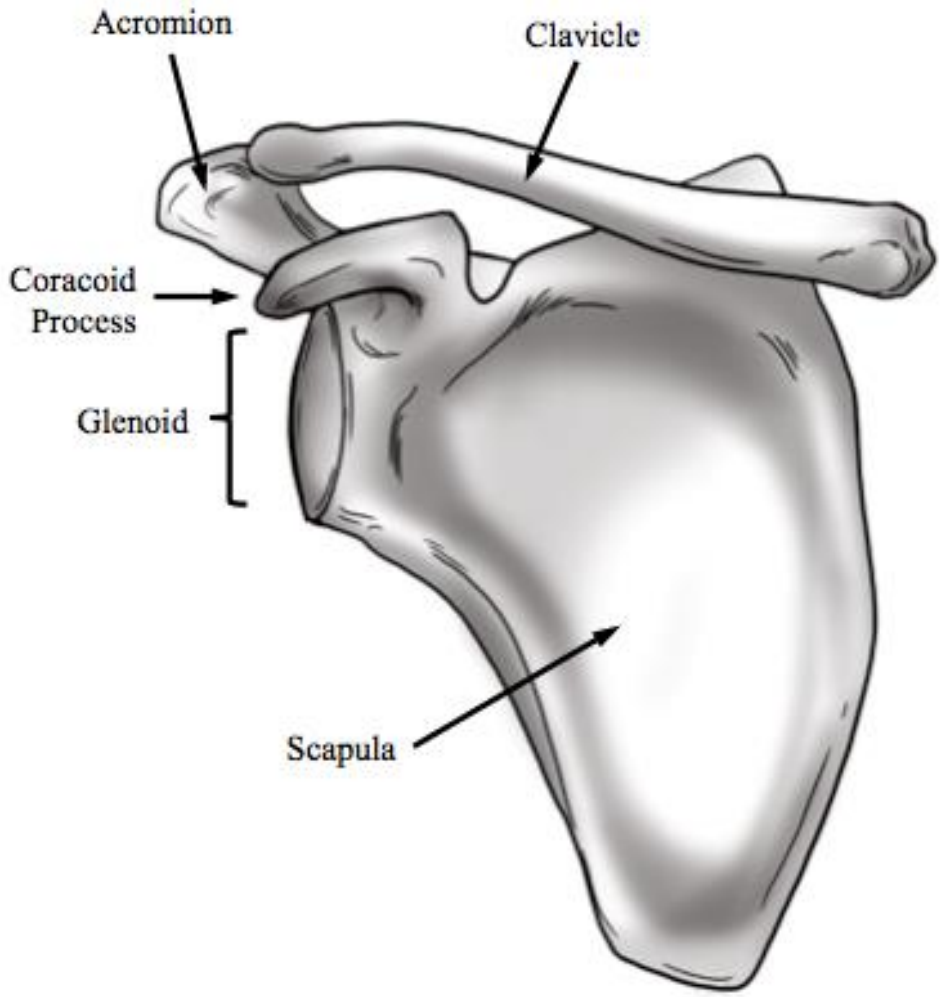

Figure 1-3: Anterior View of a Right Scapula and Clavicle

Major landmarks of the scapula and clavicle where several muscles attach to and articulations occur.

1.1.1.2 The Articulations

Joints have two very important roles in the musculoskeletal system: to allow desired motion and resist undesired motion. While the shoulder has the greatest range of motion of any joint in the body, it is also the most susceptible to dislocation (Jobe et al., 2009). Of the 4 aforementioned joints in the shoulder complex, the glenohumeral joint is the largest contributor to shoulder motion, providing three degrees of freedom between the humeral head and glenoid fossa: flexion/extension, abduction/adduction and rotation. Although this arrangement permits a wide range of motility, it provides very little articular stability. Like the surface of the humeral head, the glenoid fossa is covered by hyaline cartilage called a labrum (Dutton, 2012; Grey, 1995; Moore et al., 2011). The labrum helps to increase joint stability by deepening the glenoid cavity, increasing contact surface area of the humeral head to glenoid fossa by 75% vertically and 56% transversely (Culham et al., 1993; Dutton, 2012). The degree of motility of the shoulder joint is dependent upon the sequence of movements. The amount of abduction is limited to 60-90 degrees when the humerus is initially internally rotated. However, if the humerus is externally rotated, the degree of abduction increases to between 90 and 120 degrees (Culham et al., 1993).

Contact forces at the glenohumeral joint can vary greatly for different positions of the arm. Understanding these joint forces is of great importance in shoulder research as it forms the basis for optimizing implant design and fixation for joint replacement surgery, as well as improving and verifying critical biomechanical models of the shoulder (Bergmann et al., 2007). Bergmann *et al*. (2007) investigated the contact forces at the glenohumeral joint for various degrees of abduction (Bergmann et al., 2007). The authors' findings showed that they could better predict and measure more realistic data for movements such as abduction.

The AC joint is the main articulation that suspends the upper arm from the axial skeleton permitting scapula motion. Movement from the upper extremity is transferred horizontally from the scapula, or vice versa, through the clavicle bone, which articulates with the sternum via the sternoclavicular joint. Both the AC and SC joints are covered with a fibrocartilage that helps provide strength and elasticity, resisting repeated pressure

and friction (Dutton, 2012; Grey, 1995). While not a true synovial joint, the scapulothoracic joint also functions to permit relative motion between the scapula and torso.

1.1.2 Soft Tissue Constructs

1.1.2.1 Ligaments

Numerous passive soft tissues structures function to statically stabilize shoulder motion. Several ligaments and joint capsules cooperate to permit or limit translation and rotation by reciprocally tensioning and loosening. Movement about the glenohumeral joint is further reinforced by the glenoid labrum, which may additionally help to protect bone and assist in lubrication of the joint (Dutton, 2012; Grey, 1995).

1.1.2.2 Muscles

In addition to passive soft tissue, musculature acts to provide dynamic stabilization of the shoulder, while creating movement about the shoulder complex (Figure 1-4). Based on their attachment sites, the muscles involved in shoulder motion can be grouped into three categories: axiohumeral muscles, axioscapular muscles, and scapulohumeral muscles (Moore et al., 2011).

Attachment sites for the axiohumeral muscles are laterally to the humerus and medially to the axial skeleton. The two muscles that comprise this group are the latissimus dorsi and pectoralis major (which also has an anteromedial attachment to the clavicle) Although the latissimus dorsi and pectoralis muscles lie on opposite sides on the truck, they perform relatively the same movement; which is to adduct and medially rotate the humerus. Additionally, the latissimus dorsi aids in extension of the humerus and the clavicular head of the pectoralis major aids in flexion of the humerus (Moore et al., 2011).

The axioscapular muscles, which will not be explicitly defined, include the trapezius, levator scapulae, rhomboid minor and major, the serratus anterior, and the pectoralis major muscles. Together, these muscles produce movement and/or help to stabilize the scapula.

The scapulohumeral muscles include the deltoid, teres major, and the muscles of the rotator cuff: supraspinatus, infraspinatus, teres minor, and subscapularis. The muscles insert proximally on the scapula and distally on the humerus to perform various movements of the arm. The deltoid muscle is a very powerful muscle divided into three parts that contour the shoulder: clavicular (anterior), acromial (middle), and spinal (posterior). When all three parts of the deltoid simultaneously contract, their primary function is to abduct the arm (De Witte et al., 2014; Jobe et al., 2009; Moore et al., 2011; Rosso et al., 2014). Individual contraction from the clavicular and spinal divisions can also cause flexion and medial rotation or extension and lateral rotation of the arm respectively (Moore et al., 2011). The deltoid also acts as a shunt muscle, resisting superior and inferior displacement of the shoulder from the joint capsule (Moore et al., 2011; Rosso et al., 2014).

The muscles of the rotator cuff play an important role in the movement of the arm by fine-tuning the position of the humeral head in the glenoid cavity during arm elevation. Each muscle performs its own specific adjustment by either internally/externally rotating and/or adducting/abducting the humerus (Dutton, 2012; Moore et al., 2011).

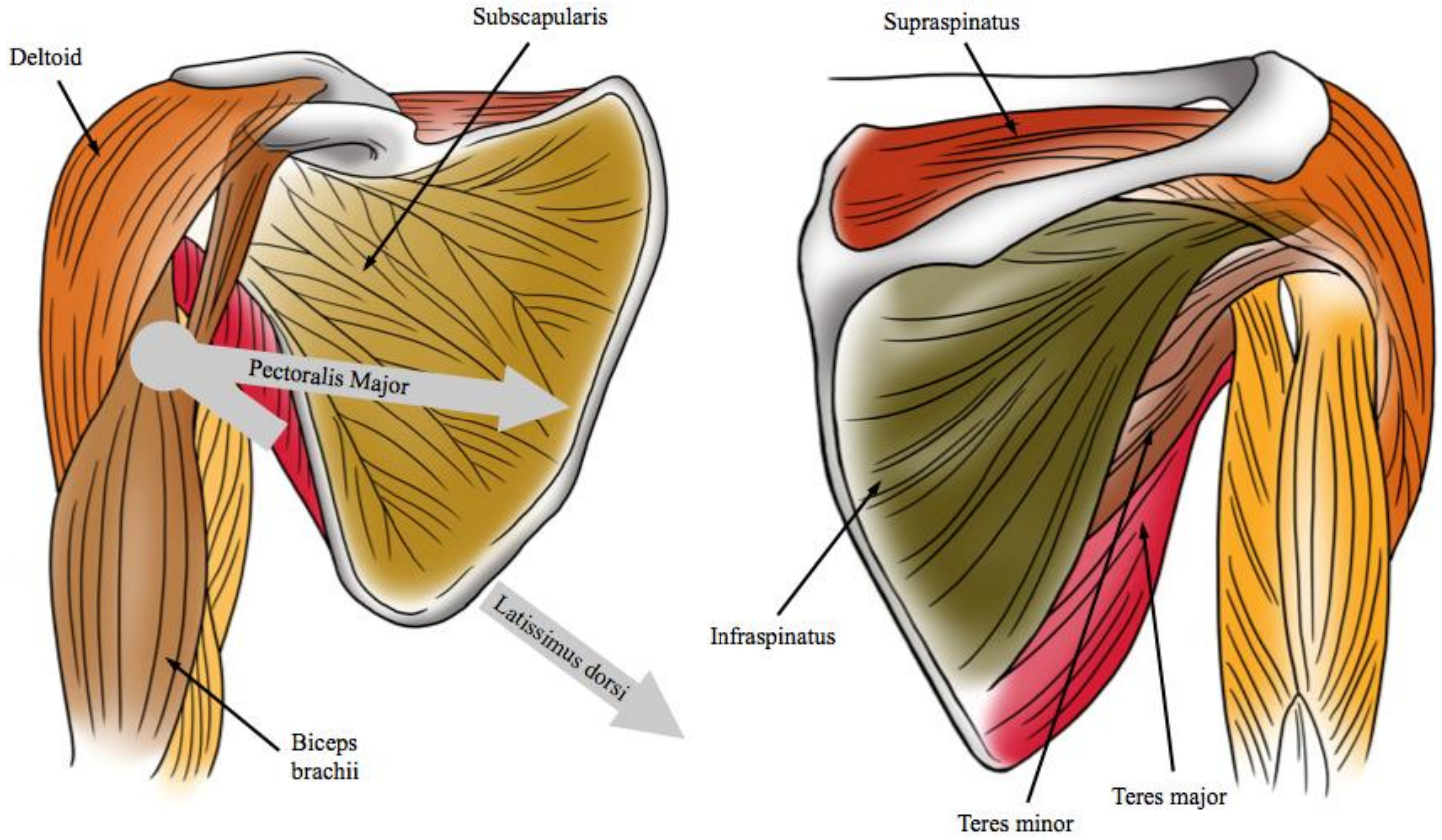

Figure 1-4: Major Muscles of the Upper Arm

Several muscles of the upper limb contribute to glenohumeral joint stability and cause motion about the shoulder joint.

1.2 Osseous (Bone) Structures

Bone is an extremely well organized composite material that provides immense structural support protecting the body and its organs. Bone material is a type of dense connective tissue with an inorganic and organic phase, which gives rise to bones structural and regulatory properties. The inorganic component of bone is made of calcium phosphate minerals giving bone its compressive properties, whereas the organic component of bone is made primarily of type I collagen fibers giving bone its tensile and viscoelastic properties. Together, these materials form a crystalline mineral, known as bone mineral, making bone very strong and hard without being brittle. Approximately two-thirds of bone is comprised of inorganic material with the remaining one-third comprised of organic material (Dalla Pria Bankoff, 2012; Grey, 1995; Ralston, 2017)

There are generally four categories of bone: long bones, short bones, flat bones, and irregular bones. The humerus, which constitutes the appendicular skeleton, is considered a long bone and is subdivided into three sections: the epiphysis (end of bone and location of articulation), the metaphysis (mid region), and diaphysis (central shaft) (Clarke, 2008). Macroscopically, bone is further divided into compact or cortical bone and cancellous or trabecular bone (Figure 1-5). Compact bone is generally limited to the cortex of long bone. A thin cortical shell surrounds the epiphysis and gradually thickens towards the diaphysis. Cancellous bone lies within in the cortical shell largely in the epiphysis region phasing out towards the outer edge at the metaphysis. No trabecular bone is present in the diaphysis, but only a “hollow” medullary canal persists (Clarke, 2008; Grey, 1995; Ralston, 2017). Compact cortical bone is much more rigid and stiff than cancellous bone. The microscopic organization of cortical bone allows for stronger mechanical properties, over cancellous bone, as the underlying structures are more uniformly arranged, with concentric cylinders parallel to the diaphysis. Microscopically, cancellous bone is inhomogeneous and porous. This structure is, however, oriented in such a way, that applied stresses can be optimally transferred to the cortical shell (Grey, 1995; Razfar et al., 2016).

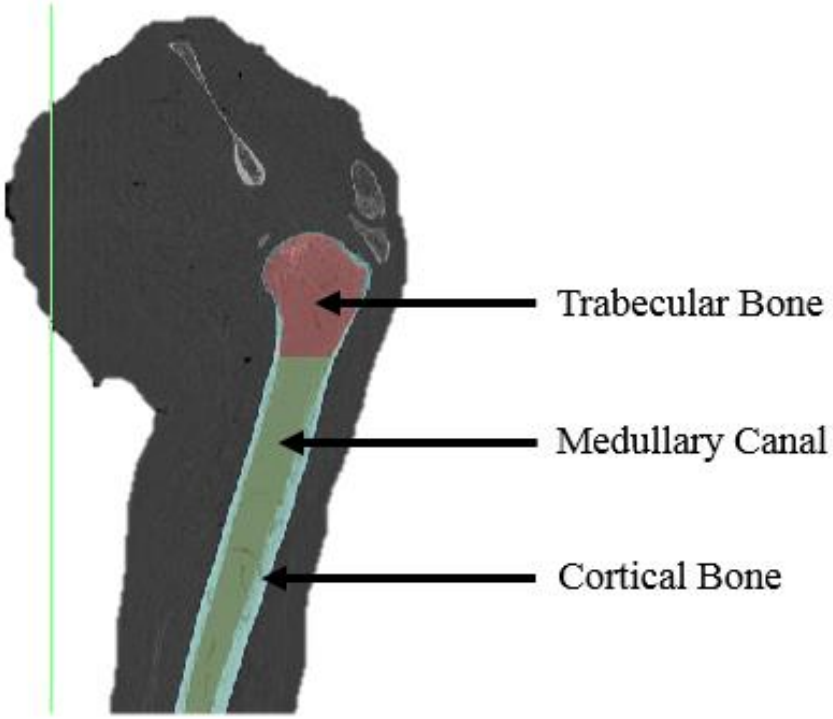

Figure 1-5: Division of Cortical and Trabecular Bone

Long bones are divided into two sections: cortical bone which is the hard-exterior shell shown in light blue and trabecular bone which is the porous interior structure labeled in red. Image obtained from a left shoulder CT scan.

Bone, being a metabolically active and dynamic tissue, is constantly adapting its structure in response to physiological influences or mechanical forces. Bone remodeling requires the resorption of mineralized bone by osteoclasts followed by the formation of new bone tissue by osteoblasts (Clarke, 2008; Dalla Pria Bankoff, 2012; Hadjidakis & Androulakis, 2006; Ralston, 2017). Since the microstructural make-up and bone material density is different between the cortical and trabecular bone, the distribution and dissipation of load and energy from the articulation, will differ, affecting the rate and degree of bone remodeling (Ralston, 2017; Wehrli, n.d.).

1.2.1 Elastic Properties of Bone

Due to the increased use of computation methods for stress analysis at the tissue level, accurate measurements of the intrinsic mechanical properties of bone tissue are extremely important for proper analyses. Throughout the literature, the modulus of elasticity (*i.e.* Young's Modulus) for cortical bone has been consistently found to be 20-22 GPa in the longitudinal axis and 12-14 GPa in the transverse axis (Turner, Rho, Takano, Tsui, & Pharr, 1999). Conversely, Young's moduli for trabecular bone tissue is more difficult to approximate due its inhomogeneous structure (Turner et al., 1999). To quantify the material properties of bone for 3D modeling, computerized tomography (CT) scans of bone are obtained. The attenuation of the bone material is attained from the CT scan and quantified in Hounsfield Units (HU), where the apparent density of the material is derived and used to determine the elastic modulus (Zannoni, Mantovani, & Viceconti, 1999). While there are a variety of empirical models on the relationship between Young's modulus and apparent bone density (Diamant, Shahar, & Gegen, 2005; Zannoni et al., 1999), the formula published by Morgan *et al*. (2003) is widely accepted and will be used to obtain material properties for cancellous bone in this thesis. Morgan *et al.* (2003) investigated the relationship between modulus and density for cancellous bone and found that the mechanical properties of trabecular bone vary across anatomical location (Morgan, Bayraktar, & Keaveny, 2003). For computational or FE models, different values of Young's modulus can be applied to individual elements of a mesh to model the inhomogeneous characteristics of cancellous bone (Zannoni et al., 1999).

1.3 Wolff's Law and Stress Shielding

In 1892 Julius Wolff discovered that mechanical loads applied to bone causes structural adaptations and remodeling, changing its architecture and composition. The resulting mechanical loads placed on bone were found to have a close relationship with the overall strength of bone. This remodeling process occurs over time and responds to optimize bone's structure (Frost, 2004; Wolff, Maquet, & Furlong, 1892). Changes to the native bone geometry, such as the insertion of an implant, result in a shared distribution of forces across sub components (*i.e.* bone and implant). The insertion of orthopaedic implants has been shown, as expected, to decrease the mechanical loading demands on the surrounding bone. This is a consequence of the implant being more rigid than the native structure and assumes more of the applied loads. This reduction in normal mechanical loading can result in the loss of bone surrounding the implant, which may lead to implant loosening and failure of the reconstructed joint. This occurrence is known as stress shielding and is a common problem resulting from shoulder arthroplasties (Collin, Matsukawa, Boileau, Brunner, & Walch, 2017; Haase & Rouhi, 2013).

1.4 Shoulder Arthroplasty

Developed in the early 1890's, the first shoulder replacement was performed to treat patients with proximal humeral fractures, successfully restoring normal range of motion and reducing pain to patients undergoing surgery (Wallace, 1998). By 1974, Neer extended the use of this proximal humeral arthroplasty to the treatment of glenohumeral arthritis, a disorder compromising the optimal performance of the shoulder resulting from congenital, metabolic, traumatic, degenerative, vascular, septic or nonseptic inflammatory factors (Matsen III et al., 2009; Neer II, 1974). To this day, shoulder arthroplasty remains the main treatment option to improve the quality of life for those who suffer from severe arthritis of the glenohumeral joint and proximal humeral fractures (Merolla, Nastrucci, & Porcellini, 2013). The current treatments options available for shoulder replacement are total shoulder arthroplasty (TSA), reverse total shoulder arthroplasty (RTSA), hemi-arthroplasty, and partial surface reconstruction (Figure 1-6).

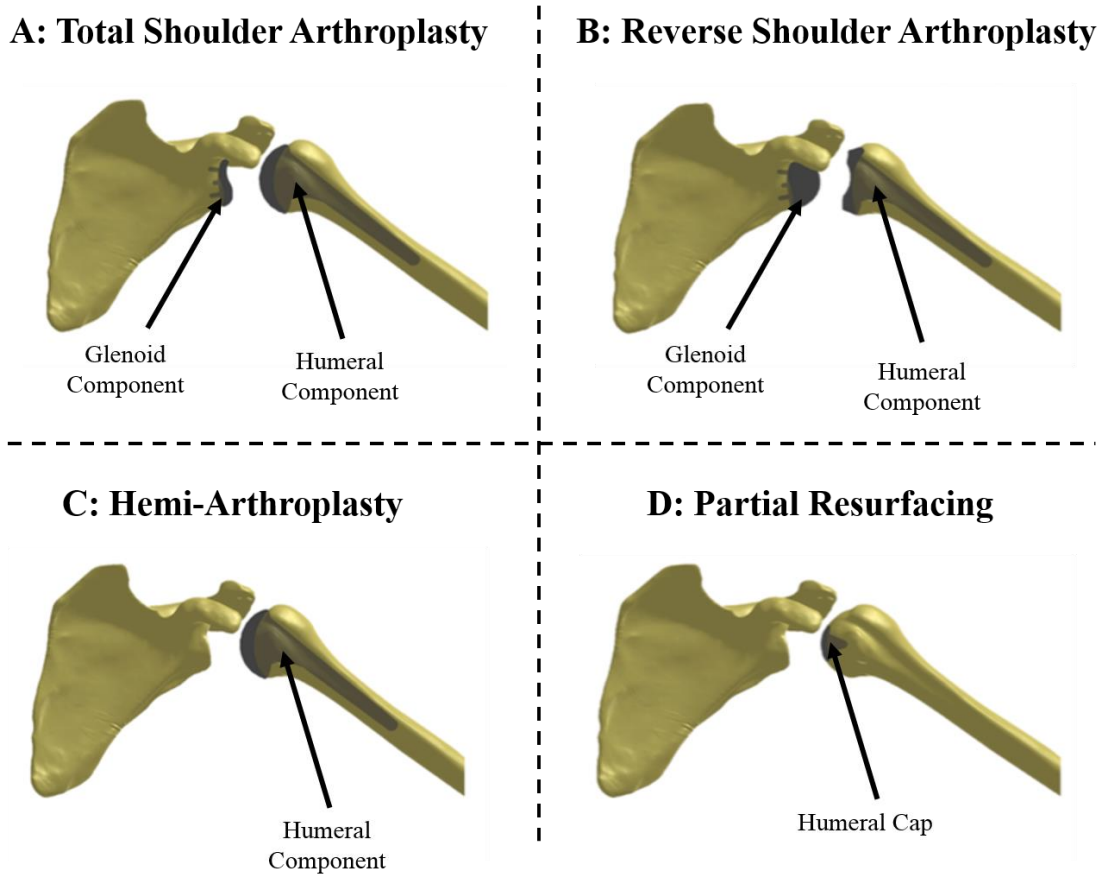

Figure 1-6: Treatment Options for Shoulder Replacement (Razfar et al., 2016)

Four current treatment options currently available to treat patients suffering from extreme arthritis and/or fractures of the proximal humerus. Figure A shows the treatment option using Total Shoulder Arthroplasty where both sides of the joint are replaced using glenoid and humeral components; Figure B shows the treatment option using Reverse Total Shoulder Arthroplasty where the native geometry of the joint is reversed; Figure C shows the treatment option using Hemi-Arthroplasty where only a humeral component is used; and Figure D shows the treatment option using Partial Resurfacing where a cap-like implant is placed on the humeral head.

In TSA and RTSA, both sides of the glenohumeral joint is replaced with a prosthesis. However, in RTSA, the native geometry of the joint is reversed, which produces a more favourable moment arm and hence reduced challenge to the deltoids when elevating the arm. Generally, the shoulder replacement prosthesis consists of three parts: a humeral head, implant stem, and glenoid structure. Hemi-arthroplasty procedures only replace one side of the joint, where only the humeral side of the joint is replaced with a humeral head and implant stem. Partial resurfacing procedures replace one of the joint surfaces, leaving most of the native bone intact.

Since the first shoulder prosthesis study was presented, several advancements have been made in implant design, innovations in materials, surgical techniques, and methods of fixation and sterilization of prostheses (Derar & Shahinpoor, 2015; Harmer, Throckmorton, & Sperling, 2016). Over the past few years, shoulder implant designs have been refined by shortening the humeral stem or eliminating the stem entirely. Shorter implant stems are becoming more favourable as there is less reaming and broaching of the humeral canal. Thus, more of the native bone is preserved, decreasing cortical bone stress and potentially reducing occurrences of perioperative periprosthetic fractures. By shortening humeral stems, studies have suggested there would also be a reduction in stress shielding by retaining more of the native bone (Harmer et al., 2016; Jost et al., 2011; Keener, Chalmers, & Yamaguchi, 2017; Romeo et al., 2017). Biomet, Arthrex, and Tornier (Figure 1-7) are some of the implant manufacturers who currently have short stem models on the market for shoulder arthroplasty (Harmer et al., 2016).

Biomet
Comprehensive®
Micro Stem
(Zimmer Biomet, 2013)

Arthrex
Univers™ Apex
(Arthrex, 2018)

Tornier
Aequalis Ascend™
Flex
(Tornier, 2018)

Figure 1-7: Current Short-stemmed Implant Models (Arthrex, 2018; Tornier, 2013; Zimmer Biomet, 2013)

Biomet, Arthrex, and Tornier are some of the current designers and manufactures of short stem humeral implants.

One of two implant fixation methods are used to create a strong and durable bond between the prosthetic and bone structure: cemented or cementless/press-fit. Depending on the type of fixation method used, different surface textures can be applied to the implant to enhance the biological response of the host (Sumner, 2015). Some of these surface finishes include, plasma spray, grit blast, trabecular metal, or smooth polished. Recent surgical approaches for humeral fixation have migrated from cemented to uncemented techniques, as uncemented fixation conserves native humeral anatomy by removing less bone, which may lead to greater long-term stability (Litchfield et al., 2011; Schmidutz et al., 2014).

1.4.1 Complications

While much advancement has been made to improve shoulder implant design, some complications do arise. Intra-operative fracture, periprosthetic fracture, implant loosening, and proximal bone loss due to osteolysis and stress shielding are still common complications experienced by humeral implants (Collin et al., 2017; Keener, Chalmers, & Yamaguchi, 2017). Denard *et al.* (2017) reported that, although short stem models resulted in less osteolysis over traditional stem length models, 18% of short stem models still resulted in cortical thinning in the lateral proximal metaphysis and 50% of short stem models showed cortical thinning in the medial metaphysis. Partial calcar bone resorption was seen in an additional 23% of short stem models. Additionally, upon implantation, 86% of short stem models were placed in anatomical alignment compared to 98% of traditional length stems. In the event of implant misalignment, malunion may occur between the implant and bone, potentially leading to functional repercussions such as joint stiffness and pain (Duparc, 2013). Schnetzke *et al.* (2016) also reported signs of cortical thinning on the medial calcar. In an evaluation of 52 short stem implant models, 83% of the short models investigated resulted in some form of bone loss. Casagrande *et al.* (2016) reported several complications while using a short stem implant: 8% of patients required revision for humeral loosening, 71% of implants developed at least 1 humeral radiolucency, and roughly 18% of patients exhibited partial or full osteolysis on the medial calcar. Radiolucencies were also observed in 21% short stem models in another study by Morwood *et al.* (2017).

Furthermore, a FE study conducted by Razfar *et al.* (2016) showed that although shorter implant models resulted in significantly less average cortical bone stresses, they were found to significantly raise trabecular bone stresses when compared to standard length humeral implants.

The long-term stability of the implant is vital to restore normal and painless function of the shoulder joint and to prevent humeral revision. In the event of humeral revision, substantial metaphyseal bone loss, periprosthetic fractures, and other high complication risks are likely to occur (Keener et al., 2017). With over 33,000 shoulder replacements conducted each year in the United States alone (American Acedamy of Orthopaedic Surgeons, 2012), high performance implants are crucial to better the lives of these patients.

1.5 Humeral Implant Design

Design of the prosthetic stem is of great interest in shoulder replacement. The overall success of the implant is very likely associated with the design of the stem geometry and material properties, as it is responsible for load transfer from the joint surface (Bobyn et al., 1992). Distribution of load at the articular surface changes when an implant is inserted into the bone. This change in load may lead to various complications, as mentioned in the previous section. Therefore, to avoid these potential complications, various mechanical properties and implant geometries have been investigated. As documented above, shoulder arthroplasties have recently changed from long-stemmed to short-stemmed implants as research suggests that short stemmed implants better mimic the intact state and result in less proximal stress shielding (Denard et al., 2017; Razfar, 2014; Shishani & Gobezie, 2017). Short stem implants prove to be a very reliable and effective treatment option for improving range of motion, decreasing osteolysis, and reducing implant loosening in patients with osteoarthritis or rheumatoid arthritis. Revision surgeries are also seeing a shift from a long stem to a short stem as proximal bone stock is preserved while providing adequate stability and low humeral complication rates (Shishani & Gobezie, 2017; Wagner et al., 2017).

1.5.1 Implant Girth/Stem Diameter

Effects of humeral stem length have been widely research; however, research investigating the effects of implant girth[2], or known in some literature studies as stem diameter, on the surrounding bone is inadequate. In the shoulder, one study examined the effects of relative stem size on proximal bone stresses. Nagels *et al.* (2003) radiographically investigated cortical bone loss at 4 regions for 70 patients who underwent shoulder replacement surgery using the same standard stem implant model. A digital template was created to measure various distances used for calculations of cortical

[2] The term implant girth will be used, over stem diameter, throughout this dissertation as it better represents the entire implant geometry (*i.e.*, changing implant girth, changes the bulk of the entire implant from the most proximal geometry to the most distal geometry)

thickness and relative stem size between subjects. Results indicated that 9% of patients had a significant reduction in cortical thickness where larger relative stem size resulted in greater incidences of stress shielding (Nagels, Stokdijk, & Rozing, 2003).

In the hip, a few studies have investigated the effects of implant stem diameter. A study conducted by Engh and Bobyn (1988), showed that larger stems (≥13.5 mm in diameter) resulted in increased occurrences of bone resorption when compared to smaller stems (≤12.0 mm in diameter). The authors classified the degree of bone loss in two categories: minor and not likely to cause clinical problems or pronounces having potentially harmful clinical consequences. Osteolysis due to the larger sized implant was classified as being pronounced. Similarly, Bobyn *et al.* (1992) showed that larger stem implants resulted in significantly higher incidences of stress shielding. Meneghini *et al.* (2006) also studied the effects of two femoral implants with different diameter stems. However, this study focused only on torsional stability of the implants.

A variety of studies conducted in dental implants have found that implants with a larger girth, resulted in more desirable outcomes (Bilhan et al., 2010; Eazhil, Swaminathan, Gunaseelan, Kannan, & Alagesan, 2016; Himmlová, Dostálová, Kácovský, & Konvičková, 2004; Hsu et al., 2017; Li et al., 2011; Olate, Lyrio, de Moraes, Mazzonetto, & Moreira, 2010). In terms of bone to implant contact (BIC) (*i.e.,* the amount of contact that occurs between the surface area of bone that is available to contact the surface area of the implant in the humeral canal) dental implants with a larger diameter produced more contact when compared to smaller diameters (Eazhil et al., 2016; Hsu et al., 2017) which resulted in increased implant stability (Bilhan et al., 2010; Eazhil et al., 2016; Li et al., 2011). Author's also reported that implants with a larger diameter decreased the maximum stresses placed on the surrounding bone when compared to smaller implant sizes (Ding, Liao, Zhu, Zhang, & Zhang, 2009; Eazhil et al., 2016; Himmlová et al., 2004), which were found to produce stresses much larger than the yield stresses for cortical and trabecular bone (McNally et al., 2013). Although the results observed in dental implants differ from the findings in the shoulder and hip, the geometries and loading conditions vary markedly and can thus affect the stress patterns observed across various bone-implant interfaces (Huiskes et al., 1987).

1.5.2 Collar versus Collarless Implant Types

Traditionally, when a humeral implant is placed into the bone, the backside of the humeral head contacts the resection surface (Figure 1-8). Recently, some surgeons have opted to leave a slight gap between the backside of the humeral head and the resection surface. A small part of the implant extends from the resection plane and allows the back of the humeral head to sit slightly above the resection surface (Figure 1-8). Execution of either surgical approach is currently subjective. To the authors' knowledge, no studies have yet been published investigating any effects of removing the collar from humeral implants. Investigation on collared or collarless humeral implants is required to guide current surgical techniques and determine the outcomes when the collar is removed.

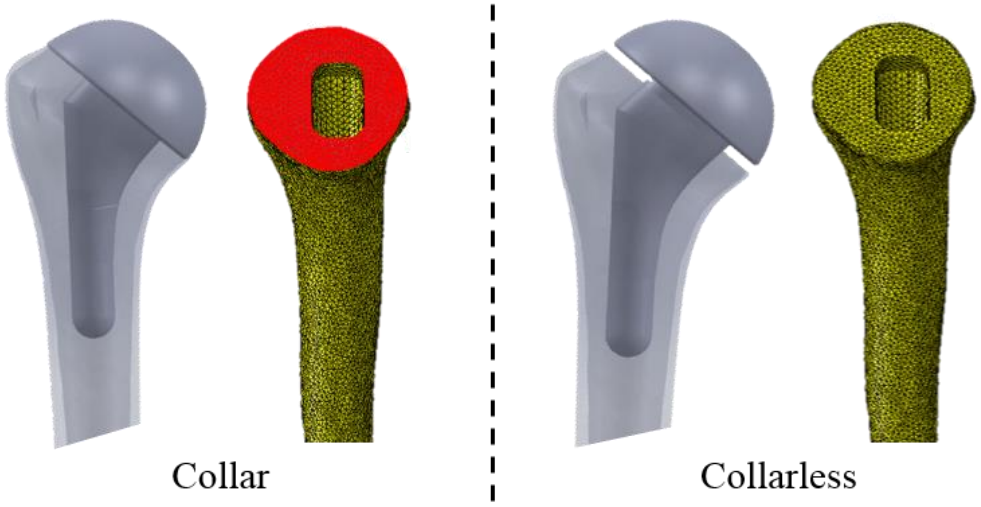

Figure 1-8: Humeral Head Contact Configurations

Some surgical techniques either employ contacting the backside of the humeral head to the resection surface or leaving a gap, characterizing either a collared implant or collarless implant, correspondingly. The figure on the left represents the collar contact state where the red indicates contact pressure to the cut plane and the figure on the right indicates the collarless state, with no contact pressure on the cut surface. N.B. The image on the right, which represents the collarless state, does not represent the true distance of the gap that was created between the backside of the humeral head and the cut surface during the FE simulation. The gap in this image is enlarged to emphasize to the reader that there is no contact of the backside of the humeral head to the cut surface.

The use of collar or collarless implants in femoral hip implants has been a topic of interest to researchers for years. Like the shoulder, the use of collared or collarless femoral implants is subjective, as clinical findings are seemingly inconclusive (Al-Dirino, 2017). The goal of the added collar is to prevent subsidence of the femoral stem, allowing for primary osseointegration and to increase axial load transfer to the calcar, preventing resorption (Jeon et al., 2011; Meding, Ritter, Keating, & Faris, 1997). However, contact between the calcar and implant collar has been found to be extremely difficult to achieve (Demey, Fary, Lustig, Neyret, & Si Selmi, 2011; Markolf, Amstutz, & Hirschowitz, 1980). In fact, authors have reported achieving perfect contact between collar and calcar in as low as 39% of cases (Meding et al., 1997). Intraoperative implant fracture may occur with collared implants, as surgeons may use increased force to obtain contact between the collar and calcar. Perfect contact is necessary to achieve biomechanical stability and proper transmission of loads. Otherwise, increased risk of calcar resorption exists and the possibility of implant tilting is introduced increasing risk of femoral fracture (Jeon et al., 2011). In the event perfect contact is achieved with the implant collar, studies have shown unpredictable results. One study conducted by Ji *et al.* (2013) found no significant difference in bone loss between collared and collarless implant types; yet, Mansour *et al.* (1995) found that bone loss was greatest in collarless femoral implants. Interestingly, a study by Allen *et al.* (1996) found that when either a collared or collarless femoral implant was used, surface strains 5 mm below the collar location were nearly identical; however, when surface strains were measured 25 mm below the collar location, the collared implant resulted in strains greater than the collarless implant, which more closely matched strains to the native state.

1.6 Finite Element Modeling

Computer based modeling and computational techniques have become a popular method to evaluate numerous biomechanical problems. These modeling techniques can be used to simulate the anatomy, movement, and joint forces of a musculoskeletal system, where information on the stress and strain throughout the system are output.

Problems involving complex geometries and material properties, such as those involved in the field of orthopaedics, can be quite challenging to solve. FE methods can be applied to simplify these parameters for easy and accurate analysis. Although *in-vitro* studies using cadaveric specimens and strain gauges can provide valuable direct data, FE methods can be used to obtain data from internal structures that may be difficult to examine or are inaccessible. In addition, computer based modeling provides a completely non-invasive method for investigating biomechanical problems, and is generally more cost and time efficient than *in-vitro* analysis.

For FE analysis, the body of interest is divided into an equal number of smaller bodies, or finite elements, connected at points common to two or more elements, called nodes (Figure 1-9). This process is known as discretization and is the first step to generating the mesh and developing the FE model. For orthopaedic-based analyses, 3D element types are most commonly used to mesh the geometry of interest. These element types are either tetrahedral or hexahedral in shape and can be linear (first-order) or quadratic (second-order). The choice of element size and type is one of the most important factors affecting the accuracy of results. Mesh size should be selected to best fit the behaviour of the system under analysis (Logan, 2002). Computational resources and time are directly affected by the size of the mesh; therefore, an appropriate size should be selected for efficient modeling. Convergence tests can be done on FE models, which help to determine the smallest mesh size necessary to maintain high accuracy without becoming computationally expensive.

Dividing the main body into smaller elements allows the performance of the system to be approximated by the local behaviour of each element. Individual elements in the mesh can be assigned a unique set of properties that can affect how the model responds to

variations in the system (such as implant geometry and applied loads). When a force is applied to the system, each node will respond according to its assigned properties. The forces and resultant displacement of each element in the system are related in terms of an overall stiffness matrix, K (Logan, 2002).

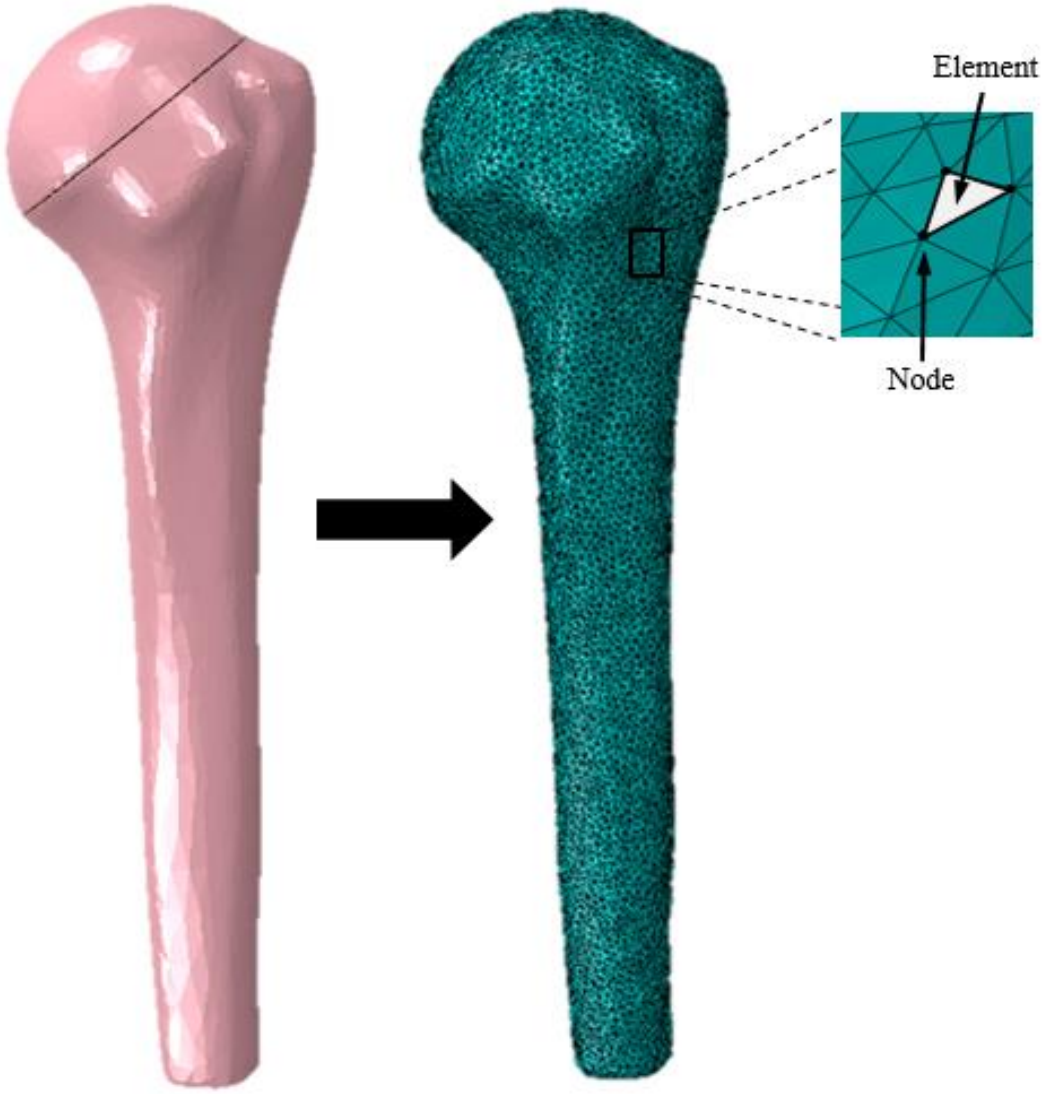

Figure 1-9: Discretization of the Humerus

A single tetrahedral element is highlighted and its surrounding 3 nodes.

1.7 Strain Energy Density

When bone is deformed, the external work on the elastic body causes it to change from its natural, unstressed state. This work is transformed into stain energy, which can be used to predict the remodeling capacity of bone. Developed by Cowin and Hegedus, the theory of adaptive elasticity examines threshold deviations from a homeostatic strain state, which can be used to predict if stress shielding may occur (Cowin & Hegedus, 1976; Neuert & Dunning, 2013). This concept has been widely studied in various reconstruction models such as elbow implants (Neuert & Dunning, 2013), knee replacements (Tissakht, Ahmed, & Chan, 1996; Van Lenthe, de Waal Malefijt, & Huiskes, 1997), orthopaedic screws (Gefen, 2002; Haase & Rouhi, 2013), and hip arthroplasties (Behrens et al., 2008; Huiskes et al., 1987) and will be used to predict bone resorption in the proximal humerus for this dissertation.

To better predict stress shielding and bone resorption, Neuert and Dunning (2013) conducted an FE study to determine a threshold value, which could be used to determine whether a region of bone would resorb, remain the same, or become stronger if changes in strain were lower, equal to, or higher than this value, respectively. Threshold values for changes in strain were tested, and the resultant steady-state density distributions were compared with values derived from micro CT images of the ulna when the model was subjected to an approximate in vivo load simulating forearm rotation. The authors found that a threshold value of 0.55 produced the most accurate results, by producing the smallest error between the predicted (*i.e.,* calculated from the FE model) and physiological (*i.e.*, derived from micro CT images) density values (Neuert & Dunning, 2013).

1.8 Motivation

Despite the widespread use of shoulder prostheses for shoulder reconstruction, there are questions regarding the effect of implant design on interface contact, load transfer, and bone stress. Studies have investigated the effects of various implant stem designs, such as stem length, surface texturing, and material stiffness in attempt to find the best implant to better match the intact state (Derar & Shahinpoor, 2015; Harmer et al., 2016; Jost et al., 2011; Keener, Chalmers, & Yamaguchi, 2017; Razfar et al., 2016; Romeo et al., 2017). One area of stem design that has received insufficient research is implant girth. To the author's knowledge only one study has examined bone stresses due to implant girth, or stem diameter, in the shoulder. Occurrences of cortical bone resorption was observed for a single implant type for multiple patients (Nagels et al., 2003); no studies have considered the effects of various implant girths on interface contact, or both cortical and trabecular bone stresses. Additionally, no studies have investigated proximal BIC, or bone stresses for collar or collarless implants in the shoulder. While some studies have investigated these concepts in the hip (Bobyn et al., 1992; Engh & Bobyn, 1988; Meneghini et al., 2006), the specific geometries of these structures differ and may result in unique findings at different anatomical locations. Examination of these concepts is needed to guide the optimization of implant sizes and designs for patients.

1.9 Objectives and Hypotheses

The goal of this dissertation is to develop and employ a FE model to determine the effects of (1) implant girth and (2) a collar shoulder implants on interface contact and bone stresses.

Objectives:

1. To develop a three-dimensional FE model of the proximal humerus to investigate the degree of BIC, changes in proximal bone stresses, and changes in SED due to changes in humeral stem girth using traditional implantation methods (*i.e.*, collared implant).
2. To use the FE model to examine the changes in BIC in the humeral canal, changes in proximal bone stresses, and changes in SED, when the implant collar was removed from the resection plane (*i.e.*, comparing collared to collarless implants).

Hypotheses:

The specific hypotheses of this work are as follows:

1. Using a traditional collared implant, it is hypothesized that the implant with the largest girth will result in the following when compared to smaller implant girth sizes:
    a. Greater degree of BIC;
    b. Greater changes in cortical and trabecular bone stresses from the intact state;
    c. Greater volume of bone expected to resorb in both cortical and trabecular bone via SED measurements.
2. It is hypothesized that removing the implant collar will result in the following:
    a. Greater degree of BIC;
    b. Greater changes in cortical and trabecular bone stresses from the intact state;
    c. Greater volume of bone expected to resorb in both cortical and trabecular bone via SED measurements.

1.10 Thesis Overview

The following chapter, Chapter 2, investigates the effect of increasing implant girth on interface contact (*i.e.*, BIC), proximal bone stresses and SED. Chapter 3 examines the implications of removing the implant collar on the same outcome measures discussed in Chapter 2 (interface contact, bone stresses, and SED). Chapters 2 and 3 will provide a description of the methods used to create each study, as well as the obtained results and detailed discussions of the findings. Chapter 4 concludes this work, mentioning the strength and limitations of this study and offers future recommendations. Additional important information can be found throughout the Appendix.

1.11 References

Allen, W. ., Beaupré, G. ., Carter, D. ., Giddings, V., Goodman, S. ., D.J, S., & van der Meulen, M. C. . (1996). *Femoral Collar Effect on bone strains after cemented hip replacement*. Stanford, CA.

Arthrex. (2018). Univers^{TM} Apex. Retrieved from https://www.arthrex.com/shoulder/univers-apex

Behrens, B., Bouquecha, A., Nolte, I., Meyer-Lindenberg, A., Stukenborg-Colsman, C., & Pressel, T. (2008). Strain adaptive bone remodelling: influence of the implantation technique. *Studies in Health Technology and Informatics*, *133*, 33–44.

Bergmann, G., Graichen, F., Bender, A., Kääb, M., Rohlmann, A., & Westerhoff, P. (2007). In vivo glenohumeral contact forces-Measurements in the first patient 7 months postoperatively. *Journal of Biomechanics*, *40*(10), 2139–2149. https://doi.org/10.1016/j.jbiomech.2006.10.037

Bilhan, H., Geckili, O., Mumcu, E., Bozdag, E., Sünbüloğlu, E., & Kutay, O. (2010). Influence of surgical technique, implant shape and diameter on the primary stability in cancellous bone. *Journal of Oral Rehabilitation*, *37*(12), 900–907. https://doi.org/10.1111/j.1365-2842.2010.02117.x

Bobyn, J., Mortimer, E., Glassman, A., Engh, C., Miller, J., Brooks, C., & CE. (1992). Producing and avoiding stress shielding: laboratory and clinical observations of noncemented total hip arthroplasty. *Clinical Orthopaedics & Related Research*, *274*, 79–96.

Clarke, B. (2008). Normal bone anatomy and physiology. *Clinical Journal of the American Society of Nephrology : CJASN*, *3 Suppl 3*, 131–139. https://doi.org/10.2215/CJN.04151206

Collin, P., Matsukawa, T., Boileau, P., Brunner, U., & Walch, G. (2017). Is the humeral stem useful in anatomic total shoulder arthroplasty? *International Orthopaedics*, 10–14. https://doi.org/10.1007/s00264-016-3371-4

Cowin, S., & Hegedus, D. (1976). Bone remodeling I: theory of adaptive elasticity. *J Elast*, *6*(3), 313–326.

Culham, E., Peat, M., & Culham, E. (1993). Functional Anatomy of the Shoulder Complex, *18*(1), 342–350.

Dalla Pria Bankoff, A. (2012). Biomechanical Characteristics of the Bone. In *Human Musculoskeletal Biomechanics* (pp. 61–86). https://doi.org/10.1016/S1067-2516(02)80064-3

De Witte, P. B., Werner, S., ter Braak, L. M., Veeger, H. E. J., Nelissen, R. G. H. H., & de Groot, J. H. (2014). The Supraspinatus and the Deltoid - Not just two arm elevators. *Human Movement Science*, *33*(1), 273–283. https://doi.org/10.1016/j.humov.2013.08.010

Demey, G., Fary, C., Lustig, S., Neyret, P., & Si Selmi, T. A. (2011). Does a Collar Improve the Immediate Stability of Uncemented Femoral Hip Stems in Total Hip Arthroplasty? A Bilateral Comparative Cadaver Study. *Journal of Arthroplasty*, *26*(8), 1549–1555. https://doi.org/10.1016/j.arth.2011.03.030

Denard, P. J., Noyes, M. P., Walker, J. B., Shishani, Y., Gobezie, R., Romeo, A. A., & Lederman, E. (2017). Proximal stress shielding is decreased with a short stem compared with a traditional-length stem in total shoulder arthroplasty. *Journal of Shoulder and Elbow Surgery*, *27*(1), 53–58. https://doi.org/10.1016/j.jse.2017.06.042

Derar, H., & Shahinpoor, M. (2015). Recent patents and designs on hip replacement prostheses. *The Open Biomedical Engineering Journal*, *9*, 92–102. https://doi.org/10.2174/1874120701509010092

Diamant, I., Shahar, R., & Gegen, A. (2005). How to select the elastic modulus for cancellous bone in patient-specific continuum models of the spine. *Medical & Biological Engineering & Computing*, *43*(4), 465–472. https://doi.org/10.1107/S0567740873002372

Ding, X., Liao, S. H., Zhu, X. H., Zhang, X. H., & Zhang, L. (2009). Effect of diameter and length on stress distribution of the alveolar crest around immediate loading implants. *Clinical Implant Dentistry and Related Research*, *11*(4), 279–287. https://doi.org/10.1111/j.1708-8208.2008.00124.x

Duparc, F. (2013). Malunion of the proximal humerus. *Orthopaedics & Traumatology: Surgery & Research*, *99*(1 Suppl), S1–S11. https://doi.org/10.1016/j.otsr.2012.11.006

Dutton, M. (2012). *Dutton's Prthopaedic Examination, Evaluation, and Intervention*. (J. Morita & B. Kearns, Eds.) (Third). NA: The McGraw-Hill Companies.

Eazhil, R., Swaminathan, S. ., Gunaseelan, M., Kannan, G. ., & Alagesan, C. (2016). Impact of implant diameter and length on stress distribution in osseointegrated implants: A 3D FEA study. *J Int Soc Prevent Communit Dent*, *6*(6), 590–596.

Engh, C. A., & Bobyn, J. D. (1988). The influence of stem size and extent of porous coating on femoral bone resorption after primary cementless hip arthroplasty. *Clinical Orthopaedics and Related Research*, *231*, 7–28. https://doi.org/10.1097/00003086-198806000-00002

Frost, H. M. (2004). A 2003 update of bone physiology and Wolff's law for clinicians. *Angle Orthodontist*, *74*(1), 3–15. https://doi.org/10.1043/0003-3219(2004)074<0003:AUOBPA>2.0.CO;2

Gefen, A. (2002). Computational simulations of stress shielding and bone resorption around existing and computer-designed orthopaedic screws. *Medical & Biological Engineering & Computing*, *40*(3), 311–322.

Grey, H. (1995). Skeletal System. In L. H. Bannister, M. M. Berry, P. Collins, M. Dyson, J. E. Dussek, & M. W. J. Ferguson (Eds.), *Grey's Anatomy* (38th ed., pp. 452–483). New York: Churchill Livingstone.

Haase, K., & Rouhi, G. (2013). Prediction of stress shielding around an orthopedic screw: Using stress and strain energy density as mechanical stimuli. *Computers in Biology*

and Medicine, *43*(11), 17481757. https://doi.org/10.1016/j.compbiomed.2013.07.032

Hadjidakis, D. J., & Androulakis, I. I. (2006). Bone Remodeling. *Annals of the New York Academy of Science*, *1092*, 385–396.

Harmer, L., Throckmorton, T., & Sperling, J. W. (2016). Total shoulder arthroplasty: are the humeral components getting shorter? *Current Reviews in Musculoskeletal Medicine*, *9*(1), 17–22. https://doi.org/10.1007/s12178-016-9313-3

Himmlová, L., Dostálová, T., Kácovský, A., & Konvičková, S. (2004). Influence of implant length and diameter on stress distribution: A finite element analysis. *THE JOURNAL OF PROSTHETIC DENTISTRY*, *91*(1), 20–25. https://doi.org/10.1016/j.prosdent.2003.08.008

Hsu, J. T., Shen, Y. W., Kuo, C. W., Wang, R. T., Fuh, L. J., & Huang, H. L. (2017). Impacts of 3D bone-to- implant contact and implant diameter on primary stability of dental implant. *Journal of the Formosan Medical Association*, *116*(8), 582–590. https://doi.org/10.1016/j.jfma.2017.05.005

Huiskes, R., Weinans, H., Grootenboer, H. J., Dalstra, M., Fudala, B., & Slooff, T. J. (1987). Adaptive bone-remodeling theory applied to prosthetic-design analysis. *Journal of Biomechanics*, *20*(11–12), 1135–1150. https://doi.org/10.1016/0021-9290(87)90030-3

Jeon, I., Bae, J. Y., Park, J. H., Yoon, T. R., Todo, M., Mawatari, M., & Hotokebuchi, T. (2011). The biomechanical effect of the collar of a femoral stem on total hip arthroplasty. *Computer Methods in Biomechanics and Biomedical Engineering*, *14*(1), 103–112. https://doi.org/10.1080/10255842.2010.493513

Ji, W. P., Wang, X. L., Ma, M. Q., Lan, J., & Li, H. (2013). Prevention of early bone loss around the prosthesis by administration of anti-osteoporotic agents and influences of collared and non-collared femoral stem prostheses on early periprosthetic bone loss. *European Journal of Orthopaedic Surgery and Traumatology*, *23*(5), 565–571.

https://doi.org/10.1007/s00590-012-1034-8

Jobe, C. M., Phipatanakul, W. P., & Coen, M. J. (2009). Gross Anatomy of the Shoulder. In C. A. Rockwood Jr, F. A. Matsen III, M. A. Wirth, & S. B. Lippitt (Eds.), *The Shoulder Volume 1* (Fourth, pp. 33–100). Philadelphia, PA: Sanders Elsevier.

Jost, P. W., Dines, J. S., Griffith, M. H., Angel, M., Altchek, D. W., & Dines, D. M. (2011). Total Shoulder Arthroplasty Utilizing Mini-Stem Humeral Components: Technique and Short-Term Results. *HSS Journal*, *7*(3), 213–217. https://doi.org/10.1007/s11420-011-9221-4

Keener, J. D., Chalmers, P. N., & Yamaguchi, K. (2017). The Humeral Implant in Shoulder Arthroplasty. *Journal of the American Academy of Orthopaedic Surgeons*, *25*(6), 427–438. https://doi.org/10.5435/JAAOS-D-15-00682

Li, T., Hu, K., Cheng, L., Ding, Y., Ding, Y., Shao, J., & Kong, L. (2011). Optimum selection of the dental implant diameter and length in the posterior mandible with poor bone quality - A 3D finite element analysis. *Applied Mathematical Modelling*, *35*(1), 446–456. https://doi.org/10.1016/j.apm.2010.07.008

Litchfield, R. B., McKee, M. D., Balyk, R., Mandel, S., Holtby, R., Hollinshead, R., … McCormack, R. (2011). Cemented versus uncemented fixation of humeral components in total shoulder arthroplasty for osteoarthritis of the shoulder: A prospective, randomized, double-blind clinical trial-A JOINTs Canada Project. *Journal of Shoulder and Elbow Surgery*, *20*(4), 529–536. https://doi.org/10.1016/j.jse.2011.01.041

Logan, D. L. (2002). Introduction. In *A First Course in the Finite Element Method* (Third, pp. 1–25). Pacific Grove, CA: Brooks/Cole Thomson Learning.

Mansour, H. ., Ray, J. ., & Mukherjee, D. . (1995). Stress shielding of femoral component with and without collar. In *In Proceedings of the IEEE Fourteenth Southern Biomedical Engineering Conference* (pp. 53–54). Shreveport, LA, USA.

Markolf, K. L., Amstutz, H. C., & Hirschowitz, D. L. (1980). The effect of calcar contact

on femoral component micromovement. A mechanical study. *The Journal of Bone and Joint Surgery. American Volume*, *62*(8), 1315–23. Retrieved from http://www.ncbi.nlm.nih.gov/pubmed/7440610

Matsen III, F. ., Clinton, J., Rockwood Jr, C. ., Wirth, M. ., & Lippitt, S. . (2009). Shoulder Arthroplasty (?) Edit. In E. V. Fehringer & J. W. Sperling (Eds.), *The Shouder Volume 2* (Fourth, pp. 1089–12). Philadelphia, PA: Saunders Elsevier.

Matsumura, N., Nakamichi, N., Ikegami, H., Nagura, T., Imanishi, N., Aiso, S., & Toyama, Y. (2013). The function of the clavicle on scapular motion: A cadaveric study. *Journal of Shoulder and Elbow Surgery*, *22*(3), 333–339. https://doi.org/10.1016/j.jse.2012.02.006

McNally, S. ., Wilcox, C., Akhter, M. P., Sheets, J. ., Danforth, J. ., & Chehal, H. . (2013). Implant diameter: Effect on stress in bone: Finite element analysis. *Journal of Dental Implants*, *3*(2), 87–90.

Meding, J. B., Ritter, M. A., Keating, E. M., & Faris, P. M. (1997). Comparison of collared and collarless femoral components in primary uncemented total hip arthroplasty. *Journal of Arthroplasty*, *12*(3), 273–280. https://doi.org/10.1016/S0883-5403(97)90023-1

Meneghini, R. M., Hallab, N. J., Berger, R. a, Jacobs, J. J., Paprosky, W. G., & Rosenberg, A. G. (2006). Stem diameter and rotational stability in revision total hip arthroplasty: a biomechanical analysis. *Journal of Orthopaedic Surgery and Research*, *1*, 5. https://doi.org/10.1186/1749-799X-1-5

Merolla, G., Nastrucci, G., & Porcellini, G. (2013). Shoulder arthroplasty in osteoarthritis: current concepts in biomechanics and surgical technique. *Translational Medicine @ UniSa*, *6*(4), 16–28. Retrieved from http://www.ncbi.nlm.nih.gov/pubmed/24251240%5Cnhttp://www.pubmedcentral.nih.gov/articlerender.fcgi?artid=PMC3829793

Moore, K. L., Agur, A. M. R., & Dalley, A. F. (2011). *Essential Clinical Anatomy*

(Fourth). Woltrs Kluwer.

Morgan, E. F., Bayraktar, H. H., & Keaveny, T. M. (2003). Trabecular bone modulus-density relationships depend on anatomic site. *Journal of Biomechanics*, *36*(7), 897–904. https://doi.org/10.1016/S0021-9290(03)00071-X

Morwood, M. P., Johnston, P. S., & Garrigues, G. E. (2017). Proximal ingrowth coating decreases risk of loosening following uncemented shoulder arthroplasty using mini-stem humeral components and lesser tuberosity osteotomy. *Journal of Shoulder and Elbow Surgery*, *26*(7), 1246–1252. https://doi.org/10.1016/j.jse.2016.11.041

Nagels, J., Stokdijk, M., & Rozing, P. M. (2003). Stress shielding and bone resorption in shoulder arthroplasty. *Journal of Shoulder and Elbow Surgery*, *12*(1), 35–39. https://doi.org/10.1067/mse.2003.22

Neer II, C. S. (1974). The of Surgery and Joint Replacement for Glenohumeral Arthroplasty Osteoarthritis *. *The Journal of Bone and Joint Surgery*, *56–A*(1), 1–13.

Neuert, M. A. C., & Dunning, C. E. (2013). Determination of remodeling parameters for a strain-adaptive finite element model of the distal ulna. *Proceedings of the Institution of Mechanical Engineers, Part H: Journal of Engineering in Medicine*, *227*(9), 994–1001. https://doi.org/10.1177/0954411913487841

Olate, S., Lyrio, M. C. N., de Moraes, M., Mazzonetto, R., & Moreira, R. W. F. (2010). Influence of Diameter and Length of Implant on Early Dental Implant Failure. *Journal of Oral and Maxillofacial Surgery*, *68*(2), 414–419. https://doi.org/10.1016/j.joms.2009.10.002

Orthopaedic Stats and Facts. (2012). In *Department of Research & Scientific Affairs*. Rosemont, IL: AAOS.

Ralston, S. H. (2017). Bone structure and metabolism. *Medicine*, *45*(9), 560–564. https://doi.org/10.1016/j.mpmed.2017.06.008

Razfar, N. (2014). *Finite Element Modeling of the Proximal Humerus to Compare Stemless , Short and Standard Stem Humeral Components of Varying Material Stiffness for Shoulder Arthroplasty*. Western Univeristy.

Razfar, N., Reeves, J. M., Langohr, D. G., Willing, R., Athwal, G. S., & Johnson, J. A. (2016). Comparison of proximal humeral bone stresses between stemless, short stem, and standard stem length: A finite element analysis. *Journal of Shoulder and Elbow Surgery*, *25*(7), 1076–1083. https://doi.org/10.1016/j.jse.2015.11.011

Romeo, A. A., Thorsness, R. J., Sumner, S. A., Gobezie, R., Lederman, E. S., & Denard, P. J. (2017). Short-term clinical outcome of an anatomic short-stem humeral component in total shoulder arthroplasty. *Journal of Shoulder and Elbow Surgery*, (16010802), 5–9. https://doi.org/10.1016/j.jse.2017.05.026

Rosso, C., Mueller, A. M., McKenzie, B., Entezari, V., Cereatti, A., Croce, U. Della, … DeAngelis, J. P. (2014). Bulk effect of the deltoid muscle on the glenohumeral joint. *Journal of Experimental Orthopaedics*, *1*(1), 14. https://doi.org/10.1186/s40634-014-0014-9

Schmidutz, F., Agarwal, Y., Müller, P. E., Gueorguiev, B., Richards, R. G., & Sprecher, C. M. (2014). Stress-shielding induced bone remodeling in cementless shoulder resurfacing arthroplasty: A finite element analysis and in vivo results. *Journal of Biomechanics*, *47*(14), 3509–3516. https://doi.org/10.1016/j.jbiomech.2014.08.029

Shishani, Y., & Gobezie, R. (2017). Does a short-stemmed humeral implant really make a difference? *Seminars in Arthroplasty*, *28*(1), 13–17. https://doi.org/10.1053/j.sart.2017.05.003

Sumner, D. R. (2015). Long-term implant fixation and stress-shielding in total hip replacement. *Journal of Biomechanics*, *48*(5), 797–800. https://doi.org/10.1016/j.jbiomech.2014.12.021

Tissakht, M., Ahmed, A. M., & Chan, K. C. (1996). Calculated stress-shielding in the distal femur after total knee replacement corresponds to the reported location of

bone loss. *Journal of Orthopaedic Research*, *14*(5), 778–785. https://doi.org/10.1002/jor.1100140515

Tornier. (2013). Aequalis Ascend Flex. Retrieved from http://www.tornier.com/epaule/ascendflex-pyro/data/AN/pdf/Aequalis_AscendFlex_brochure_UDZF131.pdf

Turner, C. H., Rho, J., Takano, Y., Tsui, T. Y., & Pharr, G. M. (1999). The elastic properties of trabecular and cortical bone tissues are similar: Results from two microscopic measurement techniques. *Journal of Biomechanics*, *32*(4), 437–441. https://doi.org/10.1016/S0021-9290(98)00177-8

Van Lenthe, G. H., de Waal Malefijt, M. C., & Huiskes, R. (1997). Stress shielding after total knee replacement may cause bone resorption in the distal femur. *The Journal of Bone and Joint Surgery. British Volume*, *79*(1), 117–22. https://doi.org/10.1302/0301-620X.79B1.6808

Wagner, E. R., Statz, J. M., Houdek, M. T., Cofield, R. H., Sánchez-Sotelo, J., & Sperling, J. W. (2017). Use of a shorter humeral stem in revision reverse shoulder arthroplasty. *Journal of Shoulder and Elbow Surgery*, *26*(8), 1454–1461. https://doi.org/10.1016/j.jse.2017.01.016

Wallace, W. A. (1998). Introduction. In *Joint Replacement in the Shoulder and Elbow* (pp. 1–5). Woburn, MA: Reed Educational and Professional Publishing.

Wehrli, F. (n.d.). Role of Cortical and Trabecular Bone Architecture in Osteoporosis. *International Society of Magnetic Resonance*, (13). Retrieved from http://cds.ismrm.org/protected/09MProceedings/files/Fri A22_07 Wehrli.pdf

Wolff, J., Maquet, P., & Furlong, R. (1892). *The law of bone remodelling*. Springer Berlin.

Zannoni, C., Mantovani, R., & Viceconti, M. (1999). Material properties assignment to finite element models of bone structures: a new method. *Medical Engineering & Physics*, *20*(10), 735–740. https://doi.org/10.1016/S1350-4533(98)00081-2

Zimmer Biomet. (2013). *Comprehensive Total Shoulder System*. Retrieved from http://www.biomet.com/patients/shoulder_replacement.cfm

Chapter 2

2 Effect of Implant Girth on Interface Contact and Bone Stresses

Finite element (FE) modeling is a very useful and effective tool to evaluate the effect of orthopaedic implants on bone. This chapter explicitly explains the steps taken to develop and analyze patient-specific FE models of the proximal humerus. These techniques were used to explore the effect of implant girth on bone to implant contact (BIC), proximal bone stresses and strain energy density (SED). While changes to implant girth (may also be referred to as stem diameter in other studies) have been studied in other joints, such as the hip, and in dental implants, there is a need to further investigate these concepts in the proximal humerus following implant reconstruction.

2.1 Introduction

Current humeral implant models have markedly improved from older generations; though, some complications, such as implant loosening and proximal stress shielding, still occur with these newer implant designs (Casagrande et al., 2016; Collin, Matsukawa, Boileau, Brunner, & Walch, 2017; Denard et al., 2017; Keener, Chalmers, & Yamaguchi, 2017; Schnetzke, Coda, Raiss, Walch, & Loew, 2016). One particular aspect of implant design that is of great interest is the design of the humeral stem, as it has been shown to play an important role in load distribution from the articular surface, which can affect the remodeling capabilities of the surrounding bone (Bobyn et al., 1992; Razfar et al., 2016).

Some aspects of humeral stem design that have been investigated, in terms of the effect on bone stress and stress shielding, are implant stem length and material stiffness or modulus (Denard et al., 2017; Dines, 2005; Razfar et al., 2016; Shishani & Gobezie, 2017; Wagner et al., 2017). However, some areas remain inadequately researched, such as the effect of implant girth. In a clinical study, Nagels *et al.* (2003) investigated the occurrences of stress shielding when a shoulder implant was inserted in patients. The relative size of the implant in the humeral canal was measured and correlated to the degree of bone loss. The results showed that humeral implants with a larger relative stem diameter increased the occurrences of stress shielding. This study only investigated radiographic changes in cortical bone and did not examine changes in trabecular bone. Additionally, the incidence of stress shielding was correlated with the use of a standard length humeral stem, and not a short stem.

With respect to the investigation of stress shielding at other joints, two separate studies by Engh and Bobyn (1988) and Bobyn *et al.* (1992) examined stress shielding in the hip with increases in femoral stem diameter. Again, these studies only determined cortical bone loss, while using a traditional length stem. Meneghini *et al.* (2006) also conducted a study investigating femoral implants with two different stem diameters; however, this study did not correlate implant stem diameter or girth with bone stresses or osteolysis.

The effects of implant girth have also been widely investigated in dental implants. In contrast to the findings in the shoulder and hip, many authors found that dental implants

with a larger diameter, or a larger implant girth, resulted in more favourable outcomes (Bilhan et al., 2010; Eazhil, Swaminathan, Gunaseelan, Kannan, & Alagesan, 2016; Himmlová, Dostálová, Kácovský, & Konvičková, 2004; Hsu et al., 2017; Li et al., 2011; Olate, Lyrio, de Moraes, Mazzonetto, & Moreira, 2010). Implants with larger diameters, when compared to smaller diameters, were found to produce more bone to implant contact (BIC) (Eazhil et al., 2016; Hsu et al., 2017) and enhance implant stability (Bilhan et al., 2010; Eazhil et al., 2016; Li et al., 2011). Studies have also shown that implants with a wider diameter produced more desirable stress patterns across the bone and implant; specifically, when implant diameter was increased, the maximum stresses in both the bone and implant decreased (Ding, Liao, Zhu, Zhang, & Zhang, 2009; Eazhil et al., 2016; Himmlová et al., 2004; McNally et al., 2013).

To better predict the capacity of bone resorption and stress shielding in orthopaedic models, various studies have investigated the changes in strain energy density (SED) when a prosthetic is implanted into bone (Behrens et al., 2008; Gefen, 2002; Haase & Rouhi, 2013; Huiskes et al., 1987; Neuert & Dunning, 2013; Tissakht, Ahmed, & Chan, 1996; Van Lenthe, de Waal Malefijt, & Huiskes, 1997). Changes in SED can be measured across several bone sites using computational methods, such as finite element (FE) analysis, and can be used to predict which regions of bone are likely to resorb when the change in SED is less than the threshold value of 55% (Neuert & Dunning, 2013).

In view of the foregoing, the objective of this FE study was to determine changes in BIC, cortical and trabecular bone stresses, as well as the changes in cortical and trabecular SED from the intact state, when implant girth was increased within the proximal humerus using a traditional collared implant. It is hypothesized that the largest implant will result in the greatest amount of BIC, greatest changes in cortical and trabecular bone stress from the intact state, as well as the greatest changes in SED; thus, resulting in an increased in the percent volume of cortical and trabecular bone expected to resorb.

2.2 Methodology

2.2.1 Developing the 3D Model

Shoulder computed tomography (CT) scans, originally DICOM format, were obtained from a database of cadaveric shoulders (eight left arm males, mean ± SD of age = 67.8 ± 5.3) (Appendix B) and processed using Mimics (Materialise, Leuven, Belgium). A 3D solid model of the proximal humerus was created distinctly showing separate regions of cortical bone and trabecular bone (Figure 2-1). These regions were separated through the combined use of automatic threshold-based segmentation and manual identification of cortical/trabecular bone boundaries. Cortical bone was separated using an applied mask with threshold of 226 Houndsfield Units (HU) (Razfar, 2014; Willing, Lalone, Shannon, Johnson, & King, 2013), while trabecular bone mask was created with manual slice-by-slice segmentation. Following appropriate cortical/trabecular bone separation, the surface geometries were exported in STL format into SolidWorks (Dassault Systèmes, S.A. (Vélizy, France)) to further develop the solid model. Please see Appendix C for more detail. Once in SolidWorks, the length of the trabecular bone was selected to be 40 mm distally from the surface of the cut-plane (see next Section: 2.2.2 Bone Resection).

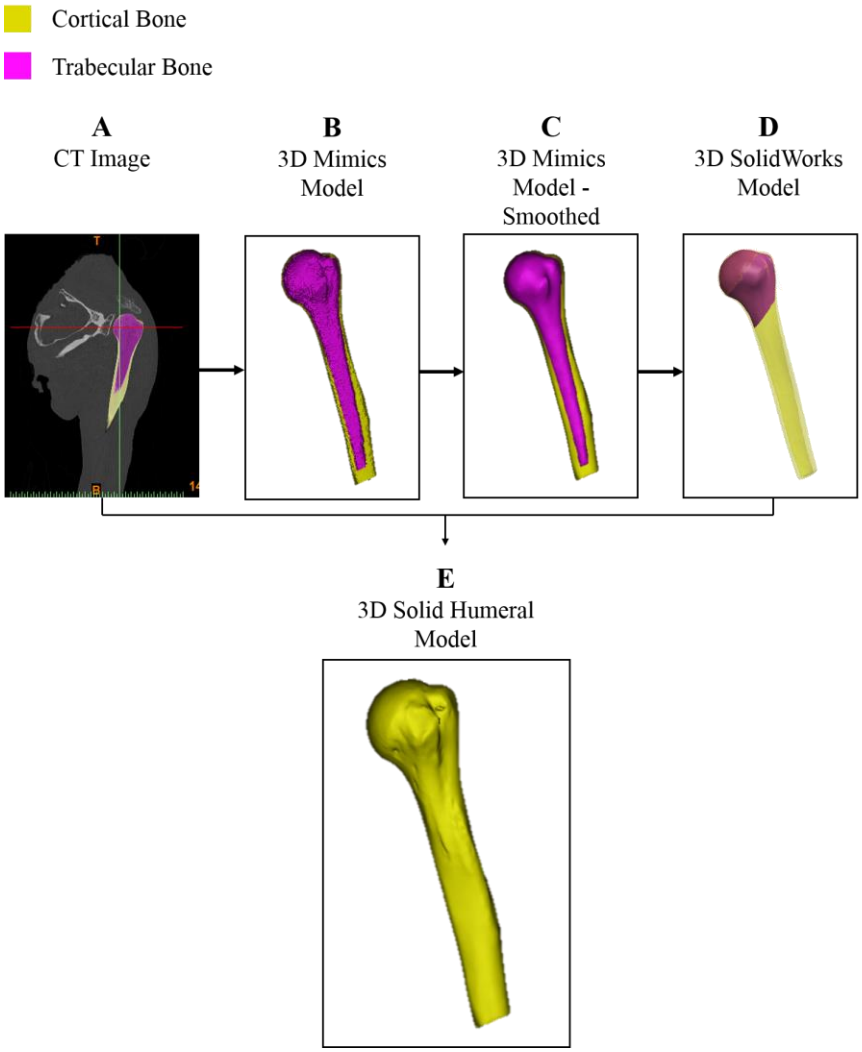

Figure 2-1: Development of 3D Humeral Model with Cortical and Trabecular Bone Regions from the CT Scan

Steps outlining the process to convert the CT image of the humerus to a smoothed 3D model in SolidWorks distinctly showing cortical and trabecular regions. Figure A shows the division of cortical and trabecular bone from the CT scan; Figure B shows the generation of the first 3D humeral model in Mimics with cortical and trabecular regions; Figure C shows the cortical and trabecular regions smoothed in Mimics, removing any sharp edges and pixilation; Figure D shows the 3D model exported into SolidWorks, where the length of the trabecular bone was shortened to 40 mm distally from the resection surface – see next section 2.2.2 Bone Resection*; Figure E shows the completed 3D solid humeral model in SolidWorks.*

2.2.2 Bone Resection

The 3D cortical and trabecular geometries were further sectioned into head and body components (Figure 2-2). To create the head component, a cut plane was created while under the supervision of an orthopaedic surgeon. This cut plane was also used as a reference plane to shorten the length of the trabecular bone to 40 mm distally from this surface (Figure 2-1; D).

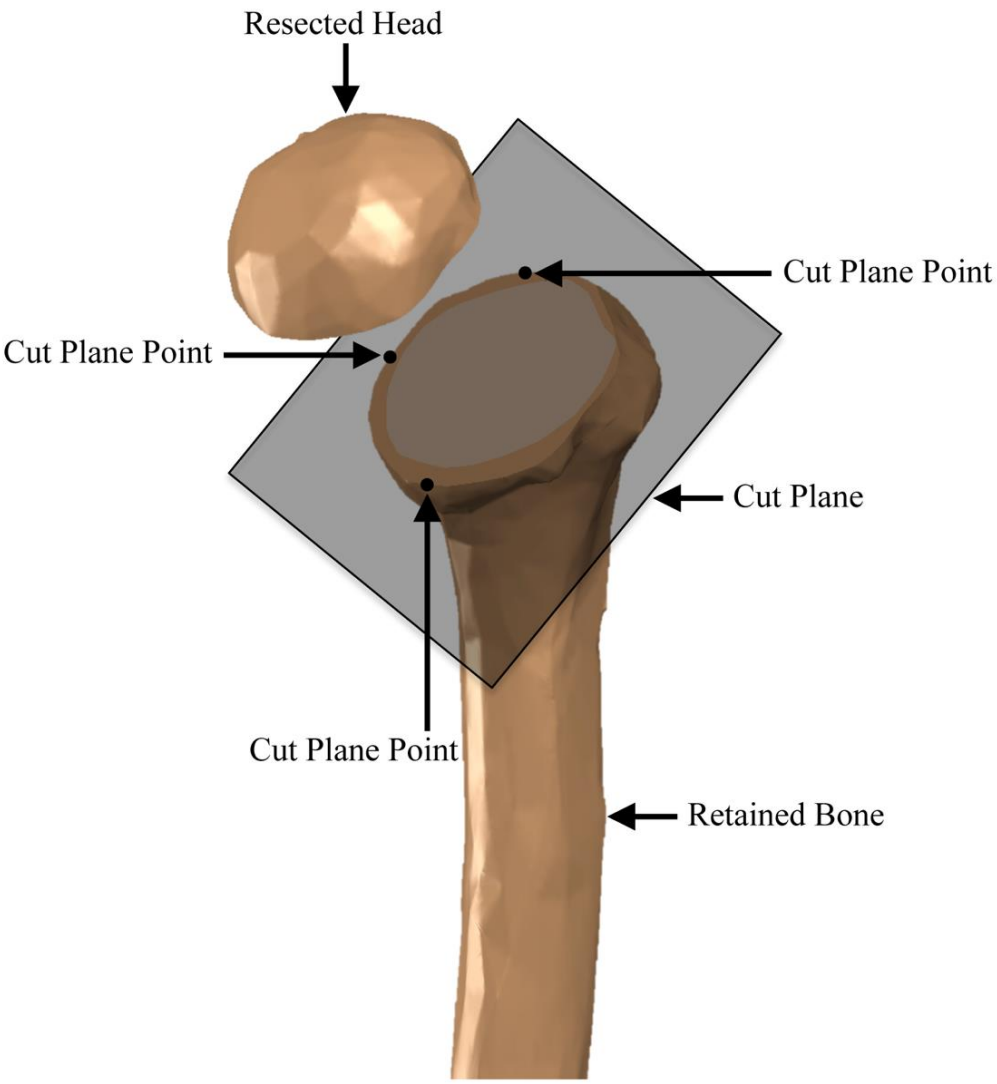

Figure 2-2: Resection of Humeral Head for Preparation of Implant Insertion (Razfar, 2014)

Superior, inferior, and medial points used to define the resection plane. Approval was obtained from an orthopaedic surgeon prior to humeral head resection. Resecting the humeral head matched the procedures conducted in clinical practice to prepare the humerus for insertion of the implant.

2.2.3 Implant Development

Three generic short stem implant models were created using SolidWorks CAD software. Implant dimensions were measured from three proximal humerus implants currently available in North America: Arthrex Univers™ Apex, Biomet Comprehensive® Mini Stem, Tornier Aequalis™ Ascend Flex (see Appendix D for details on implant measurements). Various dimensions of the three implants were averaged and used to create the generic implant model (distal stem diameter, d=12 mm). This base model was then scaled to create an implant with a smaller (d=8 mm) girth and a larger (16 mm) girth as directed by an orthopaedic surgeon (Figure 2-3). A stem length of 55 mm from the medial aspect was subjectively chosen by the surgeon to represent the length of newer clinical models. All measurements obtained from the current implant models were scaled from a known value, where measurements were then taken from a maximum stem length of 55 mm (only if the length of the stem, when scaled, exceeded this value – again, please see Appendix D).

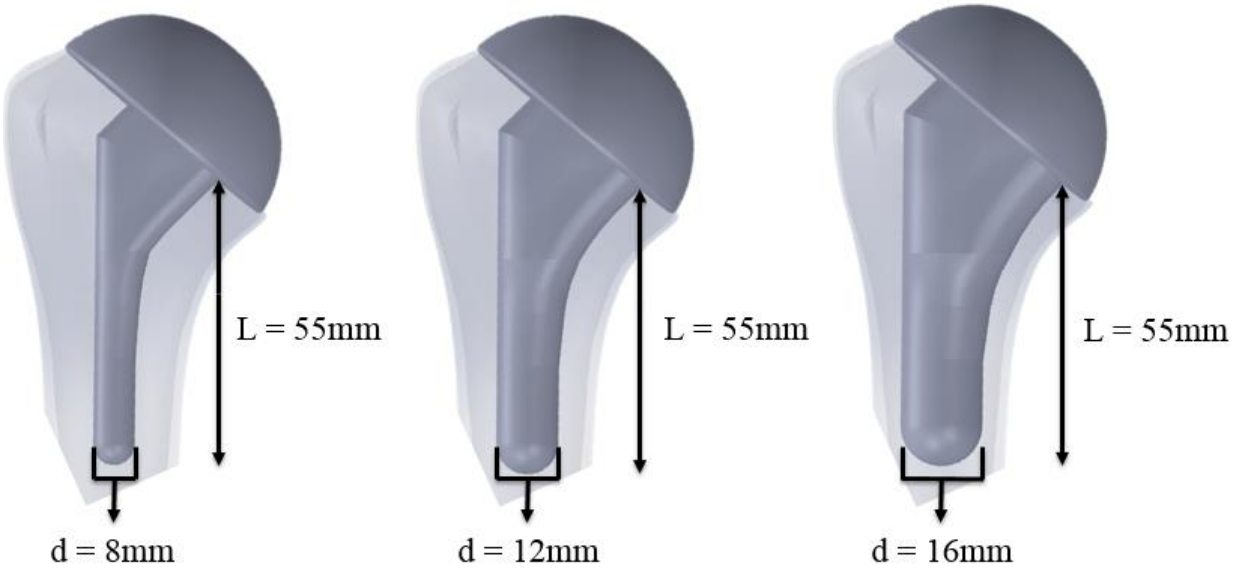

Figure 2-3: Generic Humeral Implant Models of Different Girths

One generic implant was designed from three currently available models (d=12 mm) and then scaled to create two other implants with a smaller (8 mm) and larger (16 mm) girth. The distal stem diameter represents the girth of the implant; meaning the small distal stem diameter represents the implant girth for d=8 mm, the medium distal stem diameter represents the implant girth for d=12 mm, and the large distal stem diameter represents the implant girth for d=16 mm.

Several head components were also created to ensure each patient obtained the appropriately sized implant head. Head geometry was created with an aspect ratio of 1.00:0.85 between the radius of the head and height of the head, respectively. These measurements, again, were obtained from head components currently used in practice.

2.2.4 Implant Positioning and Reference Geometry

Various reference geometries were created in SolidWorks to accurately align the implants into bone and recreate surgical placement (Figure 2-4). Two reference sites were created for the bone geometry: a central canal axis down the diaphysis, “Bone Axis”, and a plane on the cut surface, “Resection Surface Plane”. For the implant reference locations, each implant was given a central stem axis, “Implant Axis” as well as a coincident axis centered along the anterior-posterior face, “Anterior-Posterior Face Axis”. Several mates were then applied to ensure the implants were strictly confined in the bone. Bone and Implant Axes were made coincident and the Resection Surface Plane was made parallel to the Anterior-Posterior Face Axis. Lastly, the appropriate head diameter was selected for each specimen. The backside of the humeral head was made coincident with the plane on the cut surface and was appropriately positioned, once again, by an orthopaedic surgeon. Finally, the humeral head component was combined with the stem of the implant to simulate a mobile head. This current study assumed ideal alignment conditions, which may not precisely replicate the results routinely obtained clinically. To investigate the importance of alignment, a companion study was conducted that modeled a medially tilted “misaligned” implant. The distal tip of the largest implant girth was tilted such that it just contacted the lateral edge of the cortical bone. The same outcome variables defined in Section 2.2.6 (Outcome Measures) were investigated. The results of this investigation are summarized and briefly discussed in Appendix E.

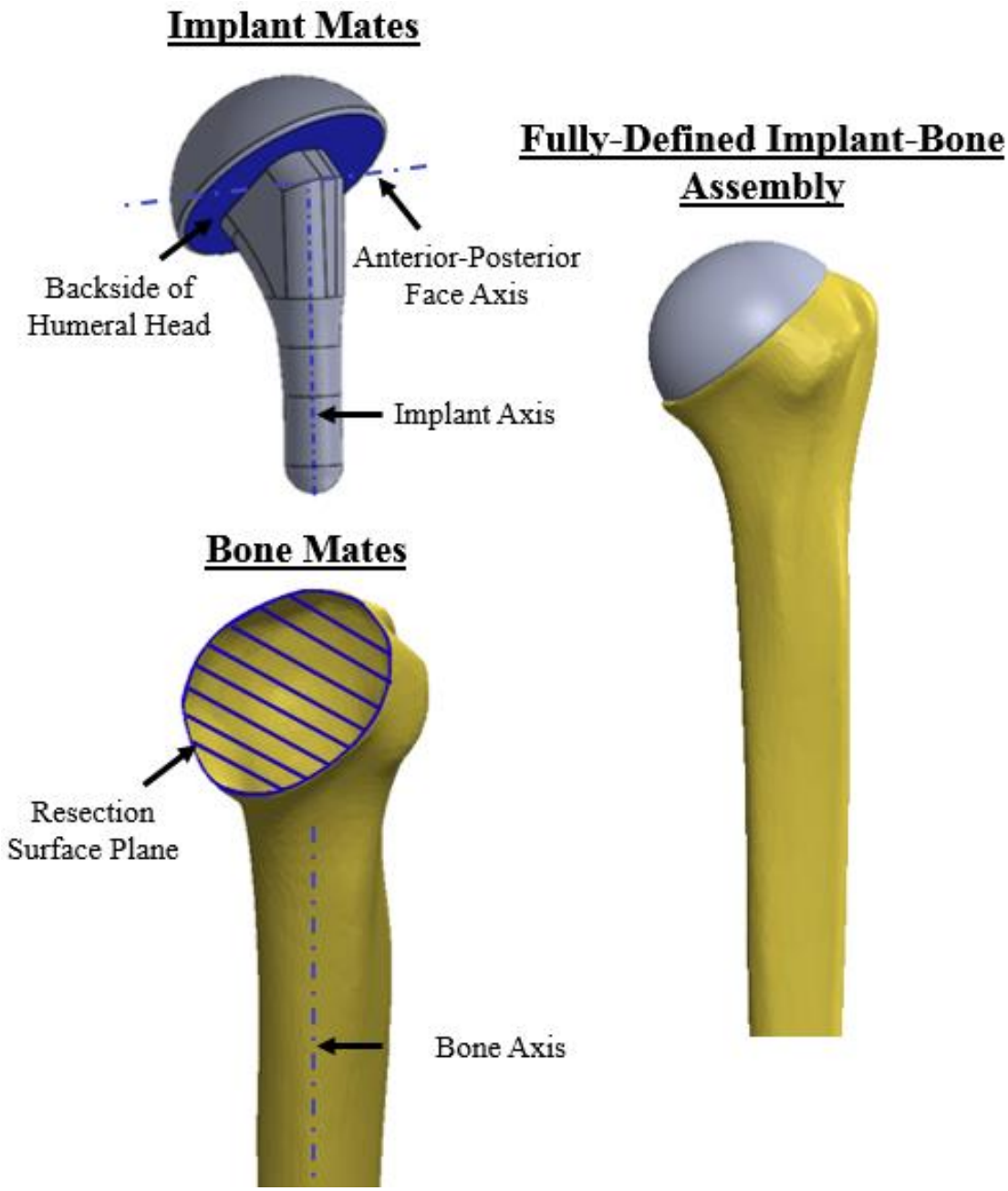

Figure 2-4: Mating Geometry for Implant and Bone

Mating surfaces and axes were created on both the implant and bone to create a fully defined implant-bone assembly. Bone Axis and Implant Axis were made coincident, Resection Surface Plane and Anterior-Posterior Face Axis were made parallel, and the Backside of the Humeral Head was made coincident to the Resection Surface Plane.

2.2.5 Creating the FE Model

Several steps were taken to create the FE model. The details of each step can be found in the following sections: mesh preparation, material properties, model assembly, and abduction angles and model fixation.

2.2.5.1 Mesh Preparation

Following implant alignment, all bone and implant geometries were exported from SolidWorks to Abaqus v6.14 (Dessault Systèmes simulia Crop., Providence, RI, USA) in STEP AP214 or ASIC format. To allow for comparison between the implanted and native state, identical meshes were required for each specimen model. For each humeral implant stem investigated, partitions were created by cutting and reaming the trabecular bone with the desired implant size (Figure 2-5). These partitions, along with the head components resected in SolidWorks (cortical and trabecular head components), were assembled and merged together maintaining the geometrical lines of the implant allowing for identical mesh generation. Thus, the intact and reconstructed state resulted in identical humeral geometries allowing for direct element-to-element comparison of changes in bone stress (Neuert & Dunning, 2013). Bone and implant were then meshed with quadratic tetrahedral elements with a maximum edge length of 2 mm and maximum deviation factor of 0.06 mm (Razfar, 2014). The number of nodes and elements for the bone region affected by insertion of the implant (*i.e.,* cortical and trabecular bone region below the resection surface) generated for the intact and reconstructed model can be found in Table 2-1**.**

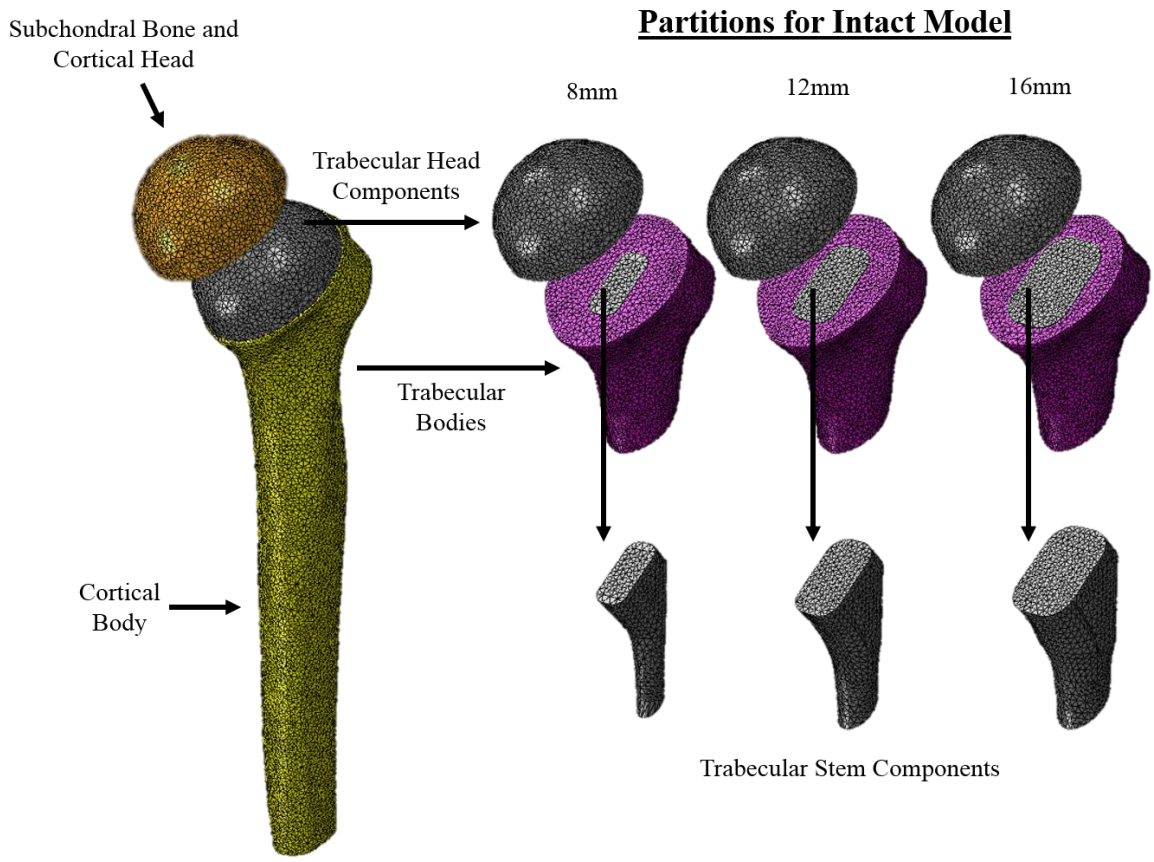

Figure 2-5: Partitions of the Intact Model for Identical Mesh Generation to the Reconstructed Model

Specific boundaries at the cut plane and proximal portion of the three sized implants were created within cortical and trabecular bone to allow for identical meshes generation between models. The trabecular head components in the intact model represent the humeral heads of the implants in the reconstructed model and the trabecular stem components in the intact model represent the region of trabecular bone that the implants engage with in the reconstructed model.

Table 2-1: Number of Nodes and Elements for the Intact and Reconstructed Models

Number of nodes and elements for all three implant sizes for both the intact and reconstructed models. Note that the number of nodes and elements are identical between intact and reconstructed models to ensure direct element-to-element comparison (N.B. For the intact model the number of nodes and elements only accounts for the region below the cut surface unoccupied by the implant).

Specimen Number	Number of Nodes (x 10^3)						Number of Elements (x$10^{3)}$					
	Model Type and Implant Size (diameter, mm)						Model Type and Implant Size (diameter, mm)					
	Intact			Reconstructed			Intact			Reconstructed		
	8	12	16	8	12	16	8	12	16	8	12	16
1	193.3	192.0	175.1	193.3	192.0	175.1	128.1	126.6	114.2	128.1	126.6	114.2
2	204.9	197.6	182.0	204.9	197.6	182.0	139.3	133.7	122.0	139.3	133.7	122.0
3	188.4	184.5	169.1	188.4	184.5	169.1	126.6	123.4	112.0	126.6	123.4	112.0
4	189.7	179.6	167.3	189.7	179.6	167.3	126.3	118.6	109.2	126.3	118.6	109.2
5	165.6	159.2	144.8	165.6	159.2	144.8	110.8	105.7	95.0	110.8	105.7	95.0
6	195.0	186.6	169.8	195.0	186.6	169.8	131.6	125.0	112.5	131.6	125.0	112.5
7	190.3	184.2	167.2	190.3	184.2	167.2	128.7	123.9	111.3	128.7	123.9	111.3
8	201.3	190.7	175.8	201.3	190.7	175.8	135.4	127.5	116.3	135.4	127.5	116.3

2.2.5.2 Material Property Assignment

Cortical bone was assigned material properties with a uniform elastic modulus of E=20 GPa and Poisson's Ratio of v=0.3 (Razfar, 2014). Trabecular bone, being an inhomogeneous structure with non-uniform properties, was assigned varying material properties based on CT attenuation. Properties were applied using the density-modulus equation reported by Morgan *et al.* (2003):

$$E = 8920 * \rho_{app}^{1.83} \qquad \text{Equation 2.1}$$

where, E is Young's modulus and ρ_{app} is the apparent density of bone.

To calculate apparent density, cadaveric CT scans were imported into Mimics, where a linear relationship was applied based on two substances of known densities placed within the scan: SB3 cortical bone (Gammex, Middleton WI; ρ=1.82 g/cm^3) and water (ρ=1.00 g/cm^3). From this, variations in density across the CT scan could be derived and determined for trabecular bone. Poisson's ratio was also set to 0.3 for trabecular bone (Razfar, 2014).

Implant models were all assigned Titanium material properties (E=110 GPa, v=0.3) with the same site-specific frictional characteristics (Figure 2-6). The under surface of the humeral heads and the distal tips of the humeral stems, where the stem became completely cylindrical, were polished (μ=0.40), and the proximal and middle region of the humeral stems were plasma sprayed (μ=0.88). Application of these frictional properties was applied to be relatively consistent with the clinical implants that the generic implants were modeled from.

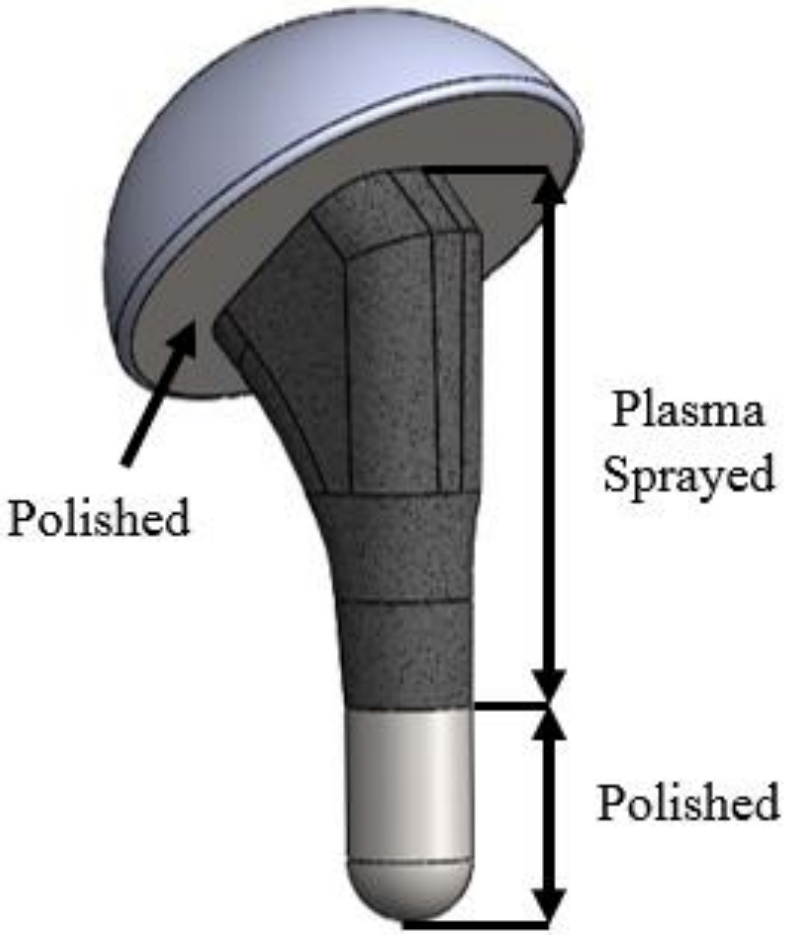

Figure 2-6: Implant Surface Textures

All implants were made using Titanium with different regions of surface textures: polished on the underside of humeral head and at the fully cylindrical tip and plasma sprayed in the metaphyseal middle region.

2.2.5.3 Model Assembly

Bone and implant components were assembled in Abaqus to create 14 finite element models (1 intact model + 3 reconstructed models [3 implant girth sizes] x 2 abduction angles/load directions (Figure 2-7)) for each of the 8 specimens used, totaling 64 models.

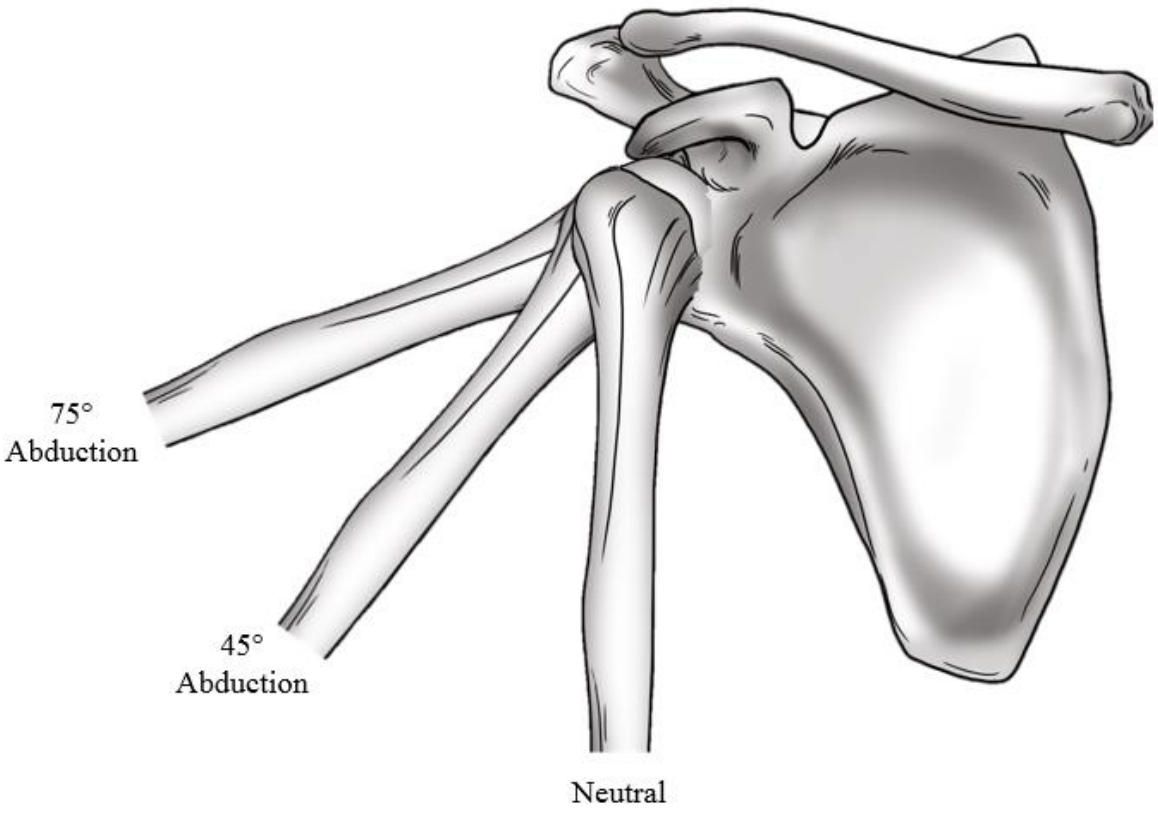

Figure 2-7: Shoulder Abduction Angles

Two abduction states investigated for this FE model that coincide with daily motion of the shoulder. The angle of arm abduction does not represent the true direction of load applied to the articular surface; the exact location of the load/joint reaction force that corresponds to the specific abduction angles investigated can be found in Table 2-2.

2.2.5.4 Abduction Angles and Model Fixation

For this experiment, two load directions were investigated that correspond to arm abduction angles of 45° and 75° (Figure 2-7). Joint reaction forces derived from telemeterized shoulder implant data, assuming 50^{th} percentile male body weight of 88.3kg, were applied at along the articular surface towards the humeral center of rotation with magnitude of 440N and 740N for 45° and 75°, respectively (Bergmann et al., 2007; McDowell, Fryar, Ogden, & Flegal, 2008). The direction of joint reaction forces, along with the associated magnitude of force, can be found in Table 2-2. To complete the development of the FE models, the distal ends of the humeri were rigidly fixed to restrict the model in space.

Table 2-2: Joint Reaction Force Components (Bergmann et al., 2007; McDowell et al., 2008)

	Components of Joint Reaction Force [N]*			
Abduction Angle	**Superior-Inferior**	**Anterior-Posterior**	**Medial-Lateral**	**Resultant**
45˚	44	-21	16	440
75˚	74	-34	25	740

*Joint reaction force broken into superior-inferior, anterior-posterior, and medial-lateral position assuming 50th percentile male body weight of 88.3kg. *Data was obtained from Bergmann et al. (2007) and converted to Newtons.*

2.2.6 Outcome Measures

Upon implantation, several changes occur to the surrounding bone. Osseointegration may begin to occur depending on the amount and quality of BIC, which is a key component required to gain fixation of the implant and prevent loosening (Goriainov, Cook, Latham, Dunlop, & Oreffo, 2014; Mueller, Basler, Müller, & Van Lenthe, 2013). Remodeling of the bone will also occur and may cause stress shielding if the bone is underloaded compared to native loading state (Wolff *et al.,* 1986). This may lead to a weaker bone structure, potentially leading to implant loosening and in some extreme cases implant failure (Collin et al., 2017; Keener et al., 2017). Following shoulder replacement surgery, the amount of BIC, changes in proximal bone stresses from the intact state to the reconstructed state, and changes in SED (used to determine risk of stress shielding) were determined from the FE simulations. Site-specific averaged values were obtained by dividing the proximal humerus into eight 5 mm thick slices parallel to the resection surface (Figure 2-8). An element was considered to be in a given slice if the centroid of that element fell within the region of that slice.

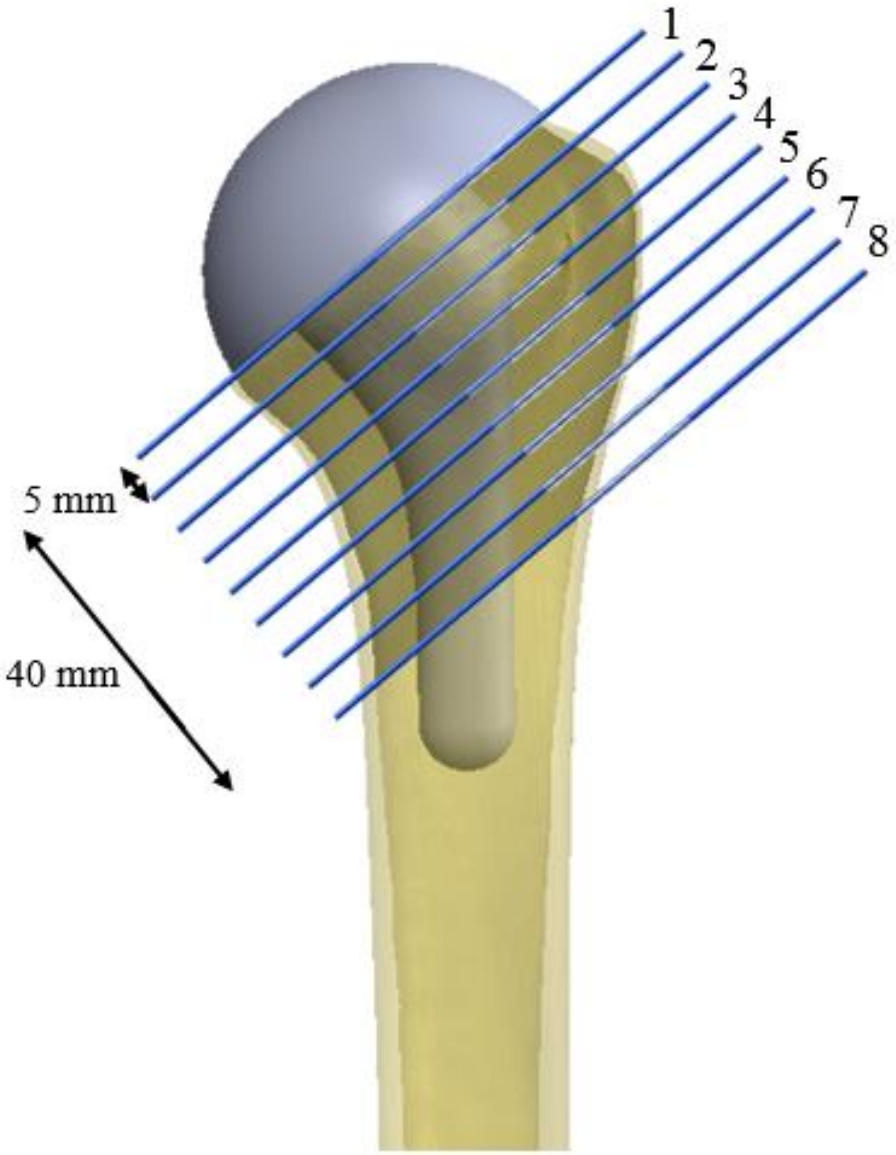

Figure 2-8: Cortical and Trabecular Bone Slices

Cortical and trabecular bone were divided into 8 equal 5 mm slices parallel to the resection surface to determine proximal bone stresses and capacity of bone resorption.

2.2.6.1 Degree of BIC

The degree of BIC was calculated using a custom-built LabVIEW (National Instruments, Austin, Texas, USA) code by determining the functional contact area (*i.e.*, contact pressure > 0, where load is being distributed between implant and bone) between the surface elements of the implant to the surrounding bone. If the surface area (SA) of an element of interest on the implant had a contact pressure greater than zero, it was considered in contact with the bone. The SA of all the elements on the surface of the implant that exhibited a functional contact pressure were summed and then divided by the total SA of the implant surface elements in the slice of interest to obtain the percentage of BIC (Equation 2.2).

$$BIC\ (\%) = \frac{A_{Contact\ Pressure>0}}{A_{Total}} * 100\% \qquad \text{(Equation 2.2)}$$

2.2.6.2 Change in Proximal Bone Stress

Changes in stress between the two states (*i.e.*, reconstructed and intact states) were calculated on an element-by-element basis for both cortical and trabecular bone using a custom code designed in LabVIEW. The six stress components (3 normal and 3 sheer) were obtained for each element in the reconstructed and intact states and then subtracted from one another (Equation 2.3) to obtain the Von Mises of the change in stress for each element (Equation 2.4).

$$\Delta\sigma_{ij} = \Delta\sigma_{ij\ RECONSTRUCTED} - \Delta\sigma_{ij\ INTACT} \qquad \text{(Equation 2.3)}$$

where *i* and *j* represent the 3D stress components.

$$\Delta\sigma_{VM} = \sqrt{0.5 * \left((\Delta\sigma_{11} - \Delta\sigma_{22)}{}^2 + (\Delta\sigma_{22} - \Delta\sigma_{33)}{}^2 + (\Delta\sigma_{11} - \Delta\sigma_{33})^2 + 6 * \left(\Delta\sigma_{12}{}^2 + \Delta\sigma_{23}{}^2 + \Delta\sigma_{13}{}^2\right)\right)}$$

(Equation 2.4)

where, $\Delta\sigma_{VM}$ represents the change in Von Mises stress. $\Delta\sigma_{11}$, $\Delta\sigma_{22}$, $\Delta\sigma_{33}$ represent the changes in normal stress between the reconstructed and intact states in the x, y, and z

directions, respectively, and $\Delta\sigma_{12}$, $\Delta\sigma_{23}$, $\Delta\sigma_{13}$ represent the changes in shear stress between the reconstructed and intact states along the x-y plane, x-z plane, and y-z plane, respectively (Figure 2-9).

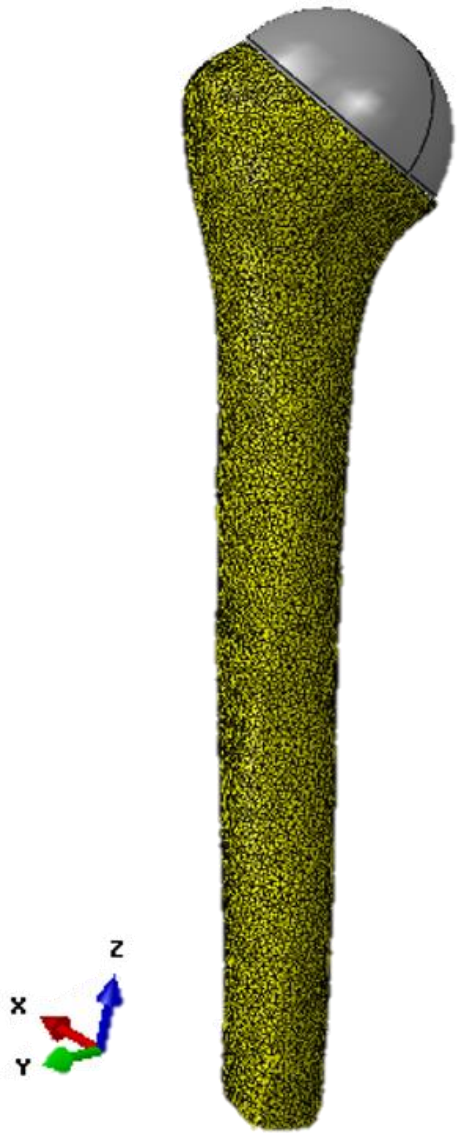

Figure 2-9: Coordinate System for Directional Stress and Strain Values for

*For changes in bone stress, the normal stresses, $\Delta\sigma_{11}$, $\Delta\sigma_{22}$, $\Delta\sigma_{33}$ occur along the x, y, and z directions, respectively; whereas the shear stresses occur along the x-y, y-z and x-z planes for $\Delta\sigma_{12}$, $\Delta\sigma_{23}$, $\Delta\sigma_{13}$ respectively. For changes in SED, $\varepsilon_{11}, \varepsilon_{22,}\ \varepsilon_{33}, \varepsilon_{12}, \varepsilon_{23}, \varepsilon_{13}$ characterize the strain values obtained from the x, y, z directions and the x-y, y-z, and x-z planes, respectively $\Delta\sigma_{11}$, $\Delta\sigma_{22}$, $\Delta\sigma_{33}$,$\Delta\sigma_{12}$,$\Delta\sigma_{23}$, $\Delta\sigma_{13}$ represent the stress in the x, y, z directions and the x-y, x-z, and y-z planes, respectively. *Important note: this is not a universal coordinate system. Coordinate system changes depending on the FE model developed for each specimen.*

For the slice of interest, the change in Von Mises stress between the two states was volume weighted, meaning that if the volume of 1 element represented 1% of the total volume in the slice of interest, the change in stress from the intact to reconstructed state, within that element, only accounted for 1% of the total change of the whole slice (Equation 2.5). The volume weighted average of the stress from the intact state when loaded was also calculated (Equation 2.6) to determine the overall percent change in stress from the intact state for the slice of interest (Equation 2.7).

$$\Delta\sigma_{VM}=\frac{\sum_{i=1}^{n}\sigma_{VM_i}*Volume_{Reconstructed\ Element}}{\sum_{i=1}^{n}Volume_i} \quad \text{(Equation 2.5)}$$

$$\sigma_{VM\ Intact}=\frac{\sum_{i=1}^{n}\sigma_{VM_i}*Volume_{Reconstructed\ Element}}{\sum_{i=1}^{n}Volume_i} \quad \text{(Equation 2.6)}$$

$$\%\Delta\sigma=\frac{\Delta\sigma_{VM}}{\sigma_{VM\ Intact}}*100\% \quad \text{(Equation 2.7)}$$

2.2.6.3 Change in SED

To determine the risk of bone remodeling and volume of bone expected to resorb, the SED for each element was calculated in the reconstructed and intact states upon loading, using a custom code designed in LabVIEW. For linear isotropic materials, SED can be calculated using Equation 2.8.

$$SED=\frac{((\varepsilon_{11}*\sigma_{11})+(\varepsilon_{22}*\sigma_{22})+(\varepsilon_{33}*\sigma_{33})+(\varepsilon_{12}*\sigma_{12})+(\varepsilon_{13}*\sigma_{13})+(\varepsilon_{23}*\sigma_{23}))}{2} \quad \text{(Equation 2.8)}$$

where, $\varepsilon_{11}, \varepsilon_{22,}\ \varepsilon_{33}, \varepsilon_{12}, \varepsilon_{23}, \varepsilon_{13}$ represent the strain in the x, y, z directions and the x-y, y-z, and x-z planes respectively and $\Delta\sigma_{11},\ \Delta\sigma_{22},\ \Delta\sigma_{33}$ characterize the stress in the x, y, z directions and the x-y, x-z, and y-z planes respectively (Figure 2-9).

The capacity of bone resorption was determined using a threshold value of change in SED of 55%, where bone would be expected to remodel and become stronger, remain the same, or resorb if the change in SED was greater than, equal to, or less than this threshold value, respectively (Neuert & Dunning, 2013) (Equation 2.9). Each element in the slice of interest was placed into one of these three categories depending on its

change in SED. To determine the overall percent volume of bone expected to resorb, the volume of the elements that exhibited change in SED less than the 55% threshold were divided by the sum of the total volume of the elements in all categories.

$$Remodel: U_{Reconstructed} > 1.55U_{Intact} \quad \text{(Equation 2.9)}$$

$$Remain\ the\ Same: 0.45U_{Intact} \leq U_{Reconstructed} \leq 1.55U_{Intact}$$

$$Resorb: U_{Reconstructed} < 0.45U_{Intact}$$

2.2.6.4 Statistical Analysis

All three outcome measures were assessed for statistical significance (α=0.05) using a three-way repeated measures (RM) ANOVA (abduction angle, slice depth, and implant girth) using SPSS (IBM, New York, USA). As previously documented, the abduction angles investigated, 45° or 75°, were used to represent the direction of corresponding load to the articular surface (Table 2-2). Independent variables for the three tests were examined for sphericity and in the event sphericity was rejected, the Greenhouse-Geisser correction was applied.

2.3 Results

Sixty-four finite element models were created to determine the changes in BIC, proximal bone stresses, and strain energy densities between an intact humeral model and three reconstructed states (distal stem diameters/implant girth sizes: 8 mm, 12 mm, and 16 mm). Changes in BIC, bone stress, and SED, which is used to determine the capacity of bone resorption, were examined in eight equal slices for both cortical and trabecular bone and are presented in the following sections. Results are presented in terms of abduction angle, which is associated with the direction of load outlined in Table 2-2 for that specific angle.

2.3.1 Effect of Implant Girth on BIC

When the three implants were implanted into the proximal humerus, implant size (45°: $p=0.080$, power=0.431; 75° $p=0.076$, power=0.444) did not significantly affect the degree of BIC (Equation 2.2), but the slice depth did have a statistically significant effect on the BIC ($p<0.001$, power=1.0 for both abduction angles) (Figure 1-10). At 45° of abduction and for all slice depths investigated (Figure 2-10), increasing implant girth from small (S) to medium (M) decreased the overall degree of BIC by 0.9 ± 0.3% ($p=0.3$) and increasing implant size from M to large (L) decreased the average degree of contact by 5.6 ± 1.1% ($p=0.07$). Examining each slice depth individually, the implant that resulted in the greatest amount of contact changed depending on slice. The S implant produced the greatest amount of contact in the first 4 slices, the M produced the most contact in slices 5-7, and the L produced the greatest amount of contact in the most distal slice (Figure 2-10. Statistically significant changes in degree of contact were only observed in the first four slices. Increasing implant size from S to M, S to L, and M to L significantly decreased the implant to bone contact in slices 3-4 ($p\leq0.04$), 1 – 3 ($p\leq0.05$), and 2 – 3 ($p\leq0.003$) respectively. When the arm was abducted 75° (Figure 2-10), increasing implant size from S to M decreased the overall degree of contact by 1.0 ± 0.3% ($p=0.3$) and increasing implant size from M to L also decreased the overall degree of contact by 6.0 ± 1.1% ($p=0.1$) for all slice depths explored. Similar to 45° of abduction, the smallest implant size produced the greatest amount of contact than the M and L implants in the first 4 slices, with the M implant producing the greatest amount of contact, again, in

slices 5-7 and the L implant in slice 8. Statistically significant decreases in degree of contact were seen when increasing the implant size from S to M ($p \leq 0.05$) in slices 1 and 4, S to L ($p \leq 0.04$) in slices 1-3, and from M to L ($p \leq 0.004$) in slices 2 and 3.

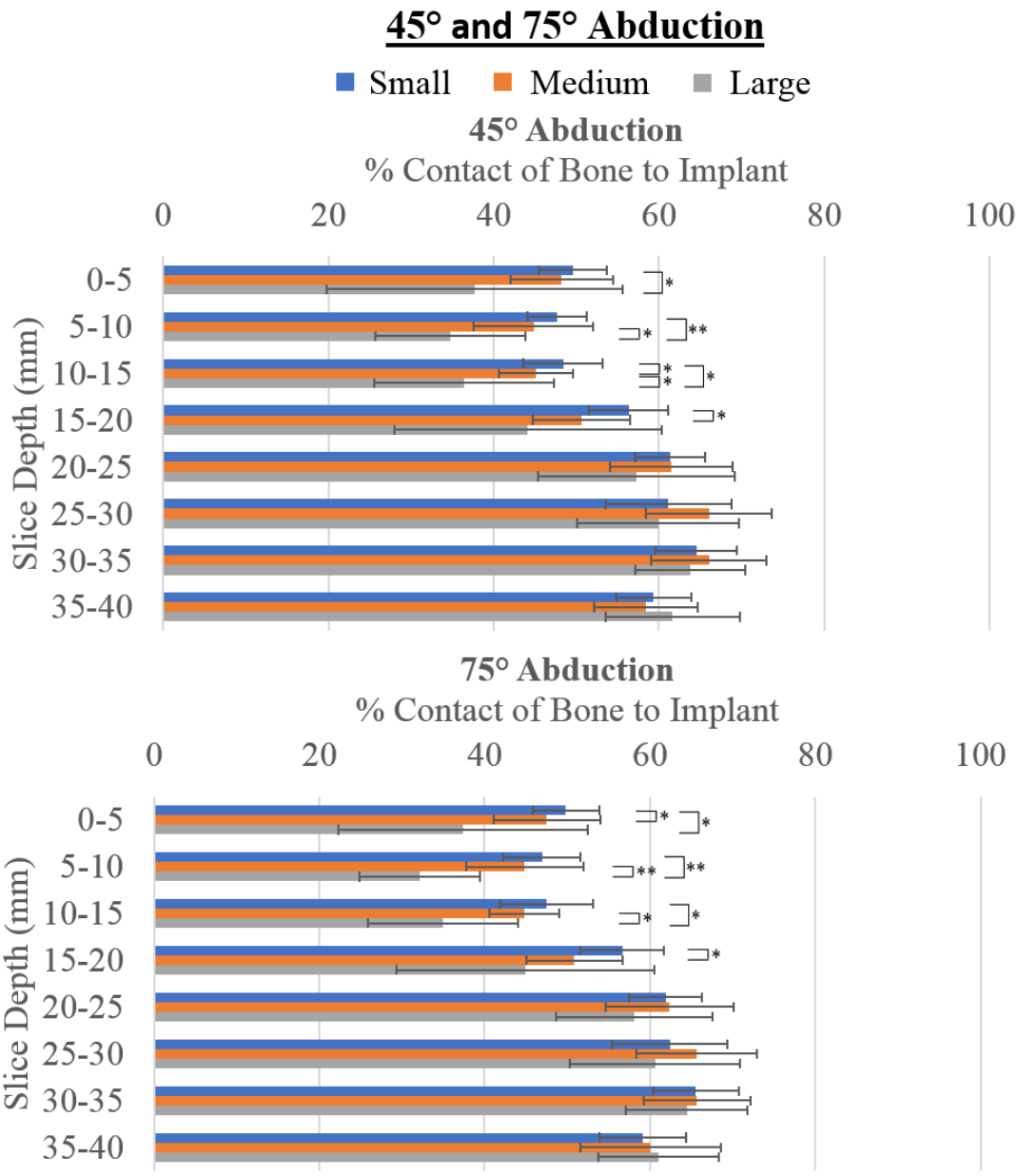

Figure 2-10: Contact of Bone with Implant at 45° and 75° Abduction (%) when Implant Girth was Increased

*The percentage of BIC (±1 SD) is shown as implant girth is changed. The degree of BIC was obtained in 8 equal 5 mm slices distal to the cut surface. Statistically significant difference is expressed with *p≤0.05 and **p≤0.001.*

2.3.2 Effect of Implant Girth on Proximal Bone Stress

Several statistically significant changes in bone stress (Equation 2.7: $\%\Delta\sigma$) were found throughout the 8 slices for cortical and trabecular bone when the articular loads were applied with their corresponding abduction angles of 45° and 75° (Figure 2-11 and Figure 2-12). The results are divided into the following sections: change in cortical bone stress and change in trabecular bone stress.

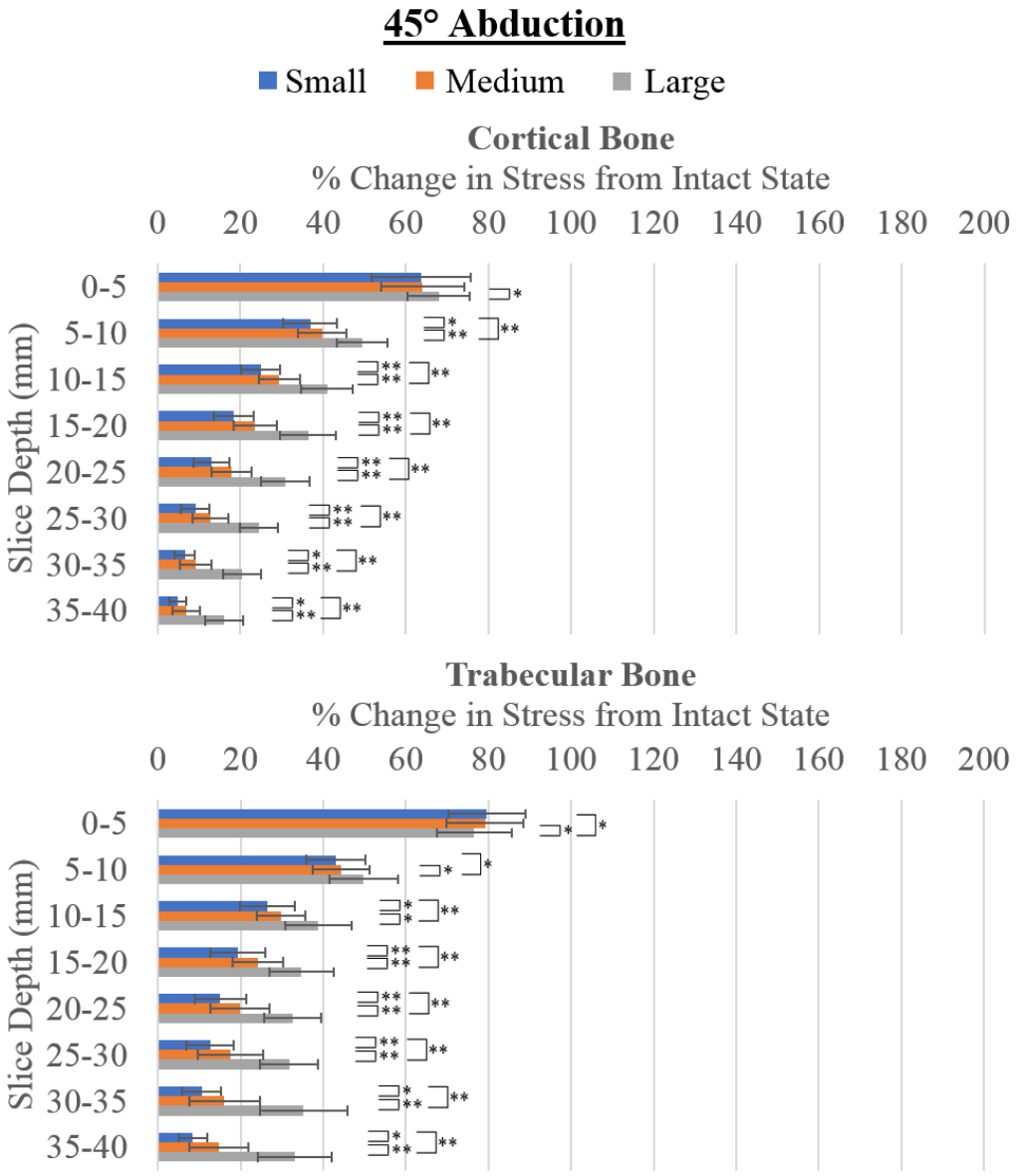

Figure 2-11: Changes in Proximal Bone Stress when Implant Girth was Increased at 45° Abduction

*The percent change (±1 SD) in proximal bone stresses from the intact to the reconstructed states when the shoulder was abducted 45° for cortical and trabecular bone. Changes in bone stress were obtained in 8 equal 5 mm slices distal to the cut surface. Statistically significant difference is expressed with *p≤0.05 and **p≤0.001 (N.B. The more favourable outcome for this variable is to the far left of the graph with 0% change in stress from the intact state being most desirable).*

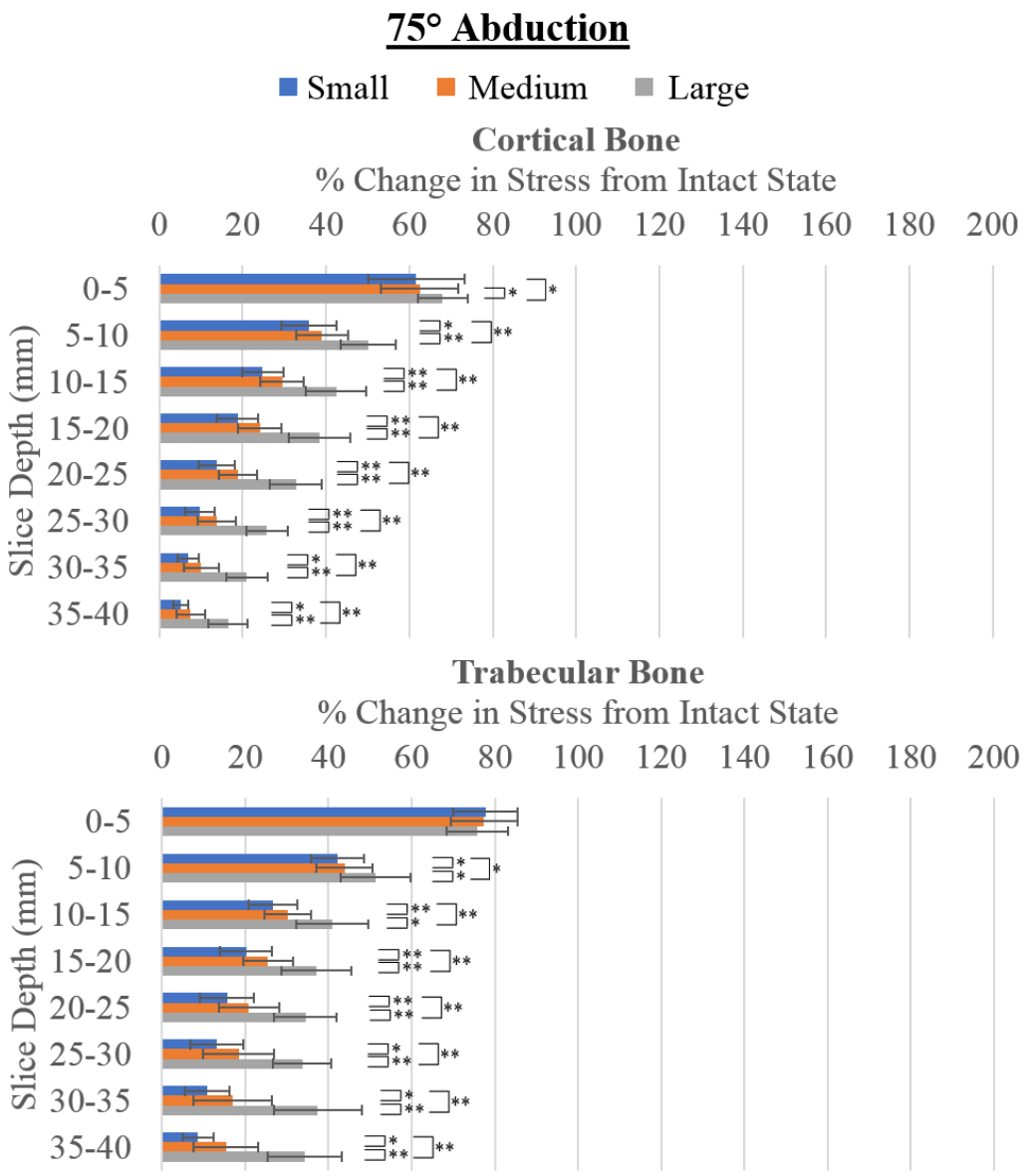

Figure 2-12: Changes in Proximal Bone Stress when Implant Girth was Increased at 75° Abduction

*The percent change (±1 SD) in proximal bone stresses from the intact to the reconstructed states when the shoulder was abducted 75° for cortical and trabecular bone. Changes in bone stress were obtained in 8 equal 5 mm slices distal to the cut surface. Statistically significant difference is expressed with *p≤0.05 and **p≤0.001 (N.B. The more favourable outcome for this variable is to the far left of the graph with 0% change in stress from the intact state being most desirable).*

2.3.2.1 Change in Cortical Bone Stress

At abduction angles of 45° and 75°, both implant size ($p<0.001$, power=1.0) and slice depth ($p<0.001$, power=1.0) had statistically significant effects on change in cortical bone stress compared to the intact state (Figure 2-11 and Figure 2-12). At 45° of abduction and for all slices depths investigated, increasing implant size from S to M increased the average change in bone stress by 3.2 ± 0.2% ($p=0.002$) and increasing the implant size from M to L increased the average change in bone stress by 10.4 ± 0.6% ($p<0.001$). The S size implant consistently produced the smallest changes in stress compared to the intact state, then both the M and L sizes for all slices. Statistically significant change in bone stress were seen in all slices, except the most proximal, when increasing implant size from S to M ($p\leq0.03$), S to L ($p\leq0.001$) and M to L ($p\leq0.02$). For the most proximal slice, no statistically significant differences were detected between the S and M ($p=0.7$) and the S and L ($p=0.06$) implants. Similar results were observed when the arm was abducted 75°. Increasing implant size from S to M increased the overall change in bone stress by 3.6 ± 0.2% ($p=0.001$) and increasing implant size from M to L increased the overall change in bone stress by 11.2 ± 0.6% ($p<0.001$) for all slice depths. The S implant size was again, consistent at producing the smallest changes in bone stress compared to the M and L sizes in all slices. All slices, except the most proximal slice, showed statistically significant changes in bone stress when increasing implant size (S-M $p\leq0.002$; S-L $p\leq0.03$; M-L $p\leq0.007$). In the most proximal slice, no significant changes in cortical bone stress were seen when increasing the implant size from S to M ($p=0.4$).

2.3.2.1.1 Change in Trabecular Bone Stress

Statistically significant changes in trabecular bone stress when compared to the intact state were observed at abduction angles of 45° and 75° for both implant size ($p<0.001$, power=1.0) and slice depth ($p<0.001$, power=1.0) (Figure 2-11 and Figure 2-12). For all slice depths investigated at 45° abduction, increasing implant size caused bone stresses to increase by an average of 3.8 ± 2% ($p<0.001$) and 10.9 ± 0.6% ($p<0.001$) for the S to M and M to L implants, respectively. Surprisingly, in the most proximal slice, the largest implant produced the smallest percent change in bone stress compared to the S and M sizes; slices 2 through 8 showed the smallest implant produced the least amount of

change compared to the M and L sizes. All slices, except slice 1 and 2, presented statistically significant changes in bone stress when increasing implant size from S to M ($p \leq 0.009$), S to L ($p \leq 0.02$), and M to L ($p \leq 0.01$). Statistically significant changes were not found in slices 1 ($p=0.4$) and 2 ($p=0.06$) when increasing the size of the implant from S to M only. Average changes in bone stress for all slices when the arm was abducted 75° increased by 4.2 ± 0.2% ($p<0.001$) and 12.0 ± 0.6% ($p<0.001$) for the S to M and M to L implant sizes, respectively. The smallest implant size resulted in the smallest percent change in bone stress for all slices, except for the most proximal slice, where the largest implant was found to more closely represented the intact state. Results showed that all slices displayed statistically significant changes in bone stress with an increase in implant size (S-M: $p \leq 0.04$; S-L: $p \leq 0.003$; M-L: $p \leq 0.002$), except for the most proximal slice where increasing implant size was not significant between all sizes ($p \geq 0.08$).

2.3.3 Effect of Implant Girth on the Risk of Bone Resorption

Several significant changes in SED were found throughout the 8 slices when increasing implant size in both cortical and trabecular bone when the arm was abducted 45° and 75° (Figure 2-13 and Figure 2-14). The results are divided into the following sections: cortical bone resorption and trabecular bone resorption. The change in SED is directly related to the risk of bone resorption; thus, results are presented in terms of percent volume expected to resorb as the change in SED was determined for the total volume of elements within a given slice.

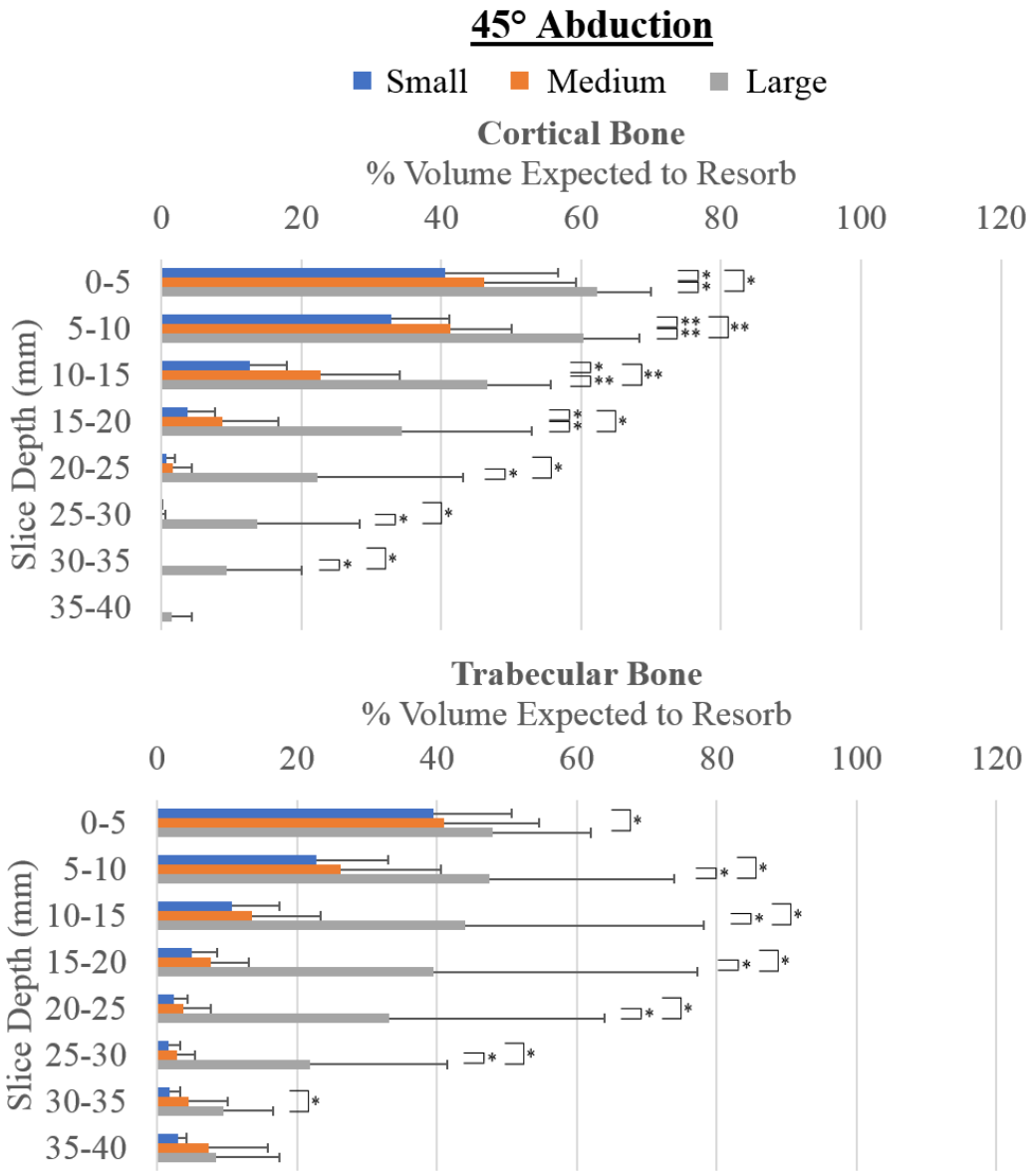

Figure 2-13: Changes in Percent Volume of Bone Expected to Resorb when Implant Girth was Increased at 45° Abduction

*The percent volume (+1 SD) of cortical and trabecular bone expected to resorb due to increasing implant girth when the shoulder was abducted 45°. Changes were observed in 8 equal 5 mm slices distal to the cut surface. Statistically significant difference is expressed with *p≤0.05 and **p≤0.001 (N.B. The more favourable outcome for this variable is to the far left of the graph with 0% volume expected to resorb being most desirable).*

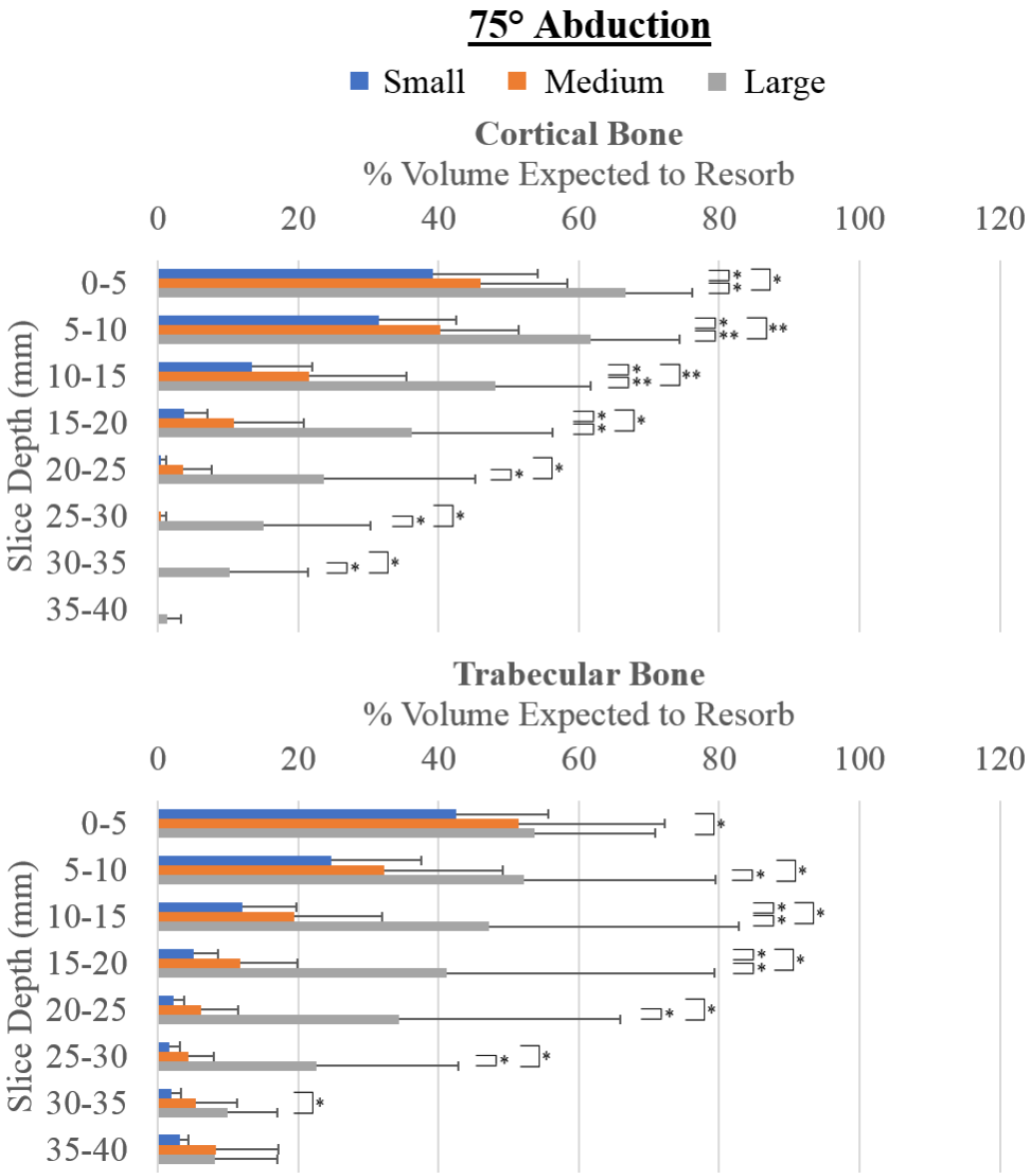

Figure 2-14: Changes in Percent Volume of Bone Expected to when Implant Girth was Increased at 75° Abduction

*The percent volume (+1 SD) of cortical and trabecular bone expected to resorb due to increasing implant girth when the shoulder was abducted 75°. Changes were observed in 8 equal 5 mm slices distal to the cut surface. Statistically significant difference is expressed with *p≤0.05 and **p≤0.001 (N.B. The more favourable outcome for this variable is to the far left of the graph with 0% volume expected to resorb being most desirable).*

2.3.3.1 Cortical Bone Resorption

For abduction angles of 45° and 75°, implant size ($p=0.002$, power≥0.9) and slice depth ($p<0.001$, power=1.0) had statistically significant effects on the change in SED and thus, the percent volume of bone expected to resorb (Figure 2-13 and Figure 2-14). For both abduction angles, the smallest implant size consistently produced the lowest volume of bone expected to resorb over the M and L implants in all 8 slices. At 45° of abduction and for all slices depths investigated, increasing implant size from S to M increased the overall percent volume of bone expected to resorb by 3.8 ± 0.3% ($p=0.002$) and increasing the implant size from M to L increased the average volume by 16.2 ± 1.3% ($p=0.004$). In all slice depths, the S implant size consistently produced the lowest volume of expected bone resorption when compared to the M and L implant sizes. Statistically significant increases in the amount of expected bone resorption were observed when increasing the implant size from S to M ($p\leq0.03$), S to L ($p\leq0.02$) and M to L ($p\leq0.004$) in slices 1-4, as well as slices 5-7 when increasing implant size from S to L ($p\leq0.04$) and M to L ($p\leq0.04$). At 75° abduction, and for all slice depths investigated, the overall volume of bone expected to resorb increased by 4.3 ± 0.4% ($p=0.008$) and 17.5 ± 1.4% ($p=0.003$) when increasing the implant size from S to M and M to L, respectively. Similar to 45° abduction, the smallest implant size presented the lowest volume of expected bone resorption in all slice depths when compared to the M and L sizes. Statistically significant increases in the volume of bone expected to resorb were observed in slices 1-4 when increasing the implant size from S to M ($p\leq0.043$), S to L ($p\leq0.003$) and M to L ($p\leq0.004$) and slices 5-7 when increasing implant size from S to L ($p\leq0.036$) and M to L ($p\leq0.036$).

2.3.3.2 Trabecular Bone Resorption

For all abduction angles, both implant size (45°: abduction $p=0.01$, power=0.8; 75° abduction: $p=0.01$, power=0.8) and slice depth (45° and 75° abduction: $p\leq0.001$, power≥0.9), significantly affected the volume of trabecular bone that may resorb. For both abduction angles, the small implant was once again, the most consistent in producing the lowest volume of expected bone resorption in all slice depths when compared to the other implant sizes. For all slices depths at 45° abduction, increasing

implant size from S to M increased the volume of expected bone resorption by 2.5 ± 0.4% ($p=0.08$) and increasing implant size from M to L increased the volume by 18.1 ± 2.1% ($p=0019$). On a per-slice basis, statistically significant changes were only found when increasing the implant size from S to L ($p\leq0.037$) and M to L ($p\leq0.039$) for slices 1-7 and 2-6, correspondingly. At 75° abduction, for all slice depths investigated, increasing implant size from S to M increased the volume of expected bone resorption by 5.8 ± 0.8% ($p=0.04$) and increasing implant size from M to L increased the volume by 16.2.3 ± 1.7% ($p=0.012$). Increasing implant size from S to L ($p\leq0.031$) and M to L ($p\leq0.032$) significantly affected the chance that bone would resorb in slices 2-6. Additional statistical significant differences were found in slices 1 and 7 when increasing the size from S to L ($p\leq0.029$) and slices 3 and 4 when increasing the size from S to M ($p\leq0.043$).

2.4 Discussion

2.4.1 Effect of Implant Girth on BIC

Statistically significant decreases in the degree of contact between bone and implant were noted in the first four slices for both abduction angles (Figure 2-10). In the most proximal bone slices (slices 1-4) the S implant size produced significantly more contact with bone than the M size in slices 3 and 4 at 45° abduction and slices 1 and 4 at 75° abduction. Significantly more contact was also observed when the S implant was used over the L implant in slices 1-3 for both abduction angles. Considering only the slice depths investigated for this study, it has shown in other studies that the greatest concentration of trabecular bone exists in the slices below the resection surface, with the highest density towards the periphery of bone, particularly in the medial region (Hepp et al., 2003; Reeves, Athwal, & Johnson, 2018; Tingart, Bouxsein, Zurakowski, Warner, & Apreleva, 2003). It is, therefore, unexpected that the smallest implant size would produce the greatest amount of BIC in the more proximal bone slices. However, individual bone and implant geometries may differ resulting in slight variations in relative implant positioning. The findings of this study may imply that, in the most proximal region (*i.e.* directly under the resection surface), the implant geometry might be more medially oriented, then perfectly symmetrical about the canal. Thus, the smallest implant may potentially be contacting more porous trabecular bone, whereas the M and L sizes are approaching more rigid cortical bone.

In contrast to the results of this study, several studies investigating dental implants, found that larger implant diameters (analogous to implant girth) were more favourable then smaller implant diameters with respect to BIC (Bilhan et al., 2010; Eazhil et al., 2016; Hsu et al., 2017; Li et al., 2011). Specifically, an in-vitro experiment conducted by Hsu *et al.* (2017) using artificial bone samples, found that larger dental implants resulted in significantly more BIC area than smaller implant diameters. Furthermore, 3D FE analyses of dental implants conducted found that larger dental implants enhanced overall implant stability (Bilhan et al., 2010; Eazhil et al., 2016; Li et al., 2011), which can be correlated to the BIC as stability is largely determined by the local bone density (Bilhan et al., 2010). Discrepancies may exist between the findings of this study and those

previous observed in the dental investigations, as the distribution and porosity of cancellous bone found throughout the mandible is generally more uniform (Hsu et al., 2017), whereas the distribution and porosity in the humerus is site dependent (Hepp et al., 2003; Reeves et al., 2018; Yamada et al., 2007). Moreover, the loading conditions are quite different, with bending being more prevalent in the shoulder. The degree of contact to bone with humeral implants may be dependent on its proximal geometry and relative location within the proximal region of the humerus. Moreover, this may suggest that if larger humeral implants are to be used, they should be designed to be more symmetrical about the proximal bone region (*i.e.* directly under the resection surface) in attempt to optimize proximal bone contact.

2.4.2 Effect of Implant Girth on Proximal Bone Stress

Statistically significant changes in bone stress were observed throughout all slices for cortical and trabecular bone at both abduction angles, except the most proximal trabecular bone slice at 75° abduction (Figure 2-11 and Figure 2-12), when implant girth was increased. On a per slice basis, the S implant was almost always more consistent at mimicking cortical and trabecular bone stresses in the intact state. The L implant, however, produced slightly less change in bone stress in the most proximal trabecular bone slice at both abduction angles when compared to the S and M implant sizes; significance was only found at 45° abduction.

According to Huiskes (1993), when an implant is placed into bone, the load applied to the joint is no longer transferred solely through the cortical shell and metaphyseal trabecular bone, but now involves the interface between the bone and implant. The load applied to the articular surface is now shared across the bone and implant (Frost, 2004; Huiskes, 1993; Wolff, Maquet, & Furlong, 1892), resulting in subnormal bone stresses when compared to the native loading state (Huiskes, 1993). It is thus logical to conclude that when an implant with a larger sized girth is implanted into bone, more of the load from the articular surface is accepted by the larger stem when compared to implants with a smaller girth. As the larger stem accepts more of the applied load, less is shared to the surrounding cortical and trabecular bone over the entire length of the implant. When an implant with a smaller girth is inserted into the bone, there is likely a greater percentage

of the load being shared to the bone; thus, better matching stress distributions in the native loading state.

In the most proximal trabecular bone slice, the larger implant may have better matched bone stresses in the native state because the implant is likely integrating with cortical bone, which in the intact bone state, normally accepts the load applied to the subchondral bone at the articular surface carrying it around the trabecular bone (Razfar, 2014; Wang, Li, Yang, & Dong, 2018). The results suggest that the implant with the largest girth may be sharing more of the load in the most proximal slice with the cortical shell that would otherwise be shared with trabecular bone when a smaller implant was used; thus, better representing the load distribution in trabecular bone as seen in the native state. Previous investigations conducted in dental implants, exhibit findings that contradict the results of this study. Many authors concluded that dental implants with larger diameters produced more favourable stress distributions, when compared to smaller diameters, by decreasing the maximum Von Mises stresses at the bone-implant interface (Ding et al., 2009; Eazhil et al., 2016; Himmlová et al., 2004; Li et al., 2011). Studies also show that stresses decreased, particularly around the implant neck, when implant diameter was increased (Baggi, Cappelloni, Di Girolamo, Maceri, & Vairo, 2008; Eazhil et al., 2016; Himmlová et al., 2004). McNally *et al.* (2013) examined the maximum Von Mises stresses in a small dental implant and compared their findings to the yield stresses in cortical and trabecular bone. The author's concluded that stresses at the bone-implant interface greatly exceeded the yield stresses in both cortical and trabecular bone. Therefore, the authors suggested that by increasing the implant diameter, there is a reduction in the risk of stress overloading (Olate et al., 2010; Vigolo & Givani, 2000), which may prevent negative outcomes such as implant fracture (Eazhil et al., 2016; Olate et al., 2010). The discrepancies between the findings in dental implants and those of the previous investigation likely pertain to the different geometries and loading conditions. Decreasing bone stresses in the mandible or maxilla with a larger implant, likely better match the stress distribution in the native loading state; whereas implants with a smaller girth better match the stress distributions throughout the proximal humerus.

2.4.3 Effect of Implant Girth on the Risk of Bone Resorption

Statistically significant changes in the percentage of cortical bone volume expected to resorb were observed within the proximal humerus because of slice depth and increasing implant size (Figure 2-13 and Figure 2-14). The findings of this experiment show that the S implant size was most consistent at producing the smallest amount of volume expected to resorb when compared to the M and L sizes in all depths. Evidence of possible stress shielding with the S implant size was found only in the most proximal 5 slices in both abduction angles and was found to present a significantly lower volume of possible resorption than the other two implant sizes (except the M implant size in slice 5). The greatest volume of cortical bone expected to resorb with the small implant size was 40.5 ± 16.2% chance of bone resorption, whereas the greatest volume of expected bone resorption with the L implant was 66.6 ± 9.4%. Thus, it is recommended that an implant with a smaller girth (distal stem diameter, d=8 mm) should be used over larger implant sizes (*i.e.,* d>8 mm) to decrease the overall risk of proximal stress shielding in cortical bone.

Significant changes were observed in trabecular bone across all abduction angles and various slice depths due to a change in implant size (Figure 2-13 and Figure 2-14). For all abduction angles increasing implant size from S to L and from M to L significantly affected the volume of bone that would be expected to resorb in numerous slices. Increasing the implant size from S to M only presented significant increases in the percent volume expected to resorb in slices 3 and 4 at 75° abduction. Although the S implant consistently produced the lowest volume of expected bone resorption across all abduction angles and slice depths the results were not statistically significant which may suggest that a M implant size (d≈12 mm) may also closely mimic bone remodeling capabilities similar to the native state when compared to the L implant size. Research has shown the adverse effect of the strain-adaptive remodeling behaviour of bone (*i.e.,* change in SED), when an implant is inserted, is caused by changes in the natural loading behaviour of the bone (Huiskes, 1993; Kaczmarczyk & Pearce, 2011; Mow & Huiskes, 2005; Wolff et al., 1892). This sharing of load between the bone and implant, ultimately reduces the mechanical loading demands of the bone leading to stress shielding (Haase &

Rouhi, 2013; Huiskes, 1993). Therefore, the overall results of this study suggest that a smaller implant may be sufficient in carrying the load applied from the joint surface to the surrounding bone, better matching the loading distribution, and thus structural changes, that would occur in the intact state for cortical bone. Findings in trabecular bone, also suggest that the S implant may also be sufficient in carrying the load by better matching stress distributions in the intact state. Increased risk of stress shielding was likely seen when the L implant was used because almost all the applied load was now being carried by the humeral stem, resulting in decreased mechanical loading to the surrounding bone (Kaczmarczyk & Pearce, 2011).

The findings of this study agree with results previously published clinical studies, suggesting that larger stem diameters lead to increased occurrences of cortical stress shielding (Bobyn et al., 1992; Engh & Bobyn, 1988; Nagels, Stokdijk, & Rozing, 2003). One study, investigating relative implant size in the humerus, found that patients who received a shoulder replacement with a larger relative stem diameter, resulted in greater incidences of cortical stress shielding particularly on the proximal-lateral aspect (Nagels et al., 2003). Studies investigating stress shielding in the hip found that larger stem diameters (≥13.5 mm), when compared to smaller stem diameters (≤12.0 mm), resulted in greater incidences (approximately 44% greater) of pronounced cortical bone resorption, meaning larger implant sizes were likely to have potentially harmful clinical consequences (Bobyn et al., 1992; Engh & Bobyn, 1988).

2.5 Conclusion

Humeral implant stem diameter, or implant girth, has been insufficiently researched. This study aimed to provide insight on the degree of BIC, changes in bone stress from the intact state, and changes in SED, which can be used to predict the expected volume of bone resorption when implant girth was increased. The results from this current study show that the greatest amount of BIC was achieved, overall, by the smallest implant, which was found to be significantly greater than the medium and large implants on a per slice basis in the most proximal bone slices (20 mm below the cut surface). These findings suggest that perhaps the larger implant is removing too much trabecular bone and is integrating with more rigid cortical bone. The implant with the smallest girth was found to produce significantly less change in both cortical and trabecular bone stresses from the intact state. Additionally, the smallest implant girth produced the lowest volume of cortical and trabecular bone expected to resorb when compared to the medium and large implants. In accordance with Huiskes and Wolff's Law, it is therefore likely that the smallest implant shares more of the load from the articular surface with the surrounding bone; thereby, increasing the mechanical load placed on surrounding bone.

2.6 References

Baggi, L., Cappelloni, I., Di Girolamo, M., Maceri, F., & Vairo, G. (2008). The influence of implant diameter and length on stress distribution of osseointegrated implants related to crestal bone geometry: A three-dimensional finite element analysis. *Journal of Prosthetic Dentistry*, *100*(6), 422–431. https://doi.org/10.1016/S0022-3913(08)60259-0

Behrens, B., Bouquecha, A., Nolte, I., Meyer-Lindenberg, A., Stukenborg-Colsman, C., & Pressel, T. (2008). Strain adaptive bone remodelling: influence of the implantation technique. *Studies in Health Technology and Informatics*, *133*, 33–44.

Bergmann, G., Graichen, F., Bender, A., Kääb, M., Rohlmann, A., & Westerhoff, P. (2007). In vivo glenohumeral contact forces-Measurements in the first patient 7 months postoperatively. *Journal of Biomechanics*, *40*(10), 2139–2149. https://doi.org/10.1016/j.jbiomech.2006.10.037

Bilhan, H., Geckili, O., Mumcu, E., Bozdag, E., Sünbüloğlu, E., & Kutay, O. (2010). Influence of surgical technique, implant shape and diameter on the primary stability in cancellous bone. *Journal of Oral Rehabilitation*, *37*(12), 900–907. https://doi.org/10.1111/j.1365-2842.2010.02117.x

Bobyn, J., Mortimer, E., Glassman, A., Engh, C., Miller, J., Brooks, C., & CE. (1992). Producing and avoiding stress shielding: laboratory and clinical observations of noncemented total hip arthroplasty. *Clinical Orthopaedics & Related Research*, *274*, 79–96.

Casagrande, D. J., Parks, D. L., Torngren, T., Schrumpf, M. A., Harmsen, S. M., Norris, T. R., & Kelly, J. D. (2016). Radiographic evaluation of short-stem press-fit total shoulder arthroplasty: Short-term follow-up. *Journal of Shoulder and Elbow Surgery*, *25*(7), 1163–1169. https://doi.org/10.1016/j.jse.2015.11.067

Collin, P., Matsukawa, T., Boileau, P., Brunner, U., & Walch, G. (2017). Is the humeral stem useful in anatomic total shoulder arthroplasty? *International Orthopaedics*, 10–

14. https://doi.org/10.1007/s00264-016-3371-4

Denard, P. J., Noyes, M. P., Walker, J. B., Shishani, Y., Gobezie, R., Romeo, A. A., & Lederman, E. (2017). Proximal stress shielding is decreased with a short stem compared with a traditional-length stem in total shoulder arthroplasty. *Journal of Shoulder and Elbow Surgery*, *27*(1), 53–58. https://doi.org/10.1016/j.jse.2017.06.042

Dines, D. (2005). *Biomet Shoulder Arthroplasty Indications and Short-Term Results*. New York, NY.

Ding, X., Liao, S. H., Zhu, X. H., Zhang, X. H., & Zhang, L. (2009). Effect of diameter and length on stress distribution of the alveolar crest around immediate loading implants. *Clinical Implant Dentistry and Related Research*, *11*(4), 279–287. https://doi.org/10.1111/j.1708-8208.2008.00124.x

Eazhil, R., Swaminathan, S. ., Gunaseelan, M., Kannan, G. ., & Alagesan, C. (2016). Impact of implant diameter and length on stress distribution in osseointegrated implants: A 3D FEA study. *J Int Soc Prevent Communit Dent*, *6*(6), 590–596.

Engh, C., & Bobyn, J. (1988). The influence of stem size and extent of porous coating on femoral bone resorption after primary cementless hip arthroplasty. *Clinical Orthopaedics and Related Research*, *231*, 7–28.

Frost, H. M. (2004). A 2003 update of bone physiology and Wolff's law for clinicians. *Angle Orthodontist*, *74*(1), 3–15. https://doi.org/10.1043/0003-3219(2004)074<0003:AUOBPA>2.0.CO;2

Gefen, A. (2002). Computational simulations of stress shielding and bone resorption around existing and computer-designed orthopaedic screws. *Medical & Biological Engineering & Computing*, *40*(3), 311–322.

Goriainov, V., Cook, R., Latham, J. M., Dunlop, D. G., & Oreffo, R. O. C. (2014). Bone and metal: An orthopaedic perspective on osseointegration of metals. *Acta Biomaterialia*, *10*(10), 4043–4057. https://doi.org/10.1016/j.actbio.2014.06.004

Haase, K., & Rouhi, G. (2013). Prediction of stress shielding around an orthopedic screw: Using stress and strain energy density as mechanical stimuli. *Computers in Biology and Medicine*, *43*(11), 17481757. https://doi.org/10.1016/j.compbiomed.2013.07.032

Hepp, P., Lill, H., Bail, H., Korner, J., Niederhagen, M., Haas, N. P., … Duda, G. N. (2003). Where Should Implants Be Anchored in the Humeral Head? *Clinical Orthopaedics and Related Research*, *415*(415), 139–147. https://doi.org/10.1097/01.blo.0000092968.12414.a8

Himmlová, L., Dostálová, T., Kácovský, A., & Konvičková, S. (2004). Influence of implant length and diameter on stress distribution: A finite element analysis. *THE JOURNAL OF PROSTHETIC DENTISTRY*, *91*(1), 20–25. https://doi.org/10.1016/j.prosdent.2003.08.008

Hsu, J. T., Shen, Y. W., Kuo, C. W., Wang, R. T., Fuh, L. J., & Huang, H. L. (2017). Impacts of 3D bone-to- implant contact and implant diameter on primary stability of dental implant. *Journal of the Formosan Medical Association*, *116*(8), 582–590. https://doi.org/10.1016/j.jfma.2017.05.005

Huiskes, R. (1993). Stress shielding and bone resorption in THA: clinical versus computer-simulation studies. *Acta Orthopaedica Belgica*, *59 Suppl 1*, 118–129. https://doi.org/URN:NBN:NL:UI:25-585440-of

Huiskes, R., Weinans, H., Grootenboer, H. J., Dalstra, M., Fudala, B., & Slooff, T. J. (1987). Adaptive bone-remodeling theory applied to prosthetic-design analysis. *Journal of Biomechanics*, *20*(11–12), 1135–1150. https://doi.org/10.1016/0021-9290(87)90030-3

Kaczmarczyk, L., & Pearce, C. J. (2011). Efficient numerical analysis of bone remodelling. *Journal of the Mechanical Behavior of Biomedical Materials*, *4*(6), 858–867. https://doi.org/10.1016/j.jmbbm.2011.03.006

Keener, J. D., Chalmers, P. N., & Yamaguchi, K. (2017). The Humeral Implant in

Shoulder Arthroplasty. *Journal of the American Academy of Orthopaedic Surgeons*, *25*(6), 427–438. https://doi.org/10.5435/JAAOS-D-15-00682

Li, T., Hu, K., Cheng, L., Ding, Y., Ding, Y., Shao, J., & Kong, L. (2011). Optimum selection of the dental implant diameter and length in the posterior mandible with poor bone quality - A 3D finite element analysis. *Applied Mathematical Modelling*, *35*(1), 446–456. https://doi.org/10.1016/j.apm.2010.07.008

McDowell, M. A., Fryar, C. D., Ogden, C. L., & Flegal, K. M. (2008). *Anthropometric reference data for children and adults: United States, 2003-2006. National Health Statistics Reports*.

McNally, S. ., Wilcox, C., Akhter, M. P., Sheets, J. ., Danforth, J. ., & Chehal, H. . (2013). Implant diameter: Effect on stress in bone: Finite element analysis. *Journal of Dental Implants*, *3*(2), 87–90.

Meneghini, R. M., Hallab, N. J., Berger, R. a, Jacobs, J. J., Paprosky, W. G., & Rosenberg, A. G. (2006). Stem diameter and rotational stability in revision total hip arthroplasty: a biomechanical analysis. *Journal of Orthopaedic Surgery and Research*, *1*, 5. https://doi.org/10.1186/1749-799X-1-5

Morgan, E. F., Bayraktar, H. H., & Keaveny, T. M. (2003). Trabecular bone modulus-density relationships depend on anatomic site. *Journal of Biomechanics*, *36*(7), 897–904. https://doi.org/10.1016/S0021-9290(03)00071-X

Mow, V. ., & Huiskes, R. (2005). *Basic orthopaedic biomechanics & mechano-biology*. Philadelphia: Lippincott Williams & Wilkins.

Mueller, T. L., Basler, S. E., Müller, R., & Van Lenthe, G. H. (2013). Time-lapsed imaging of implant fixation failure in human femoral heads. *Medical Engineering and Physics*, *35*(5), 636–643. https://doi.org/10.1016/j.medengphy.2012.07.009

Nagels, J., Stokdijk, M., & Rozing, P. M. (2003). Stress shielding and bone resorption in shoulder arthroplasty. *Journal of Shoulder and Elbow Surgery*, *12*(1), 35–39. https://doi.org/10.1067/mse.2003.22

Neuert, M. A. C., & Dunning, C. E. (2013). Determination of remodeling parameters for a strain-adaptive finite element model of the distal ulna. *Proceedings of the Institution of Mechanical Engineers, Part H: Journal of Engineering in Medicine*, *227*(9), 994–1001. https://doi.org/10.1177/0954411913487841

Olate, S., Lyrio, M. C. N., de Moraes, M., Mazzonetto, R., & Moreira, R. W. F. (2010). Influence of Diameter and Length of Implant on Early Dental Implant Failure. *Journal of Oral and Maxillofacial Surgery*, *68*(2), 414–419. https://doi.org/10.1016/j.joms.2009.10.002

Razfar, N. (2014). *Finite Element Modeling of the Proximal Humerus to Compare Stemless , Short and Standard Stem Humeral Components of Varying Material Stiffness for Shoulder Arthroplasty*. Western Univeristy.

Razfar, N., Reeves, J. M., Langohr, D. G., Willing, R., Athwal, G. S., & Johnson, J. A. (2016). Comparison of proximal humeral bone stresses between stemless, short stem, and standard stem length: A finite element analysis. *Journal of Shoulder and Elbow Surgery*, *25*(7), 1076–1083. https://doi.org/10.1016/j.jse.2015.11.011

Reeves, J. M., Athwal, G. S., & Johnson, J. A. (2018). An assessment of proximal humerus density with reference to stemless implants. *Journal of Shoulder and Elbow Surgery*. https://doi.org/10.1016/j.jse.2017.09.019

Schnetzke, M., Coda, S., Raiss, P., Walch, G., & Loew, M. (2016). Radiologic bone adaptations on a cementless short-stem shoulder prosthesis. *Journal of Shoulder and Elbow Surgery*, *25*(4), 650–657. https://doi.org/10.1016/j.jse.2015.08.044

Shishani, Y., & Gobezie, R. (2017). Does a short-stemmed humeral implant really make a difference? *Seminars in Arthroplasty*, *28*(1), 13–17. https://doi.org/10.1053/j.sart.2017.05.003

Tingart, M. J., Bouxsein, M. L., Zurakowski, D., Warner, J. P., & Apreleva, M. (2003). Three-Dimensional Distribution of Bone Density in the Proximal Humerus. *Calcified Tissue International*, *73*(6), 531–536. https://doi.org/10.1007/s00223-002-

0013-9

Tissakht, M., Ahmed, A. M., & Chan, K. C. (1996). Calculated stress-shielding in the distal femur after total knee replacement corresponds to the reported location of bone loss. *Journal of Orthopaedic Research*, *14*(5), 778–785. https://doi.org/10.1002/jor.1100140515

Van Lenthe, G. H., de Waal Malefijt, M. C., & Huiskes, R. (1997). Stress shielding after total knee replacement may cause bone resorption in the distal femur. *The Journal of Bone and Joint Surgery. British Volume*, *79*(1), 117–22. https://doi.org/10.1302/0301-620X.79B1.6808

Vigolo, P., & Givani, A. (2000). Clinical evaluation of single-tooth mini-implant restorations: A five-year retrospective study. *Journal of Prosthetic Dentistry*, *84*(1), 50–54. https://doi.org/10.1067/mpr.2000.107674

Wagner, E. R., Statz, J. M., Houdek, M. T., Cofield, R. H., Sánchez-Sotelo, J., & Sperling, J. W. (2017). Use of a shorter humeral stem in revision reverse shoulder arthroplasty. *Journal of Shoulder and Elbow Surgery*, *26*(8), 1454–1461. https://doi.org/10.1016/j.jse.2017.01.016

Wang, Y., Li, J., Yang, J., & Dong, J. (2018). Regional variations of cortical bone in the humeral head region: A preliminary study. *Bone*, *110*, 194–198. https://doi.org/10.1016/j.bone.2018.02.010

Willing, R. T., Lalone, E. A., Shannon, H., Johnson, J. A., & King, G. J. W. (2013). Validation of a finite element model of the human elbow for determining cartilage contact mechanics. *Journal of Biomechanics*, *46*(10), 1767–1771. https://doi.org/10.1016/j.jbiomech.2013.04.001

Wolff, J., Maquet, P., & Furlong, R. (1892). *The law of bone remodelling*. Springer Berlin.

Yamada, M., Briot, J., Pedrono, A., Sans, N., Mansat, P., Mansat, M., & Swider, P. (2007). Age- and gender-related distribution of bone tissue of osteoporotic humeral

head using computed tomography. *Journal of Shoulder and Elbow Surgery*, *16*(5), 596–602. https://doi.org/10.1016/j.jse.2007.01.006

Chapter 3

3 Implications of Removing an Implant Collar on Bone to Implant Contact and Load Transfer

Several aspects of humeral implant design have been previously investigated as documented in Chapters 1 and 2. However, there are apparently no studies on the effect of the implant collar, as it is a relatively new concept in shoulder implant reconstruction. This chapter compares the humeral collar to collarless stem on the same metrics used in Chapter 2, namely the degree of bone to implant contact (BIC), changes in proximal bone stresses, and changes in strain energy density (SED). Details are provided describing the steps to develop and implement the finite element (FE) method herein.

3.1 Introduction

Much advancement has been made to the design of the humeral implant since it was first developed in the early 1950's (Wallace, 1998); yet, there are some aspects that have not been explored. Historically, shoulder implants have been implanted into bone using, what is referred to in the hip literature, as a collared implant; however, in more recent practice, some surgeons have transitioned to using collarless implants, where the underside of the humeral head does not contact the resection surface.

As previously stated, this concept has been widely studied in the hip, yet results for the optimal implant type remain unsatisfactory (Al-Dirini, 2017). Ideally, the presence of a collar allows for primary osseointegration and increased axial load transfer to the calcar by preventing subsidence of the femoral stem (Jeon et al., 2011; Meding, Ritter, Keating, & Faris, 1997). However, it has been suggested that perfect contact of the implant collar to the calcar is difficult to achieve in the hip (Demey, Fary, Lustig, Neyret, & Si Selmi, 2011; Markolf, Amstutz, & Hirschowitz, 1980). If optimal contact between the backside of the collar and calcar surface is not achieved, the implant may move in a cantilever-like motion when under load, which may cause impingement on the calcar if the implant subsides, leading to resorption and possible implant failure (Al-Dirini, 2017; Demey et al., 2011; Jeon et al., 2011). Studies also show, that if perfect contact is achieved between the collar and calcar, the findings are unconvincing. Ji *et al.* (2013) found that when either a collared or collarless implant was implanted into bone, there were no significant difference in bone loss between the two implant types; however, Mansour *et al.* (1995) found that bone loss was greatest when collarless implants were used. Furthermore, Allen *et al.* (1996), found that collared or collarless implants resulted in nearly the same amount of surface strain in the femur 5 mm below the collar; but, when surface strain was measured 25 mm below the collar, the collared implant resulted in greater strain more closely matching strain in the intact state. Evidently, more research on this topic is required to determine the implant type produces more desirable outcomes.

For this current study, the objective was to develop a three-dimensional (3D) finite element (FE) model, similar to that in Chapter 2 (Section 2.2), to determine the changes in bone to implant contact (BIC), proximal bone stresses from the intact state, and SED to

predict the volume of bone expected to resorb when the implant collar was removed. It is hypothesized that the collarless implants will result in the greatest amount of BIC, produce cortical and trabecular bone stresses that more closely match the intact state, and produce less change in SED, resulting in a decreased volume of cortical and trabecular bone expected to resorb.

3.2 Methodology

The methodology of this chapter follows nearly the same procedures used to develop the FE models in Chapter 2; the only difference was that the collar of the implant was removed or "suppressed" and only one implant size was investigated: the implant with medium sized girth, was employed as this was the generic base model created from three currently available models. Therefore, only a general overview will be provided in this chapter with reference to Chapter 2.

3.2.1 Developing the 3D Model

Eight pre-operative bone scans were obtained from patients requiring total shoulder arthroplasty (left arm males, mean ± SD age = 67.8 ± 5.3) (Appendix B) and processed using MIMICS (Materialise, Leuven, Belgium). Several masks were generated using a combination of automatic threshold-based segmentation and manual identification to create the 3D models of the proximal humerus with separate cortical and trabecular bone regions (Figure 2-1) (Razfar, 2014; Willing, Lalone, Shannon, Johnson, & King, 2013). The 3D model was then exported in STL format to be further developed in SolidWorks (Dassault Systèmes, S.A. (Vélizy, France)). Please see Appendix C for details on generating the cortical and trabecular bone models in MIMICS.

3.2.2 Bone Resection

Once in SolidWorks, an orthopaedic surgeon guided the sectioning of cortical and trabecular bone into head and body components (Figure 2-2). The length of the trabecular bone was shortened to 40 mm from the surface of the cut plane.

3.2.3 Implant Development

One generic implant model was created in SolidWorks based off three clinically available short stem implants: Arthrex Univers™ Apex, Biomet Comprehensive® Mini Stem, Tornier Aequalis™ Ascend Flex. Dimensions were obtained at various points on the implant and averaged to create this model (distal stem diameter, d=12 mm) (FIG). Please see Appendix D for details on implant measurements. The length of the humeral stem was set by an orthopaedic at 55 mm from the medial aspect. Therefore, all measurements

obtained from the three currently available models were measured from this point. Head components were also developed in SolidWorks using clinically available models.

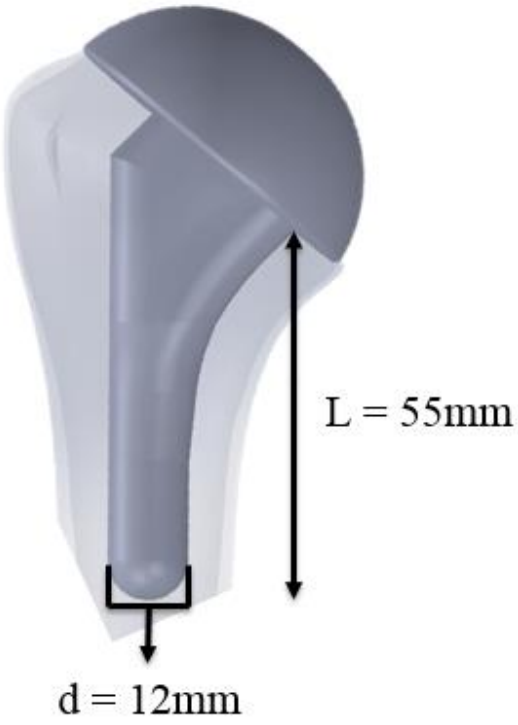

Figure 3-1: Generic Humeral Implant Model

One generic implant was designed from three currently available models (d=12 mm). The length of the implant stem was chosen by a surgeon to be 55 mm from the medial edge.

3.2.4 Implant Positioning and Reference Geometry

Reference geometries were created in SolidWorks to correctly align the implant in the humerus (Figure 2-4). For the bone geometry, two reference locations were created: a central axis down the humeral canal, termed “Bone Axis”, and a plane coincident to the resection surface, termed “Resection Surface”. On the implant geometry, additional reference sites were created: a central axis down the stem of the implants, termed “Implant Axis” and a coincident axis across the anterior-posterior face termed “Anterior-Posterior Face Axis”. To strictly define the implant in bone, the Bone Axis was made coincident to the Implant Axis and the Resection Surface was made parallel to the Anterior-Posterior Face Axis of the implant. The appropriate sized head component was selected for each specimen to accurately replicate the native humeral head. The underside of the humeral head was made coincidence to the cut plane and then combined with the implant.

3.2.5 Creating the Finite Element Model

The steps to create the FE model are divided into the following sections: mesh preparation, material properties, model assembly, and abduction angles and model fixation.

3.2.5.1 Mesh Preparation

The implant-bone models were exported from SolidWorks into Abaqus v6.14 (Dessault Systèmes simulia Crop., Providence, RI, USA) in STEP AP214 or ASIC format. Identical meshes were created for each specimen to directly compare intact and reconstructed models. To ensure identical mesh generation, the intact model was partitioned into sub-components that could be merged together (Figure 2-5, only investigating the 12 mm implant) to create geometric lines identical to the reconstructed models. Ultimately, this allows for direct element to element comparison between the two states (Neuert & Dunning, 2013). Mesh boundaries were applied to both the bone and implant models using quadratic tetrahedral elements with a maximum edge length of 2 mm and maximum deviation factor of 0.06 mm (Razfar, 2014). The number of nodes and elements created for both the intact and reconstructed states can be found in Table 3-1.

Table 3-1: Number of Nodes and Elements for the Intact and Reconstructed Models when Implant Collar was Removed

Number of nodes and elements for both the intact and reconstructed model for both the collared and collared models. Note that the number of nodes and elements are identical between intact and reconstructed models to ensure direct element-to-element comparison (N.B. For the intact model the number of nodes and elements only accounts for the region below the cut surface unoccupied by the implant).

Specimen Number	Number of Nodes ($x10^3$)			Number of Elements ($x10^3$)		
	Model and Implant Type			Model and Implant Type		
	Intact	Reconstructed		Intact	Reconstructed	
		Collar	Collarless		Collar	Collarless
1	192.0	192.0	192.0	126.6	126.6	126.6
2	197.6	197.6	197.6	133.7	133.7	133.7
3	184.5	184.5	184.5	123.4	123.4	123.4
4	179.6	179.6	179.6	118.6	118.6	118.6
5	159.2	159.2	159.2	105.7	105.7	105.7
6	186.6	186.6	186.6	125.0	125.0	125.0
7	184.2	184.2	184.2	123.9	123.9	123.9
8	190.7	190.7	190.7	127.5	127.5	127.5

3.2.5.2 Material Property Assignment

Uniform material properties were assigned to cortical bone with a Young's modulus, E=20 GPa and Poisson's Ratio, v=0.3 (Razfar, 2014). Using Equation 2.1 as previously described, trabecular bone was assigned varying material properties based on the density-modulus equation Morgan *et al.* (2003).

Apparent density was calculated and determined from the cadaveric CT scans in MIMICS. The densities of two known substances (SB3 cortical bone (Gammex, Middleton WI; ρ=1.82 g/cm^3) and water (ρ=1.00 g/cm^3)) were placed within the original CT scan and used to generate a linear relationship, which was used to derive the apparent densities of trabecular bone. Poisson's Ratio for trabecular bone was also set at 0.3 (Razfar, 2014).

Titanium material properties (E=110 GPa, v=0.3) were applied to all implant models in Abaqus with site-specific surface texturing (Figure 2-6). Both the under surface of the humeral head and the fully cylindrical portion of the distal stem were polished (μ=0.40), and the proximal and middle region of the humeral stems were plasma sprayed (μ=0.88).

3.2.5.3 Model Assembly

Forty-eight FE models were created in Abaqus ([1 intact model + 2 reconstructed models [collared or collarless implant type (Figure 3-2)]] x 2 abduction angles/load directions (Figure 2-7) x 8 specimens). To simulate the collarless implant type, the interaction between the cut plane and the underside of the humeral head that was created in the FE model to simulate the collared implant type, was "suppressed", which resulted in a loss of contact from the implant collar to the cut plane.

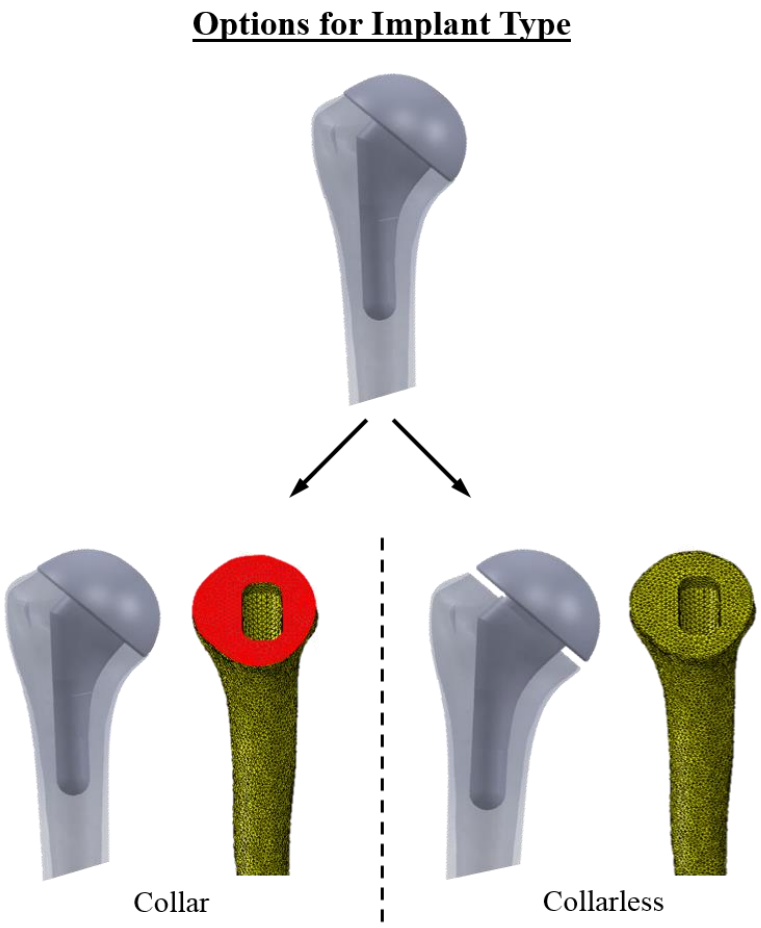

Figure 3-2: Collar and Collarless Implant Types

The two possible reconstructed states for the generic implant model (medium implant girth with distal stem diameter, d=12 mm). The humeral head may either contact the cut surface, as shown in red, representing the collared implant (bottom left) or may be left with a slight gap between the head and cut surface representing the collarless implant (bottom right). N.B. The image on the bottom right, which represents the collarless state, does not represent the true distance of the gap that was created between the backside of the humeral head and the cut surface during the FE simulation. The gap in this image is enlarged to emphasize to the reader that there is no contact of the backside of the humeral head to the cut surface. For the FE simulation, the interaction between the backside of the humeral head and the cut surface was "suppressed", meaning there was no contact between the elements on these two surfaces simulating an extremely thin and virtually immeasurable gap.

3.2.5.4 Abduction Angles and Model Fixation

As mentioned in Section 3.2.5.3 (Model Assembly), two shoulder abduction angles, or load directions, were investigated: 45° and 75° (Figure 2-7). Joint reaction forces applied at the articular surface were derived from telemeterized shoulder implant data reported by Bergmann *et al.* (2007). Assuming 50th percentile male body weight (88.3 kg), 440 N and 740 N of force were applied towards the center of humeral rotation at 45° and 75° abduction, respectively (Bergmann et al., 2007; McDowell, Fryar, Ogden, & Flegal, 2008). The specific direction and magnitude of the applied joint reaction forces are given in Table 2-2. Lastly, the distal ends of the humeri were rigidly fixed to restrict movement.

3.2.6 Outcome Measures

Following shoulder replacement using simulated FE methods, the degree of BIC, changes in proximal cortical and trabecular bone stresses from the intact state, and risk of bone resorption using changes in SED were obtained by sectioning the proximal humerus into eight 5 mm thick slices parallel to the resection surface (Figure 2-8). The three outcome measures for this experiment were measured and calculated using the same methods applied in Chapter 2; therefore, a brief description of the variables will be given.

3.2.6.1 Degree of BIC

The degree of BIC was calculated based the contact pressure of the surface elements on the implant to the surrounding bone. If this contact pressure was greater than 0, then the surface area (SA) of these elements were summed and divided by the total amount of element SA in the slice of interest (Equation 2.2).

3.2.6.2 Change in Proximal Bone Stress

The changes in stress between the intact and reconstructed states for both cortical and trabecular bone were separately calculated using Equation 2.2 and Equation 2.3 to determine the Von Mises of the change in stress for each element in a desired slice. This change was then volume weighted using Equation 2.5 and then divided by the

volume weighted average stress from the same slice in the intact state to obtain the percent change in stress from the intact state.

3.2.6.3 Change in SED

Thee volume of bone expected to resorb was determined by Equation 2.8 and Equation 2.9. The SED for each element was determined and compared to a threshold value of 55% when compared with the SED from the intact state. If the SED in the reconstructed state was less than 55% of the intact state, the element was expected to resorb. To determine the overall volume of bone expected to resorb in a desired slice, the sum of the volume of elements in that slice that were determined to be less than the 55% threshold were divided by the total volume of all the elements within that slice.

3.2.6.4 Statistical Analysis

All outcome measures were assessed for statistical significance (α=0.05) through a three-way repeated measures (RM) ANOVA (abduction angle/load direction, slice depth, and implant type (collared versus collarless)) using SPSS (IBM, New York, USA). Spherical significance was taken into consideration, and in the event sphericity was rejected, the Greenhouse Geisser correction was applied.

3.3 Results

3.3.1 Effect of Collar Status on BIC

When the implant model was inserted into the bone (Figure 3-3), implant type (45°: $p=0.001$, power=1.0; 75° $p=0.001$, power=1.0) and slice depth (45°: $p=0.001$, power=1.0; 75° $p=0.001$, power=1.0) significantly affected the degree of BIC. For all slice depths investigated at 45° abduction, removing the implant collar increased the overall amount of BIC by 15.8 ± 1.0% ($p<0.001$). Investigation of each slice show that the collarless implant produced significantly more contact than the collared implants ($p\leq0.01$), except in the slice 6 and 8 where the increase in BIC was not found to be significant ($p\geq0.09$). The greatest difference in BIC between the collared and collarless implant types was observed in slice 3, which resulted in an increase of contact by 24.7% when the collar was removed. At 75° abduction, the collarless implant resulted in an overall increase in contact by 16.2 ± 1.0% ($p=0.001$) Removing the implant collar, again, resulted in significantly more BIC in all slices ($p\leq0.004$) but slice 6 and 8, where no statistically significant increase in BIC was detected ($p\geq0.1$). Similarly to 45° abduction, the greatest increase in BIC was observed in slice 3, where 27.9% more contact was observed when the implant collar was removed.

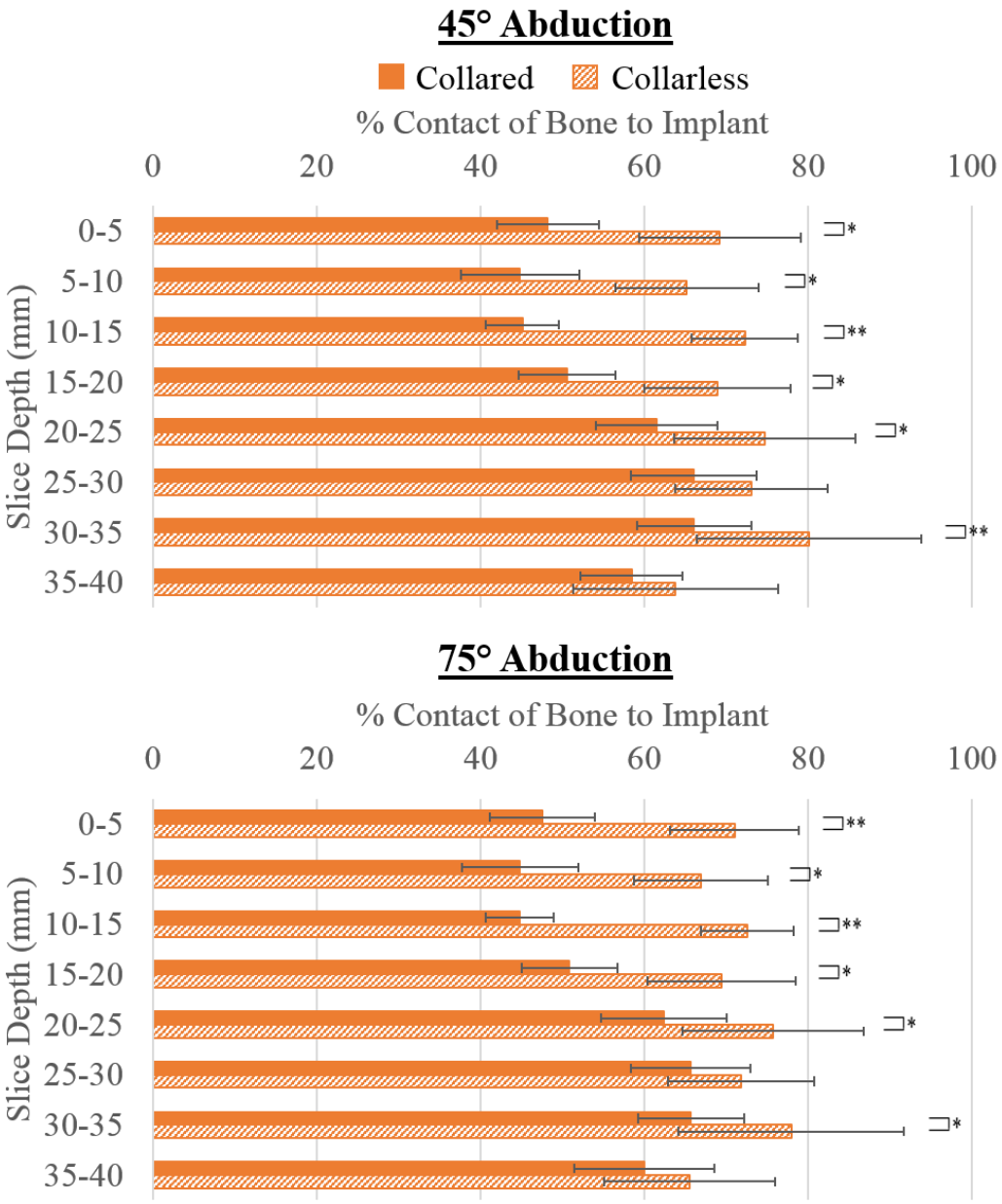

Figure 3-3: Contact of Bone with Implant at 45° and 75° Abduction (%) when Implant Collar was Removed

*The percentage of BIC (±1 SD) is shown for the collared and collarless models. Degree of BIC was obtained in 8 equal 5 mm slices distal to the cut surface. Statistically significance difference is expressed with *p≤0.05 and **p≤0.001.*

3.3.2 Effect of Collar Status on Proximal Bone Stress

3.3.2.1 Cortical Bone Stress

Statically significant changes in overall cortical bone stress when compared to the intact state were observed at abduction angles of 45° and 75° for both implant type ($p<0.001$, power=1.0) and slice depth ($p<0.001$, power=1.0) (Figure 3-4 and Figure 3-5). For all slice depths investigated at 45° abduction, removal of the implant collar caused the change in bone stress to increase by an average of 32.2 ± 0.8% ($p<0.001$). The collarless implant type significantly produced the greatest changes in stress from the intact state in all slice depths ($p<0.001$). When the collar was removed, the greatest increase in stress on a per slice basis was 44.6% in slice 2. Average changes in bone stress for all slices when the arm was abducted 75° increased by 33.3 ± 0.9% ($p<0.001$). Again, the collarless implant resulted in statistically significant larger changes in bone stress for all slice depths ($p<0.001$). Investigation of all slice depths show that the greatest increase in the change in bone stress was 46.4% in slice 2, when the implant collar was removed.

3.3.2.2 Trabecular Bone Stress

Statistically significant changes in overall trabecular bone stress when compared to the intact state were observed for both implant type (45° and 75° abduction: $p<0.001$, power=1.0) and slice depth (45° and 75° abduction: $p<0.001$, power=1.0) (Figure 3-4 and Figure 3-5). When the changes in stress values were pooled for all slices depths investigated at 45° abduction, removing the implant collar increased the average change in bone stress by 57.4 ± 1.7% ($p<0.001$). Removing the implant collar consistently produced the greatest changes in stress from the intact state for all slice depths investigated. Significant increases in the change in trabecular bone stress were observed in all slices when the collar was removed ($p<0.001$). The greatest change in bone stress was observed in slice 4, with an increase in the change in bone stress by 90.3% when the collar of the implant was removed. Similar results were observed when the load was applied with the arm abducted 75°. Removing the implant collar resulted in an overall increase in bone stress by 58.5 ± 1.8% ($p<0.001$) for all slice depths. Again, the collarless implant consistently produced the largest change in stress from the intact; results were

statistically significant across all slice depths ($p \leq 0.001$). On a per slice basis, the largest increase in the change in stress was found to be 92.4% in slice 4 when the implant collar was removed.

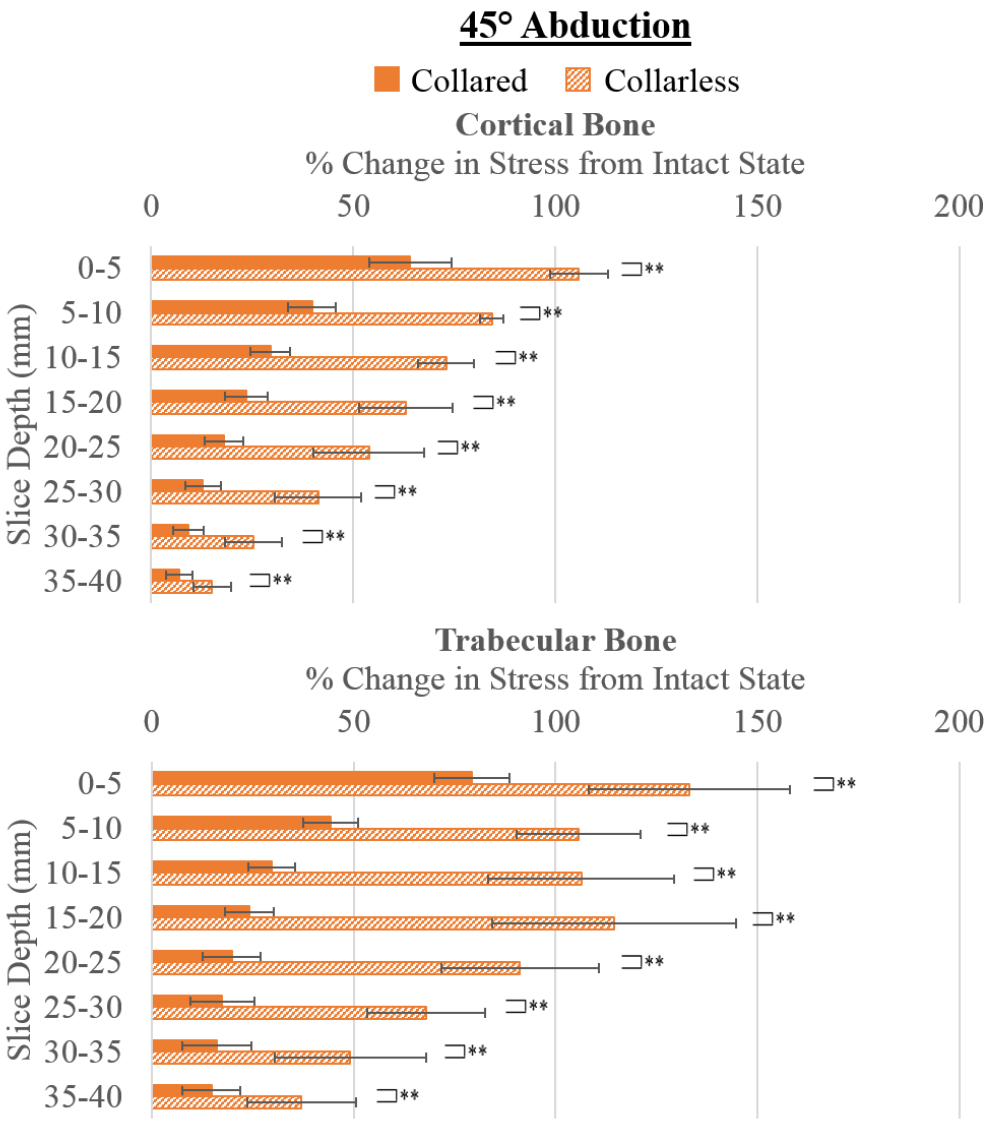

Figure 3-4: Changes in Proximal Bone Stress when Implant Collar was Removed at 45° Abduction

*The percent change (±1 SD) in proximal bone stresses from the intact to the reconstructed states is shown for the collared and collarless models when the shoulder was abducted 45° for cortical and trabecular bone. Changes in bone stress were obtained in 8 equal 5 mm slices distal to the cut surface. Statistically significance difference is expressed with *p≤0.05 and **p≤0.001 (N.B. The more favourable outcome for this variable is to the far left of the graph with 0% change in stress from the intact state being most desirable).*

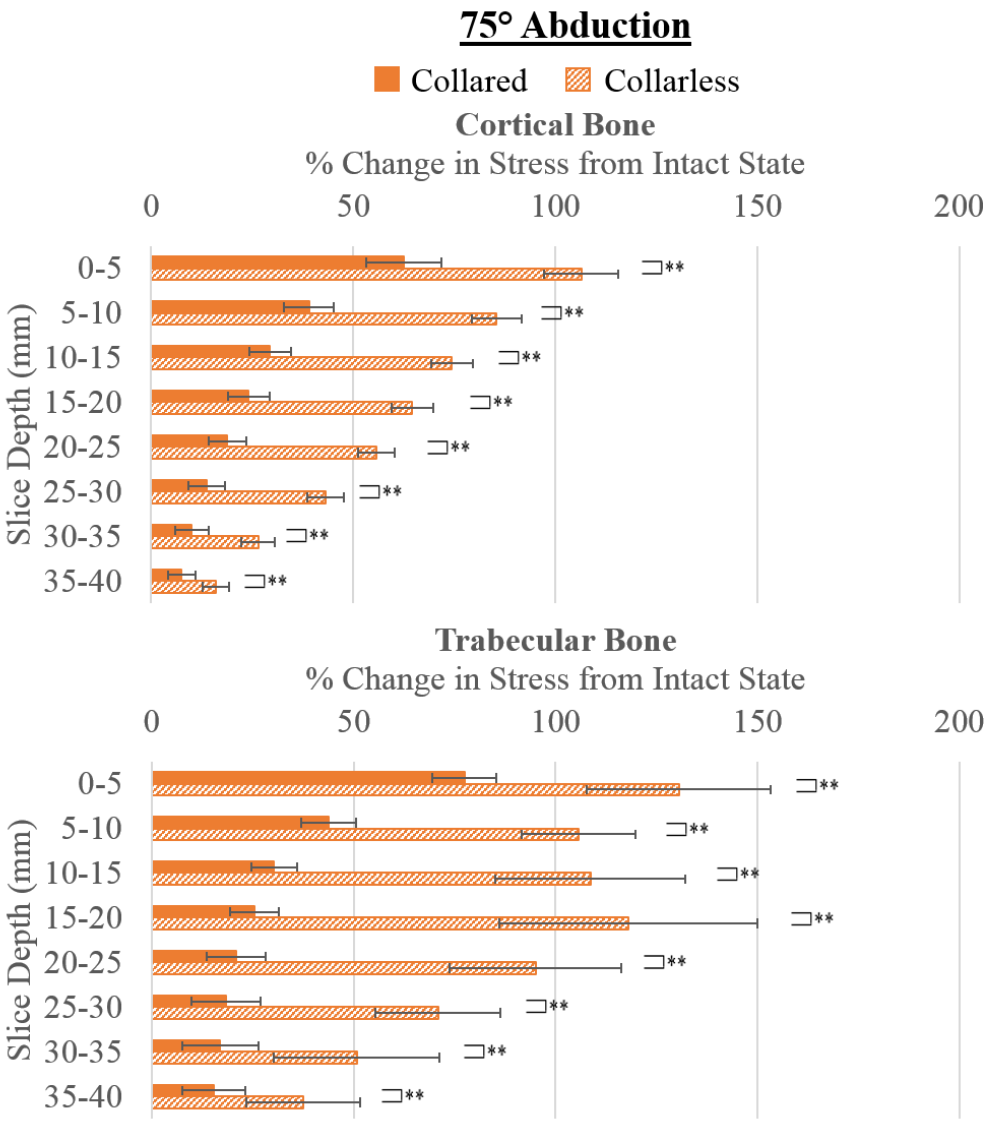

Figure 3-5: Changes in Proximal Bone Stress when Implant Collar was Removed at 75° Abduction

*The percent change (±1 SD) in proximal bone stresses from the intact to the reconstructed states is shown for the collared and collarless models when the shoulder was abducted 75° for cortical and trabecular bone. Changes in bone stress were obtained in 8 equal 5 mm slices distal to the cut surface. Statistically significance difference is expressed with *p≤0.05 and **p≤0.001 (N.B. The more favourable outcome for this variable is to the far left of the graph with 0% change in stress from the intact state being most desirable).*

3.3.3 Effect of Collar Status on the Risk of Bone Resorption

3.3.3.1 Cortical Bone Resorption

For all abduction angles, statistically significant changes in the percent volume of bone expected to resorb were found for both implant type ($p<0.001$, power=1.0) and slice depth ($p<0.001$, power=1.0) (Figure 3-6 and Figure 3-7). When the data from all slice depths were pooled at 45° abduction, removing the implant collar caused the percent volume of cortical bone expected to resorb to increase by an average of 19.5 ± 1.0% ($p<0.001$). The collarless implant type produced the greatest volume of bone expected to resorb in all slice depths, with statistically significance differences found in slices 1 to 5 ($p\leq0.003$). When the collar was removed, the greatest increase in the percent volume of cortical bone expected to resorb, on a per slice basis, was 36.2% in slice 2. The average percent volume of expected bone loss for all slices combined, when the arm was abducted 75° increased by 19.3 ± 1.0% ($p<0.001$). The collarless implant, once again, resulted in the greatest percent volume of bone expected to resorb in all slice depths, with statistically significant differences presented in slices 1-6 ($p\leq0.04$). Observation across all slice depths, show that the greatest increase in the percent volume of bone expected to resorb, when the implant collar was removed, was found to be 37.4% in slice 2.

3.3.3.2 Trabecular Bone Resorption

In trabecular bone, implant type (45°: p=0.4, power=0.1; 75° p=0.8, power=0.05) did not result in significant changes to the percent volume of bone expected to resorb, whereas changes in slice depth (45° abduction: p=0.001, power=1.0; 75° abduction: p=0.001, power=1.0) did (Figure 3-6 and Figure 3-7). At 45° abduction, when the values from all slice depths were pooled, removing the implant collar increased the overall percent volume at risk of resorption by 2.9 ± 1.0% (p=0.4). Although no statistical significance was found in any of the 8 slice depths investigated ($p\geq0.08$), the collarless implant resulted in a reduction in the volume of bone expected to resorb in slices 2,7, and 8. The largest change in the volume of expected bone loss was observed in slice 4. When the implant collar was removed, the volume of expected trabecular bone resorption increased by 11.1%. At 75° abduction, and for all slice depths investigated, removing the implant

collar resulted in an overall decrease in the volume of expected bone resorption by 0.60 ± 1.1% ($p=0.8$). On a per slice basis, the collarless implant resulted in less volume of expected bone resorption in slices 1-2 and 6-7; yet, no results were found to be statistically significant ($p\geq0.09$). The greatest change in the percent volume of bone expected to resorb was, again, observed in slice 4. The volume of expected bone loss increased by 7.6% when the implant collar was removed.

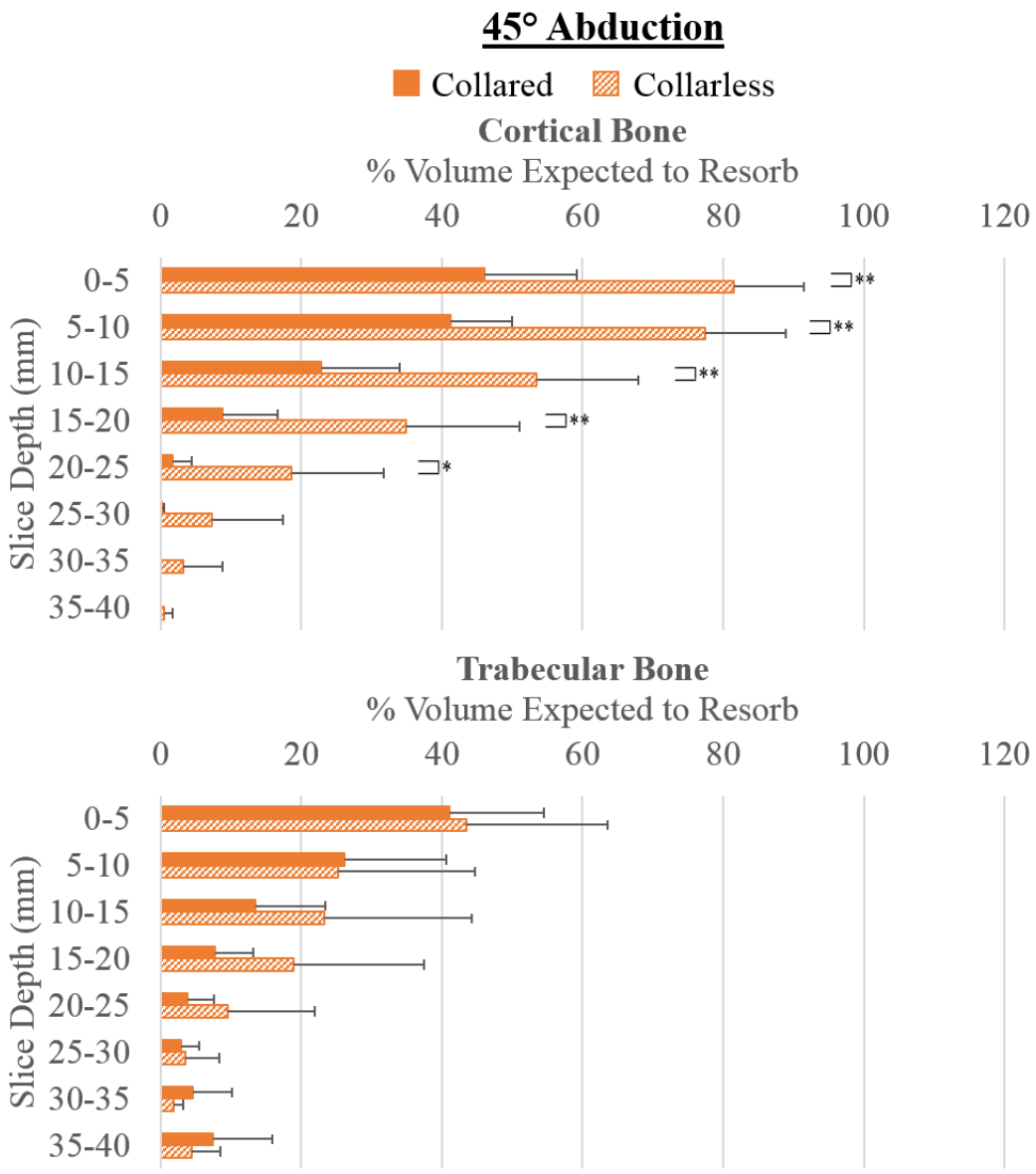

Figure 3-6: Changes in Percent Volume of Bone Expected to Resorb when Implant Collar was Removed at 45° Abduction

*The percent volume (+1 SD) of cortical and trabecular bone expected to resorb when the implant collar was removed and the shoulder was abducted 45°. The change in SED, and therefore risk of bone resorption, were obtained in 8 equal 5 mm slices distal to the cut surface. Statistically significant difference is expressed with *p≤0.05 and **p≤0.001 (N.B. The more favourable outcome for this variable is to the far left of the graph with 0% volume expected to resorb being most desirable).*

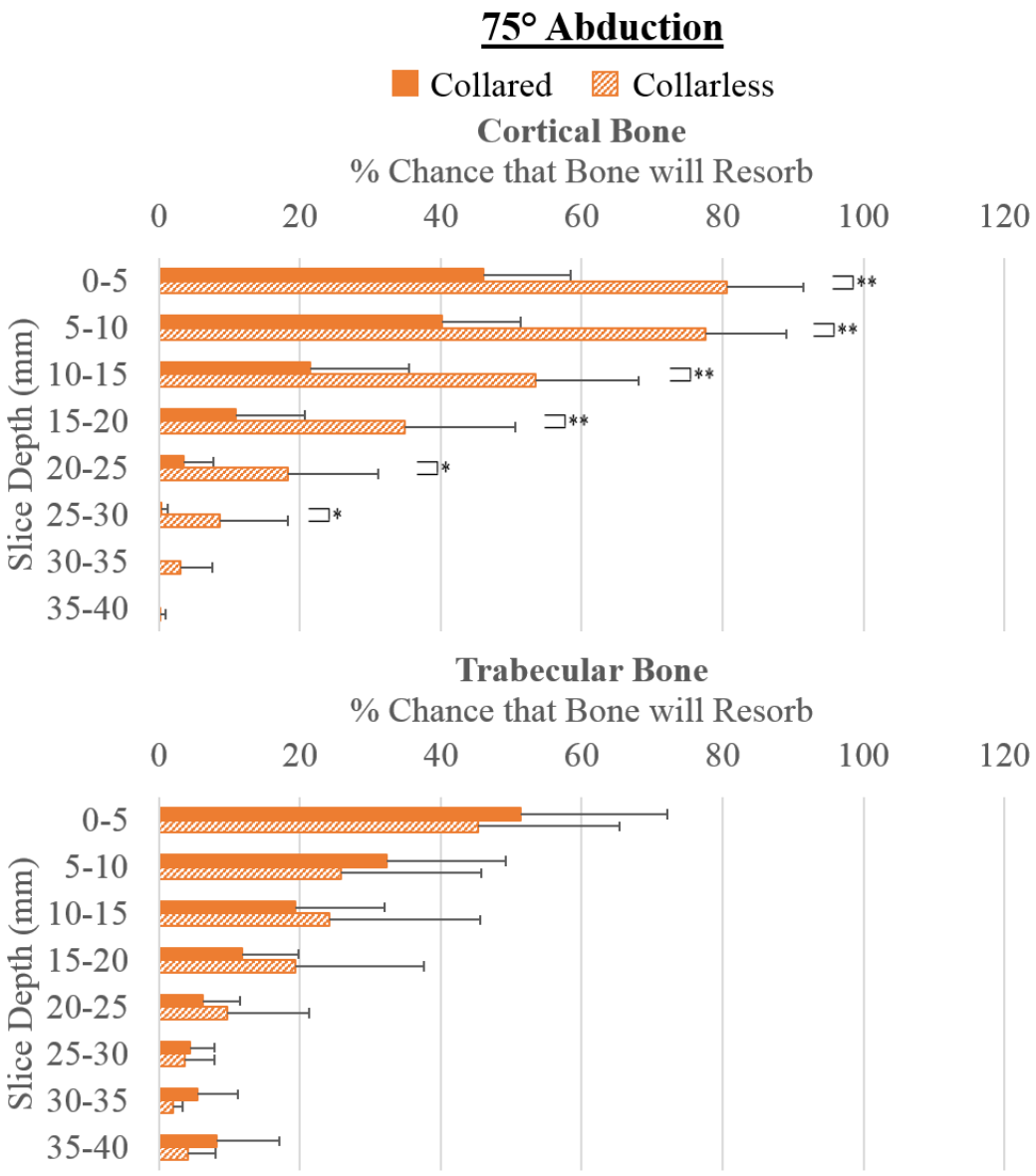

Figure 3-7: Changes in Percent Volume of Bone Expected to Resorb when Implant Collar was Removed at 75° Abduction

*The percent volume (+1 SD) of cortical and trabecular bone expected to resorb when the implant collar was removed and the shoulder was abducted 75°. The change in SED, and therefore risk of bone resorption, were obtained in 8 equal 5 mm slices distal to the cut surface. Statistically significant difference is expressed with *p≤0.05 and **p≤0.001 (N.B. The more favourable outcome for this variable is to the far left of the graph with 0% volume expected to resorb being most desirable).*

3.4 Discussions

3.4.1 Effect of Collar Status on BIC

Significant increases in the degree of BIC resulted for the first five bone slices, with additional significance found in the 7th bone slice, when the implant collar was removed (Figure 3-3). Greater contact was also achieved in slices 6 and 8, when the collar was disengaged, but results were not found to be significant.

When the collar contact is removed from the cut plane, the stem of the implant must now accept the entire load transferred from the articular surface before distributing it to the surrounding bone. This loss of support from the cut plane may be causing the implant to move in a cantilever-like motion resulting in some micro-movement medial-laterally; thereby driving the implant into more contact with the surrounding bone.

Additionally, there may be some early gentle subsidence of the implant vertically into the canal resulting in a tighter fit of the implant into the bone. While a large degree of subsidence has been shown to negatively affect the long term survival of the implant (Selvaratnam, Shetty, & Sahni, 2015; Whiteside, Amador, & Russel, 1988), by increasing the risk of implant loosening and subsequently requiring revision (Vestermark, 2011; Yildirim et al., 2016), small amounts of subsidence may be beneficial if immediate stability is inadequate to permit secondary integration (Demey et al., 2011; Girard, Roche, Wavreille, Canovas, & Le Béguec, 2011; Meding et al., 1997).

In agreement with the findings from the FE conducted in Section 3.3.1 (Effect of Collar Status on BIC), a study conducted by Malfroy Camine *et al.* (2018) found that subsidence was greater with a collarless implant. They also showed that in both compression and torsion, micromotion was lower with collarless femoral implants than collared implants. It may be postulated that this reduction in micromotion with the collarless implant is due in part to the subsidence of the implant creating a tighter fit within the surrounding bone, and thus resulting in a higher degree of BIC (Meltzer, 2009).

Early subsidence with collarless femoral implants was also observed in other clinical studies (Hutt et al., 2014; Selvaratnam et al., 2015; Ström, Nilsson, Milbrink, Mallmin, &

Larsson, 2007). Some author's reported subsidence of the collarless implants used in their studies occurring up to six months postoperatively. Once subsidence ceased, sufficient stabilization of the implant was reported (Hutt et al., 2014; Selvaratnam et al., 2015; Ström et al., 2007), which may be due, in part, to an increase in the degree of contact between bone and implant (Bilhan et al., 2010; Hsu et al., 2017; Javed, Ahmed, Crespi, & Romanos, 2013; Shukla, Fitzsimmons, An, & O'Driscoll, 2012; Swami, Vijayaraghavan, & Swami, 2016). Authors have speculated that early subsidence in collarless implants may be an effect of impaction rather than true vertical displacement due to instability of the implant (Selvaratnam et al., 2015); thus, supporting the idea that some early gentle subsidence to achieve a tighter fit and greater BIC is likely beneficial to increase the survivability of the implant.

The surface roughness of the implant used in the current study (*i.e.*, surface texturing and coefficient of friction such as the plasma spray in this experiment) likely also plays a role in the degree of implant subsidence and BIC. The FE model generated for this experiment attempted to simulate a press fit model. However, a true press fit implantation method was not fully achieved since the bone was "cut" with the implant, meaning the size of the humeral canal was not undersized for the implant used. Therefore, the added friction from the plasma spray to the implant surface acted to resist some of the axial displacement of the load when the implant collar is removed, possibly preventing too much subsidence that may occur with a fully polished implant. While some displacement may prove to be beneficial (Demey et al., 2011; Girard et al., 2011; Meding et al., 1997), this added surface texture may help to prevent continuous migration of the implant allowing for osseoconduction; therefore, increasing early fixation and enhancing long term stability (Daugaard, Elmengaard, Bechtold, Jensen, & Soballe, 2010; Harrison, McHugh, Curtin, & McDonnell, 2013). The surface roughness of the implant may prove to be beneficial in cases where the canal is over-reamed for the size of the implant. It may therefore, be important for future investigations to examine the effects of different surface texturing on the degree of BIC and amount of subsidence.

3.4.2 Effect of Collar Status on Proximal Bone Stress

When the generic implant was implanted into the bone statistically significant changes in bone stress were observed throughout all slices for cortical and trabecular bone at both abduction angles (Figure 3-4 and Figure 3-5). On a per slice basis, removing the implant collar consistently produced statistically greater changes in cortical and trabecular bone stresses from the intact state than when the collar was present.

When a load is applied at the articular surface of the non-reconstructed joint (*i.e.*, intact bone state), the subchondral bone normally accepts the load and dissipates the majority of it distally through the cortical shell (Razfar, 2014; Wang, Li, Yang, & Dong, 2018). In a reconstructed joint, the load is now shared across the bone and the implant (Frost, 2004; Huiskes, 1993; Wolff, Maquet, & Furlong, 1892). When a traditional collared implant is inserted into the bone, the load applied to humeral head of the implant is shared between the cut surface and implant stem; both the cortical and trabecular bone will experience some direct transfer of load via contact of the implant collar to the cut surface. However, when the implant collar is removed, the entire load from the joint surface is transferred to the stem of the implant with no direct transfer of load to the cortical shell. This loss of load sharing directly to the cortical bone likely reduces the stress placed on the cortical shell resulting in stress changes further from the intact state than if an implant collar was present.

In terms of the changes in stress observed in trabecular bone, removing the implant collar may cause an increase in the stress placed on the surrounding bone when compared to the collared state. Some of the applied load is likely now being shared directly below the cut plane resulting in a possible cantilever like motion. This bending moment may be increasing the stress placed on the surrounding trabecular bone, driving the change in stress further away from the intact state then if the collar was present.

The findings related to bone stresses for the two implant models are in agreement with previous work by others. Studies on the effect of implant collar on bone stresses in the hip have shown that the presence of an implant collar, when contacted to the calcar, increases proximal bone stresses to the medial calcar (Jeon et al., 2011; Kelley, Fitzgerald

Jr, Rand, & Ilstrup, 1993; Whiteside et al., 1988), which better match the distribution of stress in the intact state (Jeon et al., 2011). Jeon *et al.* (2011) also reported greater lateral tilting with a collarless implant, which resulted in greater stress placed on trabecular bone when compared to a collar implant. When the stresses in both the collared and collarless implants were compared to the intact state, the collared implant was found to better match the overall stress distribution in the native loading state (Jeon et al., 2011).

3.4.3 Effect of Collar Status on the Risk of Bone Resorption

Removing the implant collar resulted in a greater percent volume of cortical bone expected to resorb in all bone slices, with statistically significant differences found in at least the first five slice depths (Figure 3-6 and Figure 3-7). As stated previously, when the collar of the implant is removed, there is a loss of load transfer to the cut plane, and consequently, a loss of direct load transfer to the cortical shell. As per Wolff's law, when an implant is placed into bone, the normal remodeling capabilities of bone changes as the applied load is now shared across bone and implant (Frost, 2004; Huiskes, 1993; Wolff et al., 1892). Accordingly, the mechanical loading demands of the bone are decreased, which causes stress shielding of the bone (Collin, Matsukawa, Boileau, Brunner, & Walch, 2017; Haase & Rouhi, 2013). Evidently, when the implant collar is removed, the direct loading of the cortical bone is removed, therefore, decreasing the load demand on the bone, causing significantly greater underloading of the cortical bone than if the implant collar was present.

In trabecular bone, when the implant collar was removed, the volume of expected bone resorption closely matched the volume of expected bone loss observed in the collared implant type, particularly in slices 1-2 and 6-8. It can be postulated that when the implant collar is removed, some medial-lateral motion may be occurring producing some bending moment about the implant. As discussed in Section 3.4.2 (Effect of Collar Status on Proximal Bone Stress), the implant may be experiencing some bending moment that is likely increasing the stress placed on the trabecular bone. Although the implant stem is accepting all of the applied load from the joint surface, the possible bending moment likely increases the stress and thus, allows for greater load sharing to the trabecular bone reducing the risk of bone resorption (Collin et al., 2017; Haase & Rouhi, 2013; Huiskes,

1993; Wolff et al., 1892), which more closely matches the risk of trabecular bone loss in the collared state.

While this concept has yet to be investigated in the shoulder, studies have examined the removal of an implant collar in the hip and have reported inconsistent findings. Findings from some investigations show that collarless implants resulted in greater occurrence of stress shielding (Allen et al., 1996; Jeon et al., 2011; Kelley et al., 1993; Mansour, Ray, & Mukherjee, 1995), while others show no significant differences in bone loss between collar and collarless implant types (Allen et al., 1996; Ji, Wang, Ma, Lan, & Li, 2013). The results of this investigation (Effect of Collar Status on the Risk of Bone Resorption) are in partial agreement with the hip literature as the results found in cortical bone, show that removing the implant collar significantly increased the risk of bone loss. However, results in trabecular bone show that removing the implant collar did not produce significant changes in the volume of bone expected to resorb when compared to the collar state. More research on this topic is recommended to determine which implant type is more optimally suited for patients. Additionally, it may be beneficial to examine the effects of removing implant collar with implants of various sizes.

3.5 Conclusion

Surgical implantation methods for a shoulder replacement have begun to see a shift from traditional methods, where the backside of the humeral head contacts the resection surface (analogous to a collared implant in the hip), to leaving a small gap between the humeral head and humeral stem (representing a collarless implant). While this concept has been widely studied in the hip, results remain inconclusive on the optimal implant type. Furthermore, to the author's knowledge, no studies have investigated removing the implant collar in shoulder arthroplasties. For this investigation, the effects of removing the implant collar on the degree of BIC, changes in proximal bone stresses from the intact state, and risk of bone resorption were examined. Results were determined throughout the proximal humerus (total depth of 40 mm distal to the cut plane) using FE methods. When a generic implant was implanted into the bone (distal stem diameter, d= 12mm) and the implant collar was removed, more BIC was achieved throughout all slice depths, with statistically significant differences found in 75% of the slices investigated. In terms of the changes in bone stress from the intact state, statistically significant increases were observed in all slice depths for both cortical and trabecular bone. Lastly, when the implant collar was removed, the volume of bone expected to resorb increased in all slice depths for cortical bone, with statistically significant differences found in at least the first 25 mm distal to the cut plane. No statistically significant changes were found in the volume of trabecular bone expected to resorb when the implant collar was disengaged. However, the changes in stress were less pronounced than the changes in the risk in cortical bone and more closely resembled the risk of bone loss in the collar implant state. The findings of this study are of importance to the design of future humeral implant models, as they will ideally help to reduce some of the complications seen with current implant models.

3.6 References

Al-Dirini, R. M. A. (2017). Influence of collars on the primary stability of cementless femoral stems: A finite element study using a diverse patient cohort. *Journal of Orthopaedic Research*, 1–11. https://doi.org/10.1002/jor.23744

Allen, W., Beaupré, G., Carter, D., Giddings, V., Goodman, S., D.J, S., & van der Meulen, M. C. (1996). *Femoral Collar Effect on bone strains after cemented hip replacement*. Stanford, CA.

Bergmann, G., Graichen, F., Bender, A., Kääb, M., Rohlmann, A., & Westerhoff, P. (2007). In vivo glenohumeral contact forces-Measurements in the first patient 7 months postoperatively. *Journal of Biomechanics*, *40*(10), 2139–2149. https://doi.org/10.1016/j.jbiomech.2006.10.037

Bilhan, H., Geckili, O., Mumcu, E., Bozdag, E., Sünbüloğlu, E., & Kutay, O. (2010). Influence of surgical technique, implant shape and diameter on the primary stability in cancellous bone. *Journal of Oral Rehabilitation*, *37*(12), 900–907. https://doi.org/10.1111/j.1365-2842.2010.02117.x

Collin, P., Matsukawa, T., Boileau, P., Brunner, U., & Walch, G. (2017). Is the humeral stem useful in anatomic total shoulder arthroplasty? *International Orthopaedics*, 10–14. https://doi.org/10.1007/s00264-016-3371-4

Daugaard, H., Elmengaard, B., Bechtold, J. E., Jensen, T., & Soballe, K. (2010). The effect on bone growth enhancement of implant coatings with hydroxyapatite and collagen deposited electrochemically and by plasma spray. *Journal of Biomedical Materials Research - Part A*, *92*(3), 913–921. https://doi.org/10.1002/jbm.a.32303

Demey, G., Fary, C., Lustig, S., Neyret, P., & Si Selmi, T. A. (2011). Does a Collar Improve the Immediate Stability of Uncemented Femoral Hip Stems in Total Hip Arthroplasty? A Bilateral Comparative Cadaver Study. *Journal of Arthroplasty*, *26*(8), 1549–1555. https://doi.org/10.1016/j.arth.2011.03.030

Frost, H. M. (2004). A 2003 update of bone physiology and Wolff's law for clinicians.

Angle Orthodontist, *74*(1), 3–15. https://doi.org/10.1043/0003-3219(2004)074<0003:AUOBPA>2.0.CO;2

Girard, J., Roche, O., Wavreille, G., Canovas, F., & Le Béguec, P. (2011). Stem subsidence after total hip revision: 183 cases at 5.9 years follow-up. *Orthopaedics and Traumatology: Surgery and Research*, *97*(2), 121–126. https://doi.org/10.1016/j.otsr.2010.10.006

Haase, K., & Rouhi, G. (2013). Prediction of stress shielding around an orthopedic screw: Using stress and strain energy density as mechanical stimuli. *Computers in Biology and Medicine*, *43*(11), 17481757. https://doi.org/10.1016/j.compbiomed.2013.07.032

Harrison, N., McHugh, P. ., Curtin, W., & McDonnell, P. (2013). Preclinical trial of a novel surface architecture for improved primary fixation of cementless orthopaedic implants. *Journal of the Mechanical Behavior of Biomedical Materials*, *21*, 37–46. https://doi.org/10.1016/j.clinbiomech.2014.07.007

Hsu, J. T., Shen, Y. W., Kuo, C. W., Wang, R. T., Fuh, L. J., & Huang, H. L. (2017). Impacts of 3D bone-to- implant contact and implant diameter on primary stability of dental implant. *Journal of the Formosan Medical Association*, *116*(8), 582–590. https://doi.org/10.1016/j.jfma.2017.05.005

Huiskes, R. (1993). Stress shielding and bone resorption in THA: clinical versus computer-simulation studies. *Acta Orthopaedica Belgica*, *59 Suppl 1*, 118–129. https://doi.org/URN:NBN:NL:UI:25-585440-of

Hutt, J., Hazlerigg, A., Aneel, A., Epie, G., Dabis, H., Twyman, R., & Cobb, A. (2014). The effect of a collar and surface finish on cemented femoral stems: A prospective randomised trial of four stem designs. *International Orthopaedics*, *38*(6), 1131–1137. https://doi.org/10.1007/s00264-013-2256-z

Javed, F., Ahmed, H. B., Crespi, R., & Romanos, G. E. (2013). Role of primary stability for successful osseointegration of dental implants: Factors of influence and

evaluation. *Interventional Medicine and Applied Science*, *5*(4), 162–167. https://doi.org/10.1556/IMAS.5.2013.4.3

Jeon, I., Bae, J. Y., Park, J. H., Yoon, T. R., Todo, M., Mawatari, M., & Hotokebuchi, T. (2011). The biomechanical effect of the collar of a femoral stem on total hip arthroplasty. *Computer Methods in Biomechanics and Biomedical Engineering*, *14*(1), 103–112. https://doi.org/10.1080/10255842.2010.493513

Ji, W. P., Wang, X. L., Ma, M. Q., Lan, J., & Li, H. (2013). Prevention of early bone loss around the prosthesis by administration of anti-osteoporotic agents and influences of collared and non-collared femoral stem prostheses on early periprosthetic bone loss. *European Journal of Orthopaedic Surgery and Traumatology*, *23*(5), 565–571. https://doi.org/10.1007/s00590-012-1034-8

Kelley, S., Fitzgerald Jr, R. ., Rand, J. ., & Ilstrup, D. . (1993). A prospective randomized study of a collar versus a collarless femoral prosthesis. *Clinical Orthopaedics & Related Research*, (294), 114–122.

Mansour, H., Ray, J., & Mukherjee, D. (1995). Stress shielding of femoral component with and without collar. In *Proceedings of the IEEE Fourteenth Southern Biomedical Engineering Conference* (pp. 53–54). Shreveport, LA, USA.

Markolf, K. L., Amstutz, H. C., & Hirschowitz, D. L. (1980). The effect of calcar contact on femoral component micromovement. A mechanical study. *The Journal of Bone and Joint Surgery. American Volume*, *62*(8), 1315–23. Retrieved from http://www.ncbi.nlm.nih.gov/pubmed/7440610

McDowell, M. A., Fryar, C. D., Ogden, C. L., & Flegal, K. M. (2008). *Anthropometric reference data for children and adults: United States, 2003-2006. National Health Statistics Reports*.

Meding, J. B., Ritter, M. A., Keating, E. M., & Faris, P. M. (1997). Comparison of collared and collarless femoral components in primary uncemented total hip arthroplasty. *Journal of Arthroplasty*, *12*(3), 273–280.

https://doi.org/10.1016/S0883-5403(97)90023-1

Meltzer, A. M. (2009). and Restoration of Dental Implants. *Journal of Implant and Reconstructive Dentistri*, *1*(1).

Morgan, E. F., Bayraktar, H. H., & Keaveny, T. M. (2003). Trabecular bone modulus-density relationships depend on anatomic site. *Journal of Biomechanics*, *36*(7), 897–904. https://doi.org/10.1016/S0021-9290(03)00071-X

Neuert, M. A. C., & Dunning, C. E. (2013). Determination of remodeling parameters for a strain-adaptive finite element model of the distal ulna. *Proceedings of the Institution of Mechanical Engineers, Part H: Journal of Engineering in Medicine*, *227*(9), 994–1001. https://doi.org/10.1177/0954411913487841

Razfar, N. (2014). *Finite Element Modeling of the Proximal Humerus to Compare Stemless , Short and Standard Stem Humeral Components of Varying Material Stiffness for Shoulder Arthroplasty*. Western Univeristy.

Selvaratnam, V., Shetty, V., & Sahni, V. (2015). Subsidence in Collarless Corail Hip Replacement. *The Open Orthopaedics Journal*, *9*(1), 194–197. https://doi.org/10.2174/1874325001509010194

Shukla, D. R., Fitzsimmons, J. S., An, K. N., & O'Driscoll, S. W. (2012). Effect of stem length on prosthetic radial head micromotion. *Journal of Shoulder and Elbow Surgery*, *21*(11), 1559–1564. https://doi.org/10.1016/j.jse.2011.11.025

Ström, H., Nilsson, O., Milbrink, J., Mallmin, H., & Larsson, S. (2007). The Effect of Early Weight Bearing on Migration Pattern of the Uncemented CLS Stem in Total Hip Arthroplasty. *Journal of Arthroplasty*, *22*(8), 1122–1129. https://doi.org/10.1016/j.arth.2006.11.015

Swami, V., Vijayaraghavan, V., & Swami, V. (2016). Current trends to measure implant stability. *The Journal of Indian Prosthodontic Society*, *16*(2), 124. https://doi.org/10.4103/0972-4052.176539

Vestermark, M. (2011). Strontium in the bone-implant interface. *Danish Medical Journal*, *58*(5), B4286.

Wallace, W. A. (1998). Introduction. In *Joint Replacement in the Shoulder and Elbow* (pp. 1–5). Woburn, MA: Reed Educational and Professional Publishing.

Wang, Y., Li, J., Yang, J., & Dong, J. (2018). Regional variations of cortical bone in the humeral head region: A preliminary study. *Bone*, *110*, 194–198. https://doi.org/10.1016/j.bone.2018.02.010

Whiteside, L., Amador, D., & Russel, K. (1988). The effects of the collar on total hip femoral component subsidence. *Clinical Orthopaedics & Related Research*, 120–126.

Willing, R. T., Lalone, E. A., Shannon, H., Johnson, J. A., & King, G. J. W. (2013). Validation of a finite element model of the human elbow for determining cartilage contact mechanics. *Journal of Biomechanics*, *46*(10), 1767–1771. https://doi.org/10.1016/j.jbiomech.2013.04.001

Wolff, J., Maquet, P., & Furlong, R. (1892). *The law of bone remodelling*. Springer Berlin.

Yildirim, G., Gopalakrishnan, A., Davignon, R. A., Parker, J. W., Chawla, H., & Pearle, A. D. (2016). Comparative Fixation and Subsidence Profiles of Cementless Unicompartmental Knee Arthroplasty Implants. *Journal of Arthroplasty*, *31*(9), 2019–2024. https://doi.org/10.1016/j.arth.2016.02.034

Chapter 4

4 Thesis Closure

This chapter summarizes the objectives and hypothesis, as well as the important outcomes from the two studies presented in Chapters 2 and 3. Additionally, the strengths and limitations of this work are reviewed, and as well, the future directions to expand on this research.

4.1 Summary

Finite element (FE) methods were used to determine the effects of increasing implant girth (from a small implant with distal stem diameter, d=8 mm, to a medium implant d=12 mm and to a large implant d=16 mm), as well as the implications of removing the implant collar, on interface contact and proximal bone stresses in the humerus. Specifically, the changes in the degree of bone to implant contact (BIC), changes in cortical and trabecular bone stress from the intact state, and changes in SED (used to predict the risk of bone resorption) in cortical and trabecular were investigated.

Eight clinical CT scans were obtained from cadaveric specimens and used to generate intact and reconstructed models of the proximal humerus. Simulated joint reaction forces were applied to the humeral head corresponding to arm abduction angles of 45° and 75°. A review of the hypotheses presented in Chapter 1 and results of Chapter 2 (Effect of Implant Girth on Interface Contact and Bone Stresses), and Chapter 3 (Implications of Removing an Implant Collar on Bone to Implant Contact and Load Transfer) can be found within the following two sections.

4.1.1 Chapter 2: Effect of Implant Girth on Interface Contact and Bone Stresses

For this investigation it was hypothesized that increasing implant girth using a traditional collared implant would result in the following:

1a. Greater degree of BIC;
1b. Greater changes in bone stress from the intact state in both cortical and trabecular bone;
1c. Greater volume of bone expected to resorb in both cortical and trabecular bone via SED measurements.

4.1.1.1 Effect of Implant Girth on BIC

For the first hypothesis (1a), the findings of this study do not agree with the expected results. Surprisingly, the smallest implant size produced greater overall contact to the bone than the medium or large implant sizes. Results were found to be selectively

significant, depending on the increase in girth size (*i.e.*, small to medium, small to large, or medium to larger), in only the first 4 slices. Accordingly, hypothesis 1a is rejected as the large implant girth did not produce a greater amount of BIC, except in the most distal bone slice, but results were not significant.

These findings perhaps suggest that the larger implant size may be removing too much porous trabecular bone and may likely be interacting with more rigid cortical bone; thus, reducing the volume of bone available for contact. Additionally, the results suggest that perhaps the degree of BIC is dependent on the proximal geometry of the implant and its relative location within the humerus (*i.e.*, proximal orientation of the implant lies closer to the medial aspect than perfectly symmetrical about the anatomical neck).

4.1.1.2 Effect of Implant Girth on Proximal Bone Stress

The results pertaining to the proximal bone stresses (related to Hypothesis 1b) indicated that the largest implant size resulted in overall cortical and trabecular bone stresses that were significantly worse at representing bone stresses produced in the intact state, except in the most proximal bone slice where significance varied depending on the increase in implant girth (*i.e.*, small to medium, small to large, or medium to larger), and abduction angle. Therefore, the hypothesis for this investigation is accepted.

The results of this investigation suggest that as implant girth is increased, more of the load applied to the articular surface is shared to the stem of the implant; whereas, an implant with a smaller girth likely shares more load with the surrounding bone matching the native loading state.

4.1.1.3 Effect of Implant Girth on the Risk of Bone Resorption

The results of the third investigation (related to Hypothesis 1c) showed that the largest implant resulted in significantly more volume of expected cortical and trabecular resorption. Although results varied depending on the slice depth and increase between sizes, the overall results show that the large implant resulted in an increase in the volume of bone expected to resorb in the majority of slices. Therefore, it was correctly

hypothesized that the increasing implant girth would increase the volume of expected proximal bone resorption in both cortical and trabecular bone.

Overall, these results suggest the small implant size likely shares more load with the surrounding bone over the larger implant sizes, which is removing more bone proximally and accepting more of the distributed load causing larger changes in bone stress from the intact state. Ultimately, as the stem accepts more of the load, the surrounding bone becomes underloaded, which increases the risk of stress shielding and bone resorption.

4.1.2 Chapter 3: Implications of Removing an Implant Collar on Bone to Implant Contact and Load Transfer

It was hypothesized that when the implant collar was removed the following would occur:

2a. Greater degree of BIC;
2b. Greater changes in cortical and trabecular bone stresses from the intact state;
2c. Greater volume of bone expected to resorb in both cortical and trabecular bone via SED measurements.

4.1.2.1 Effect of Implant Collar on BIC

The findings of this study are in agreement with the Hypothesis 2a. When the implant collar was removed, the results showed that more BIC was achieved in all slice depths for both abduction angles, with significance presented in at least the first 5 bone slices. Accordingly, this hypothesis is accepted.

It is postulated that removing the implant collar resulted in some medial-lateral micromotion driving the implant into more contact with the surrounding bone. Additionally, some early gentle subsidence of the implant may have occurred, resulting in a tighter fit within the humeral canal. The surface texturing modeled on the implant surface likely plays a key role in the amount of subsidence that may have been experienced by the implant, which may affect the overall BIC. Since this was not a true press-fit model, the surface texturing may have helped to prevent excessive subsidence of

the implant; thus, promoting a more optimal degree of contact between the bone and implant.

4.1.2.2 Effect of Collar Status on Proximal Bone Stress

The results of the second investigation (related to Hypothesis 2b) indicated that removing the implant collar caused significantly greater changes to both cortical and trabecular bone stresses when compared to the intact state. The findings were found to be significant across all slice depths. Therefore, it was correctly hypothesized that the removing the implant collar would increase the change in cortical and trabecular bone stresses from the intact state.

When the collar was removed, the entire load applied to the joint surface was now being accepted by the stem of the implant; whereas when the collar is present, the load was shared between the cut surface and implant stem. Removing the implant collar resulted in a loss of direct load distribution to the cortical bone; thus, reducing the stress placed on the bone and driving the change in stress further away from the intact state then when the implant collar was present. The findings in terms of trabecular bone suggest that, as noted above, there may a cantilever like motion occurring under the resection surface resulting in an increase in the stress placed on the surrounding bone, and hence, driving the change in trabecular bone stress further away from the intact state.

4.1.2.3 Effect of Collar Status on the Risk of Bone Resorption

The results of the final investigation (related to Hypothesis 2c) showed that the volume of bone expected to resorb was increased in all cortical bone slices when the implant collar was removed; statistically significant differences were found in at least the first 5 bone slices. The change in the volume of trabecular bone expected to resorb was not found to change dramatically when the implant collar was removed. In fact, removing the implant collar resulted in nearly the same volume of expected bone loss as when the implant collar was employed, specifically in slices 1-2 and 6-8. Thus, the hypothesis for this investigation is accepted for cortical bone and rejected for trabecular bone.

As mentioned in the previous investigation (Effect of Collar Status on Proximal Bone Stress), removing the implant collar resulted in the entire load applied to the joint surface now being accepted by the stem causing a loss of direct load distribution to the cortical bone. Therefore, the results showed that this loss of load due to the removal of the implant collar increased the risk of cortical bone resorption, which can be expected according to Wolff's Law. The findings in trabecular bone suggested that there may some bending moment occurring under the resection surface. This possible increase in stress likely allowed more load to be shared to the trabecular bone from the humeral stem which ultimately led to a risk in bone loss similar to that observed in the collared implant state.

4.2 Strengths and Limitations

For this present work, there are some limitations to be noted. First, the application of joint reaction forces was restricted to 45° and 75° abduction and specific to the 50th percentile male with a body weight of 85kg (Bergmann et al., 2007; McDowell, Fryar, Ogden, & Flegal, 2008). Ideally, the values of the joint reaction forces would be patient-specific based on individual body weights; however, to minimize variations in loading across specimens, this method was used. Another limitation is the use of clinical CT scans over more detailed micro-CTs. By doing so, the precision of the scanned images was decreased as the size of the voxel, in which CT attenuation was quantified, was increased, hence resulting in a less accurate bone model. However, the cadaveric shoulders that were used for this experiment would not fit within the capture range of a micro-CT scanner; thus, larger clinical scanners were required. Resolution of the clinical scanners was maximized to obtain the highest possible resolution of the CT image. Lastly, the use of manual segmentation of the humerus to identify regions of trabecular bone is variable and should be investigated for its reliability in the future.

Despite the limitations to this work, there are several important strengths. Inhomogeneous trabecular material properties were applied based on the modulus-density equation formulated by Morgan *et al.* (2003) to permit more realistic bone response. Although this equation was not specific to trabeculae in the humerus, several trabecular bone sites (n=147) throughout the body (*i.e.* vertebra, proximal tibia, and proximal femur) were pooled to obtain an averaged based value.

The development of generic implant models was another strength to this work. Ideally, this would allow the results of this study to be comparable to other implant models. All measurements obtained to design and develop the generic model were scaled based off clinically available models, which truly represented an average implant model. Furthermore, the small (d=8 mm) and large (d=16 mm) implant models were scaled about the central axis of the original model (d=12 mm), holding implant length constant. This allowed for identical placement of all implants within the humerus.

The generation of identical meshes is an obvious strength to this work. This allowed each element in the model to be directly compared between the intact and reconstructed models, which could then determine local effects of implant size and type (collar versus collarless) as opposed to an overall effect. This also contributed to the repeatability of the study, which controlled for inter-specimen variability.

4.3 Future Investigations

The investigations conducted throughout Chapters 2 and 3 successfully achieved the objectives presented in Chapter 1 of this thesis. This research contributes to a greater understanding of the implications on proximal BIC and bone stresses due to implant girth and the presence or absence of an implant collar. However, there still exists future opportunity to further investigate the complex mechanical behaviour of the humerus during reconstruction.

To the author's knowledge, the present work was the first to investigate the effects of increasing implant girth on the degree of BIC in the proximal humerus. In contrast to the hypothesis for this particular investigation (Hypothesis 1a), the results showed that the implant with the smallest girth size produced significantly more contact with the bone (in slices 1-4) than implants with a larger girth. The most proximal geometry of the generic implants designed for this study seemed to be oriented more medially about the anatomical neck (*i.e.*, region right below resection surface). Examination of Figure 2-3 in Chapter 2, shows that the most proximal geometry of the implants does not lie perfectly symmetrical between the inferior-medial and superior-lateral points directly below the resection surface. Future investigations could focus on design of the proximal geometry of the implant to be more evenly positioned about this region, as the distribution of trabecular bone in the most proximal region of the humerus likely affects these results.

When the implant collar was removed, it was postulated that the implants used for this investigation experienced some gentle subsidence to increase the degree of BIC. Future studies could look to verify this speculation to determine if in fact, there was some micromotion occurring, causing the implant to subside. This could also be paired with testing various surface textures, which may affect the amount of displacement possibly experienced by a collarless implant and consequently the degree of BIC.

Future work should also look to investigate the stresses transferred from the load at the articular surface to the various implants, particularly when the implant collar was removed. As the stem accepts all the load, the potential for implant fracture may arise if

the stresses are too great for the implant; this may be specifically true if a smaller implant is inserted into the bone.

4.4 Significance and Conclusions

As the occurrences of shoulder arthroplasties continues to increase, a greater understanding of the effects of implant design and surgical approaches are critical as they can affect the overall survivability of the implant. This work shows the importance of implant girth and implant collar on interface contact and proximal bone stresses. The humeral stem of the implant has been known to play an integral role in the distribution of load from the articular surface to the surrounding bone. The findings of this study show that the interaction between the undersurface of the humeral head and the resection plane also plays a significant role This new understanding will help to guide surgical techniques and determine the ideal implant size for patients receiving a shoulder replacement.

4.5 References

Bergmann, G., Graichen, F., Bender, A., Kääb, M., Rohlmann, A., & Westerhoff, P. (2007). In vivo glenohumeral contact forces-Measurements in the first patient 7 months postoperatively. *Journal of Biomechanics*, *40*(10), 2139–2149. https://doi.org/10.1016/j.jbiomech.2006.10.037

McDowell, M. A., Fryar, C. D., Ogden, C. L., & Flegal, K. M. (2008). *Anthropometric reference data for children and adults: United States, 2003-2006. National Health Statistics Reports*.

Appendix A: Glossary of Medical Terminology

Abduction: Movement away from the midplane of the body, specifically, the humerus away from the rib cage.

Acromion: The lateral extension of the spine of the scapula, forming the highest point of the shoulder.

Acromioclavicular (AC): Pertaining to the acromion and clavicle.

ANOVA: Analysis of variance, a statistical test between groups.

Anterior: Near or closet to the front of the body.

Arthritis: Medical condition of joint leading to inflammation caused or metabolic causes or infectious.

Arthroplasty: Repair of a joint by implanting an artificial component.

Articular: Referring to adjacent moving components (*e.g.* joint).

Axiohumeral: Pertaining to the torso and humerus.

Axioscapular: Pertaining to the torso and scapula.

Cartilage: Firm flexible tissue that lines the articular surface of joints.

Clavicle: Typically known as the 'Collar Bone', horizontally placed linking the thorax to the scapula.

Diaphysis: The center region of a long bone typically slender.

Distal: Referring to the position further away from torso.

Glenoid: A fossa resembling a pit or socket located on the lateral scapula.

Glenohumeral: The joint formed by the proximal head of the humerus and the glenoid of the scapula.

Humerus: Long bone of the upper arm which connects the shoulder to the elbow.

***In-silico*:** Refers to studies performed on computer or using computer simulation.

Lateral: Refers to the side that is further away from the median axis of the body.

Ligament: Tough fibrous band or tissue that link articulating bone.

Medial: Refers to the side that is closer to the median axis of the body.

Moment: Tendency of a force to rotate an object about an axis when that forces is applied at a distance.

Muscle: An organ which by contraction produces movement of an animal organism.

Musculoskeletal: Pertaining to the musculature and skeleton together.

Orthopaedics: Surgical discipline that deals with the restoration and preservation of the skeletal system (including articular structures).

Osteoblasts: Cells that produce and secrete proteins, which form the matrix for bone formation.

Osteoclasts: Cells that breakdown and absorb bone tissue.

Osteolysis: Pathological destruction or resorption of bone tissue by osteoclasts.

Posterior: Near or closet to the back of the body.

Proximal: Referring to the position closes to the torso.

Scapula: Medial bone of the shoulder connecting the humerus to the torso.

Scapulohumeral: Pertaining to the scapula and humerus.

Scapulothoracic: Pertaining to the scapula and thorax.

Shear: A motion or force parallel to the face of an object.

Shunt Muscle: Muscle that contracts to resist dislocating forces occurring at a joint

Sternoclavicular (SC): Pertaining to the sternum and clavicle.

Tendon: Fibrous tissue linking muscle to bone.

Torso: The center structure of the human body from which extend the limbs and neck.

Appendix B: Cadaveric Information

Table B-1 displays the demographic information (age and gender) of the eight cadaveric specimens used for these studies.

Table B-1: Demographic Information

Subject Number	Age	Sex
1	64	Male
2	71	Male
3	76	Male
4	62	Male
5	66	Male
6	61	Male
7	75	Male
8	67	Male

Appendix C: 3D Bone Model Generation

The following six figures demonstrate how the 3D bone model was generated from the CT scan in Mimics.

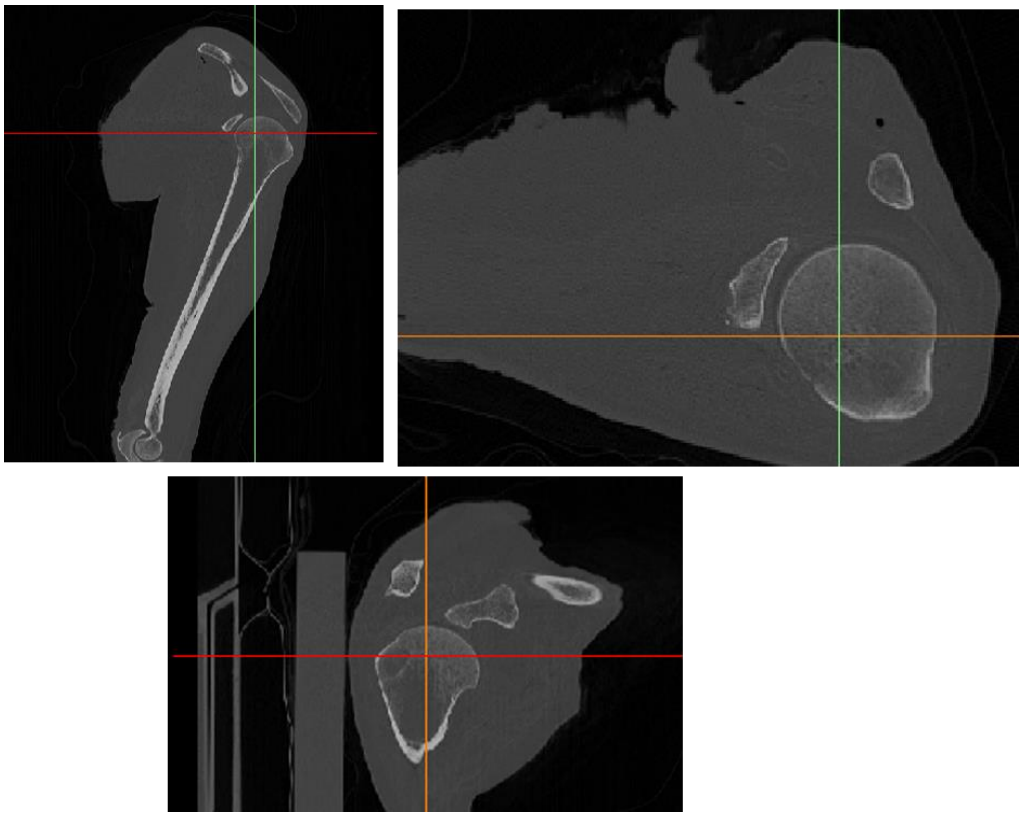

Figure C-1: Importing the DICOM Files into Mimics

DICOM files were imported into Mimics software, where the cortical bone was separated from the trabecular bone to make 3D models of the bone that would be later exported into SolidWorks.

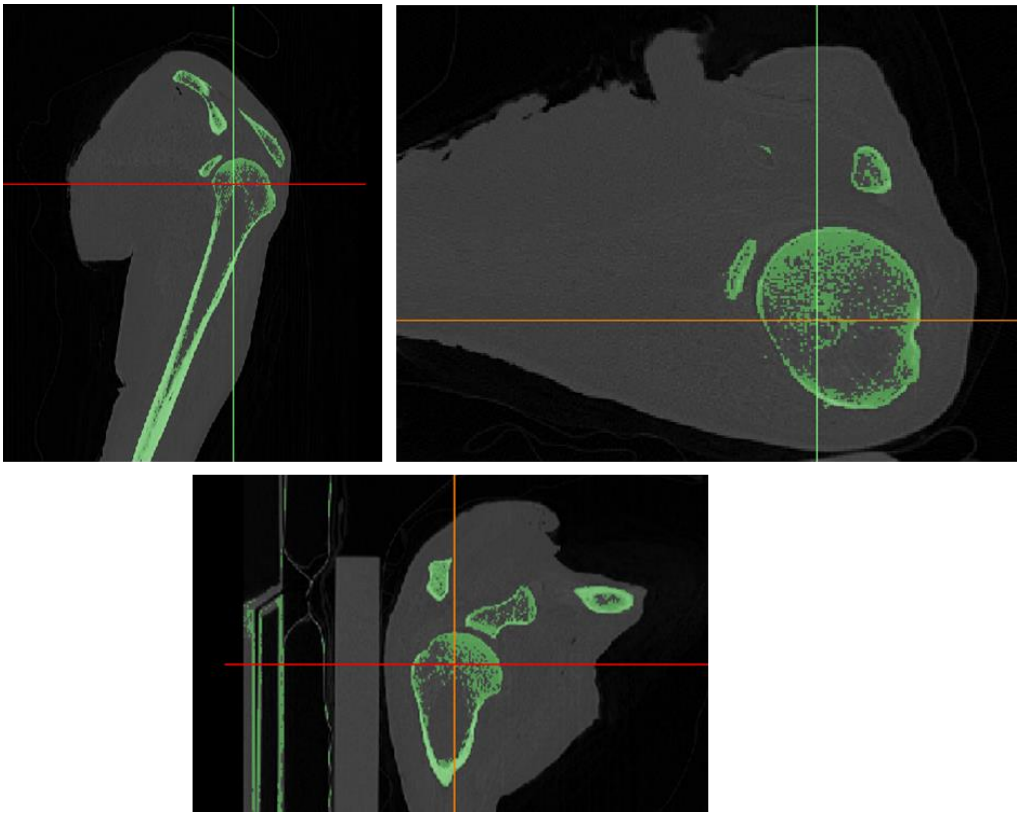

Figure C-2: Generation of Bone Mask

A bone mask was created using the Threshold function to identify all types of bone present in the CT scan.

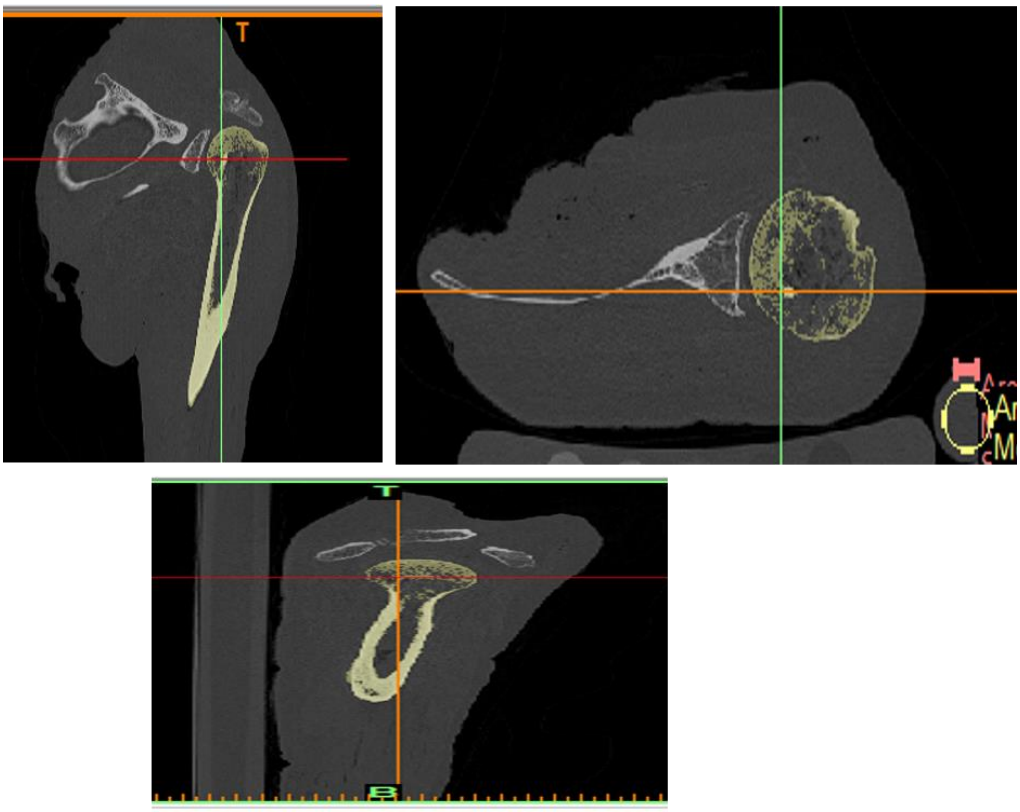

Figure C-3: Identification of Cortical Bone

A second mask was generating from the original bone mask using the Region Growing function to identify cortical bone in the humerus.

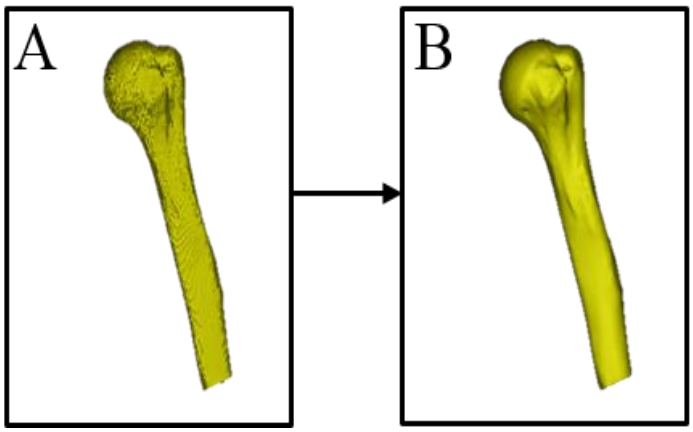

Figure C-4: Generating the 3D Cortical Bone Model

From the cortical bone mask, the 3D model of cortical bone was generated (A). Wrapping and Smoothing features were then used to further refine the bone (B), giving it a smoother finish consistent with natural bone. The 3D cortical bone model was exported as an STL file, where it would later be imported into SolidWorks and combined with the trabecular bone.

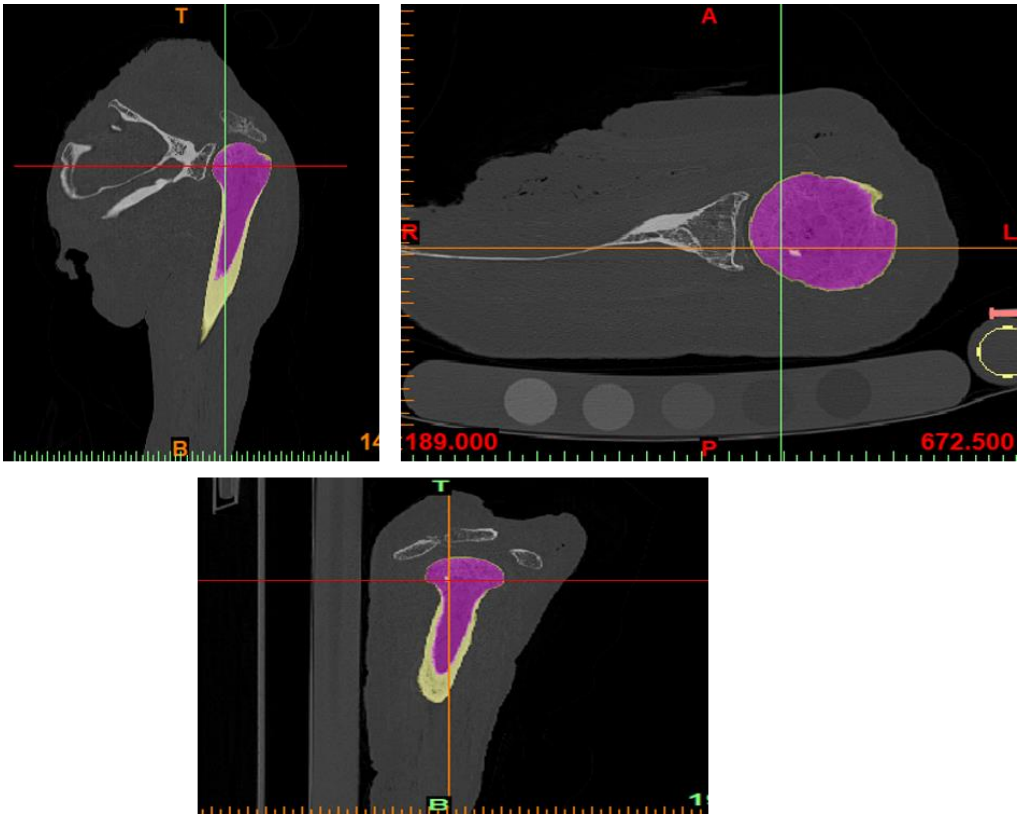

Figure C-5: Identification of Trabecular Bone

A distal point in the humerus was chosen and capped to create the trabecular bone mask. The "Cavity Fill" function was then used to fill in the region enclosed by the cortical bone.

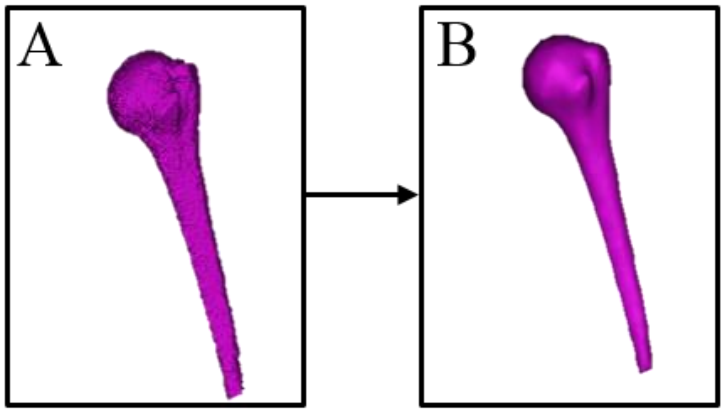

Figure C-6: Generating the 3D Trabecular Bone Model

From the trabecular bone mask, the 3D model of trabecular bone was generated (A). Wrapping and Smoothing features were then used to further refine the bone (B), giving it a smoother finish. The 3D trabecular bone model was exported as an STL file, where it would later combine with the cortical bone in SolidWorks to create the model of the proximal humerus.

Appendix D: Generating the Generic Implant Model

Three current short stem implant models, Biomet Comprehensive® Micro Stem, Arthrex Univers™ Apex, and Tornier Aequalis Ascend™ Flex, were scaled and measured using AutoCAD (Autodesk, San Rafael, CA, USA) to create the generic implant used for this experiment. The location points of interest are shown in Figure D-1 to Figure D-3 and the approximate measurements from these locations are displayed in Table D-1

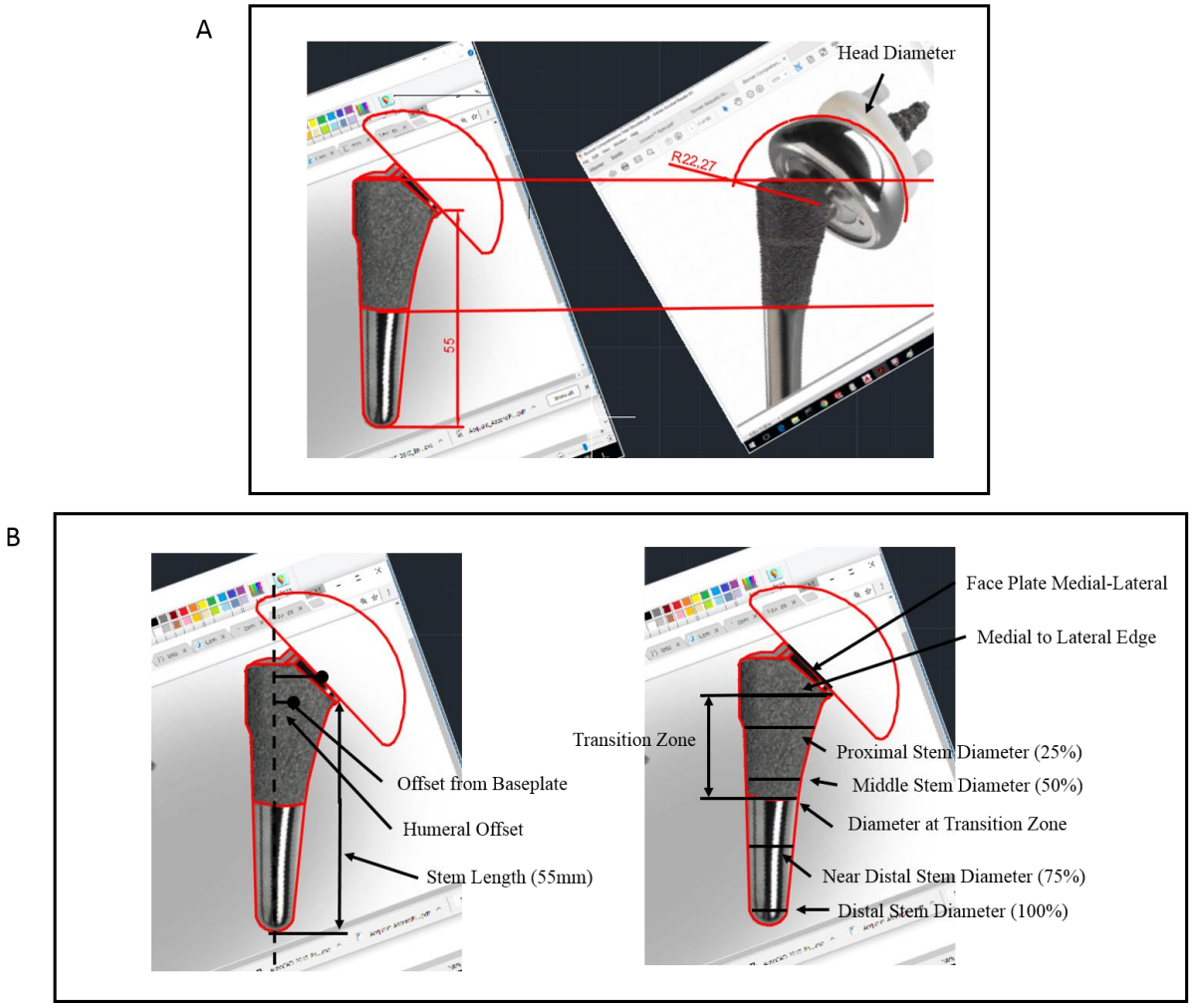

Figure D-1: Implant Measurements for the Biomet Comprehensive® Micro Stem (Zimmer Biomet, 2013)

The Biomet Comprehensive® Micro Stem was imported into AutoCAD and scaled according to a known dimension found in Figure D-1A (known stem length). This dimension was used to create a scaled drawing in Figure D-1B. Several locations along the implant were measured to generate a generic model with averaged values of the three market models as shown in Table D-1.

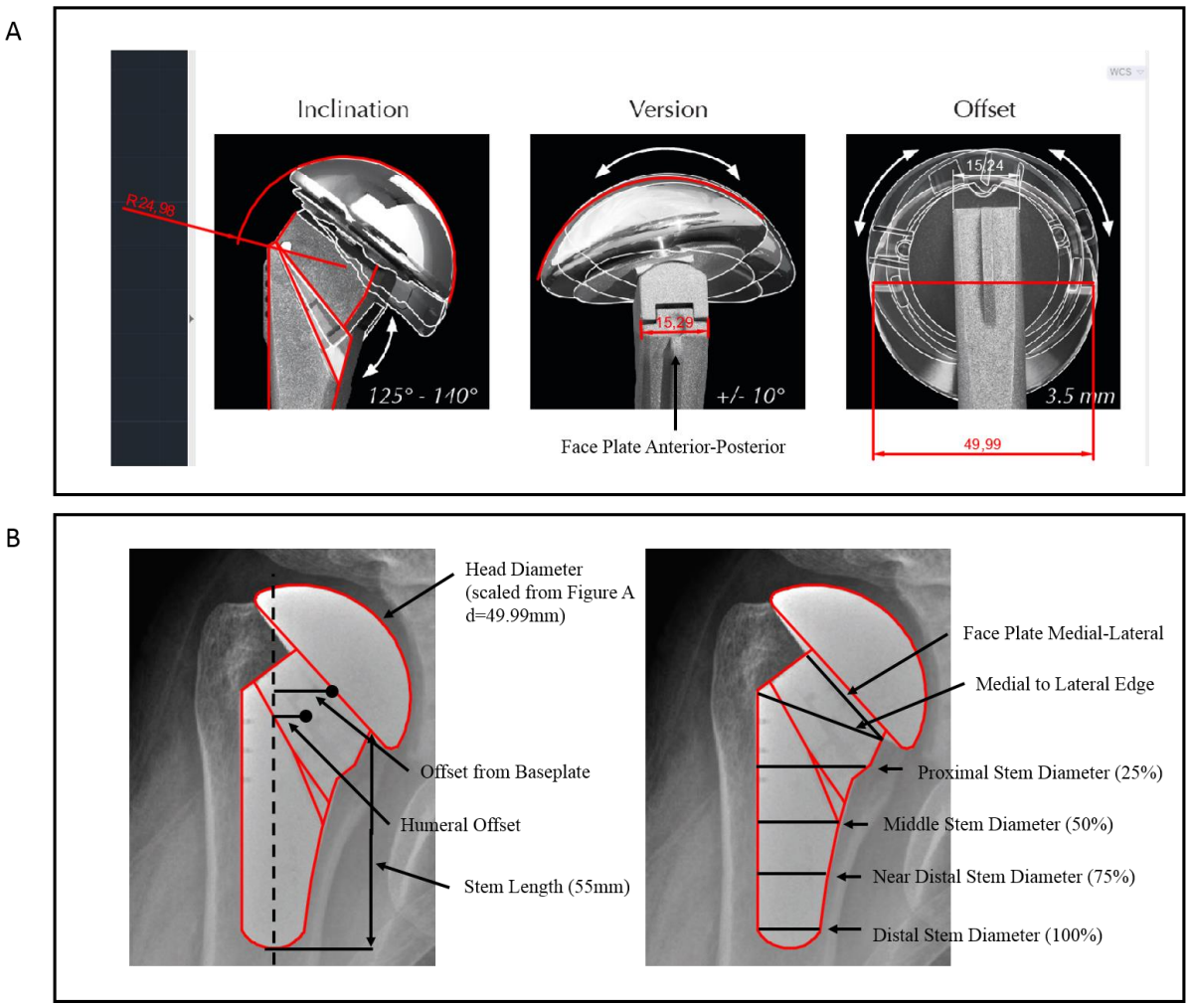

Figure D-2: Implant Measurements for the Arthrex Univers™ Apex (Arthrex, 2018)

The Arthrex Univers™ Apex was imported into AutoCAD and scaled according to known dimensions found in in Figure D-2A (known Anterior-Posterior width and head diameter). These dimensions were used to create a scaled drawing in Figure D-2B. Several locations along the implant were measured to generate a generic model with averaged values of the three market models as shown in Table D-1.

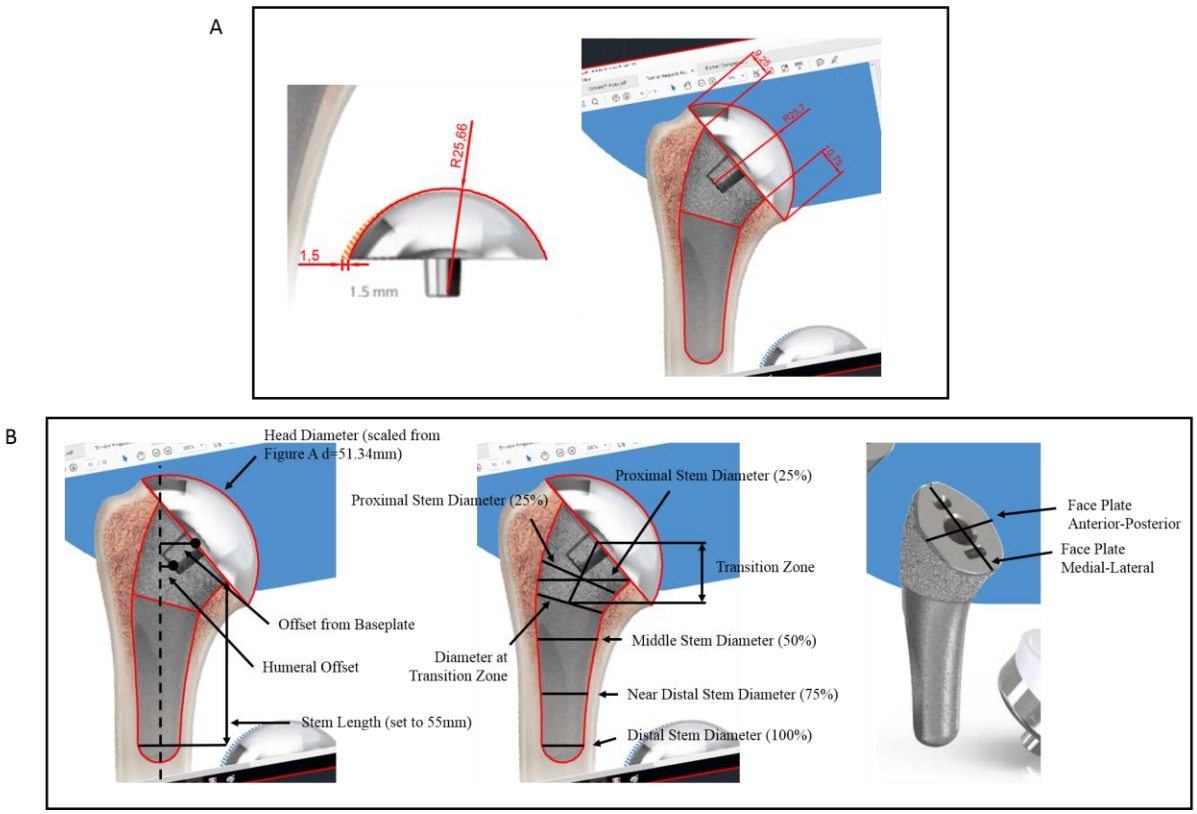

Figure D-3: Implant Measurements for the Tornier Aequalis Ascend™ Flex
(Tornier, 2013)

The Tornier Aequalis Ascend™ Flex was imported into AutoCAD and scaled according to known dimensions found in in Figure D-3A (known head offset to determine head diameter). These dimensions were used to create a scaled drawing in Figure D-3B. Several locations along the implant were measured to generate a generic model with averaged values of the three market models as shown in Table D-1.

Table D-1: Measurements of Current Implant Models

Table D-1 *displays the measurements from the 3 current implant models used to develop the generic model used for this study. Please refer to* Figure D-1 to Figure D-3*for dimension location.*

	Implant Dimensions (mm)			
Dimension Description	Arthrex	Tornier	Biomet	***Average***
Head Diameter	50.00	58.20	44.54	***50.91***
Face Plate Anterior-Posterior	15.29	19.30	N/A	***17.30***
Face Plate Medial-Lateral	25.31	33.36	22.75	***27.14***
Medial to Lateral Edge	28.33	30.42	22.53	***27.09***
Proximal Stem Diameter (25% Stem Length)	27.88	28.83	16.19	***24.30***
Middle Stem Diameter (50% Stem Length)	19.59	20.51	12.46	***17.52***
Near Distal Stem Diameter (75% Stem Length)	16.09	16.79	10.60	***14.49***
Distal Stem Diameter (100% Stem Length)	14.07	13.33	8.60	***12.00***
Transition Zone (between surface texturing)	N/A	23.09	30.20	***26.65***
Diameter at Transition Zone	N/A	22.30	12.27	***17.29***
Humeral Offset	5.80	4.17	6.04	***5.34***
Offset from Baseplate	10.98	12.29	11.11	***11.46***

Appendix E: Misaligned Large Stem Implant

The effects of a misaligned large stem (diameter=16 mm) implant were investigated in one (1) specimen. The degree of bone to implant contact (BIC), percent changes in proximal bone stress from the intact state, and changes in SED (percent volume of bone expected to resorb) were investigated throughout 8 equal 5mm slice depths for one specimen, at 75° abduction. The effects on cortical and trabecular bone are presented when the implant was medial tilted, contacting the distal tip of the stem to the lateral aspect of the humeral canal. As mentioned in Chapter 1, there have been some cases of misaligned implants (Duparc, 2013); therefore, the goal here was to investigate the preliminary changes in the degree in BIC, changes in bone stresses from the intact states, and changes in SED and risk of bone resorption. The methods used to create this study were the same as those found in Chapter 2 and 3, only just the large implant was used. The preliminary findings show that future investigation on this topic may present some important findings (Figure E-1 to Figure E-5).

For the degree of BIC with the collared implants (Figure E-1), both implant types produced nearly the same amount of contact in the proximal 3 slices, but in the distal 5, the aligned implant produced greater BIC. This could be expected because the misaligned implant is contacting stiffer cortical bone distally, which provides less surface area for contact compared to more porous trabecular bone. However, when the collar contact was disengaged from the cut surface, the findings were reversed. In the proximal 6 slices, the aligned implant contacted more bone than the misaligned implant, and in the distal 2 slices, the BIC was approximately the same. This may be because when the collar is removed, the implant may experience a cantilever like motion. The proximal region of the aligned implant may be forced to contact more trabecular bone that it may not be contacting without this induced moment. Distally, the tip of the aligned implant may now be approaching stiffer cortical bone, producing roughly the same amount of contact as the misaligned implant.

In terms of the changes in bone stress, the misaligned implant, when paired with a collar (Figure E-2), resulted in a greater change in cortical and trabecular bone stress from the intact state compared to the aligned implant. This may be due to the fact that the aligned

implant is likely contacting more cortical bone and hence increasing the stresses. In terms of the trabecular bone, the misaligned implant may be overloading regions of trabecular bone, which is resulting in greater changes in bone stress from the intact when compared to the aligned implant.

When the collar was disengaged from the cut surface (Figure E-3), the aligned implant produced slighter greater change in cortical bone stress from the intact in slices 1, 4 and 5 when compared to the misaligned implant. In trabecular bone, the aligned implant produced greater changes in stress than the misaligned implant for the most proximal 5 slices. When the collar contact is employed, the load is distributed between the cut plane and stem; however, when the collar is removed, the stem accepts the entire load. This may be resulting in greater distribution of force directly under the cut plane, which may result in a cantilever like motion of the implants. However, the misaligned implant is medial tilted into stiffer cortical bone and may be resisting more of the moment than the aligned implant; which may explain why the change in cortical stress from the intact is less for the misaligned implant. In the most distal slices (7 and 8), the misaligned implant produced greater changes in stress from the intact when compared to the aligned implant. This can be expected because the distal tip of the misaligned implant is already in contact with cortical bone. Furthermore, the change in stress may be larger due to a cantilever-like moment driving the tip of the implant further into the cortical shell. For trabecular bone, the misaligned implant may better represent stresses in the intact state because it may be resisting more of the cantilever motion, when compared to the aligned implant, as it is in contact with the stiff cortical bone. This may ultimately reduce the stress placed on trabecular bone.

Results of the change in SED data, show that the aligned implant, when paired with a collar (Figure E-4), resulted in less volume of cortical bone expected to resorb in the proximal 3 slices. For trabecular bone, the aligned implant actually increased the volume of bone expected to resorb in all slices but the most proximal (slice 1). These findings may suggest that the aligned implant actually applies more load overall to the cortical shell than the misaligned implant. Perhaps when the implant is misaligned to the medial aspect, there is an overall reducing in the distribution to all other areas of the cortical

shell, resulting in increased risk of proximal resorption across all regions. Distally, however, the tip of the misaligned implant is in contact with the cortical bone, which may be overloading the bone, resulting in very little to no risk of bone resorption.

When the collarless implants were used (Figure E-5), the aligned and misaligned implants resulted in similar volumes of cortical bone expected to resorb. This may be because, in both cases, the loss of load distributed to the cut plane is underloading the stress placed on the cortical bone in both implant types. The volume of expected bone resoption may be slightly higher for the aligned implant, because the misaligned implant is in contact with more cortical bone medial, which may increase the overall stress distribution when compared to the aligned implant. In trabecular bone, the aligned implant resulted in a greater volume of bone expected to resorb in the most proximal 5 slices. These findings may suggest that the misaligned implant overloads the trabecular more than the aligned implant, resulting in less risk of proximal stress shielding.

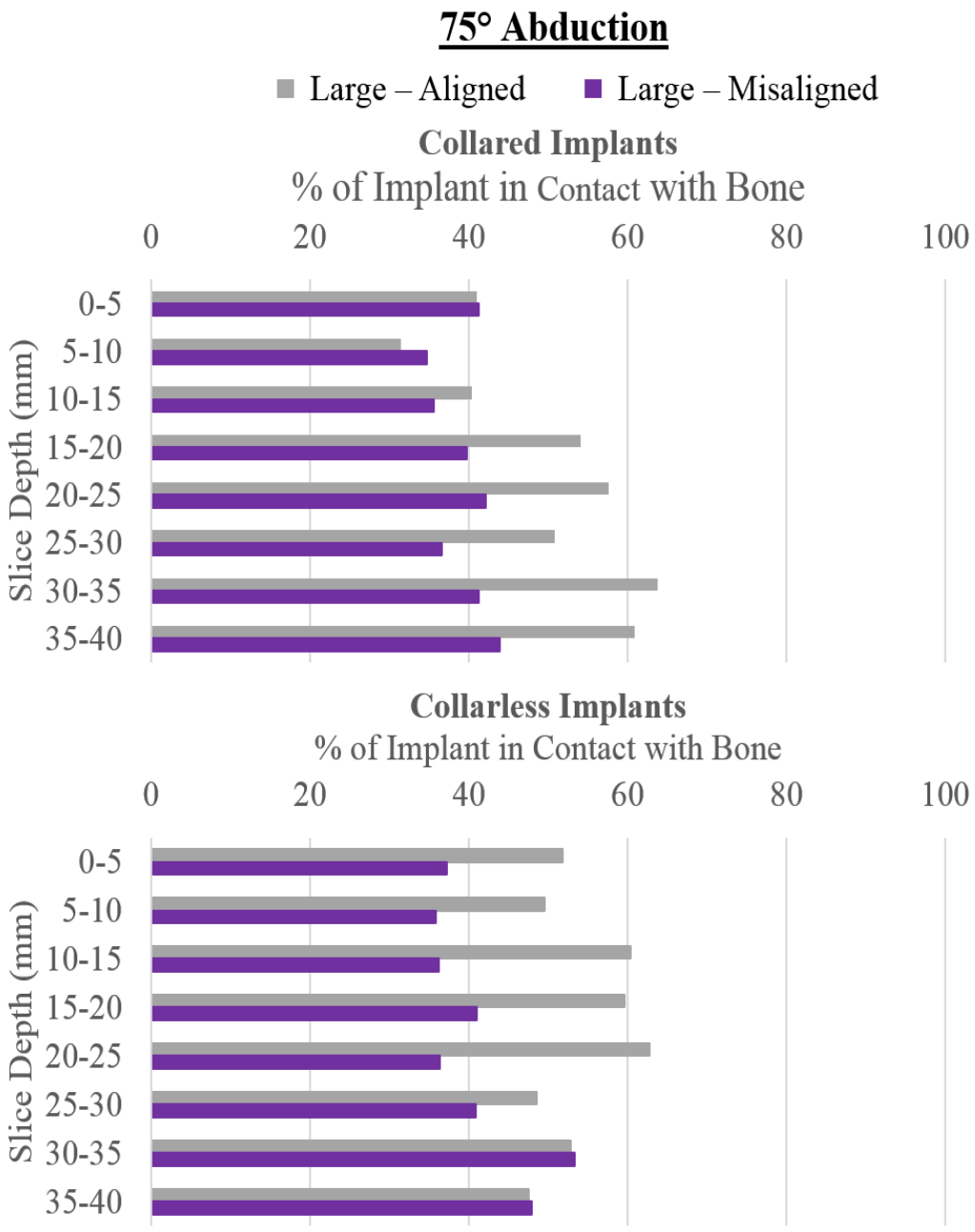

Figure E-1: Contact of Bone with a Large Implant at 75° Abduction (%)

Percent contact of bone to implant throughout 8 equal 5 mm slices when either the large collared or collarless implant was correctly aligned or misaligned with a medial tilt contacting the distal tip of the stem to the lateral humeral wall.

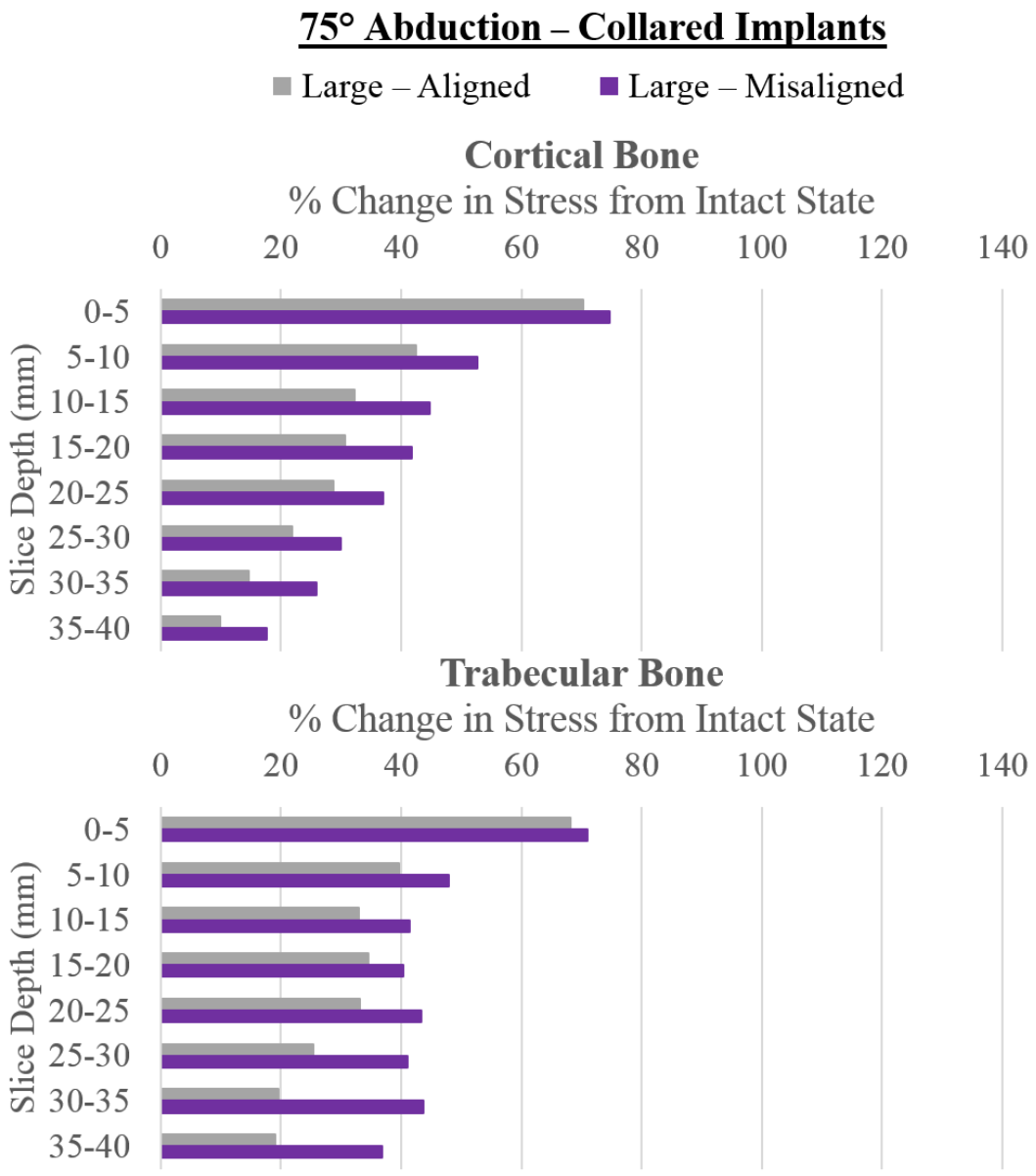

Figure E-2: Changes in Proximal Bone Stress with a Large Collared Implant at 75° Abduction

Percent change in cortical and trabecular bone stresses from the intact to the reconstructed state when the large collared implant was either correctly aligned or misaligned with a medial tilt contacting the distal tip of the stem to the lateral humeral wall. Changes in bone stress were obtained in 8 equal 5 mm slices distal to the cut surface.

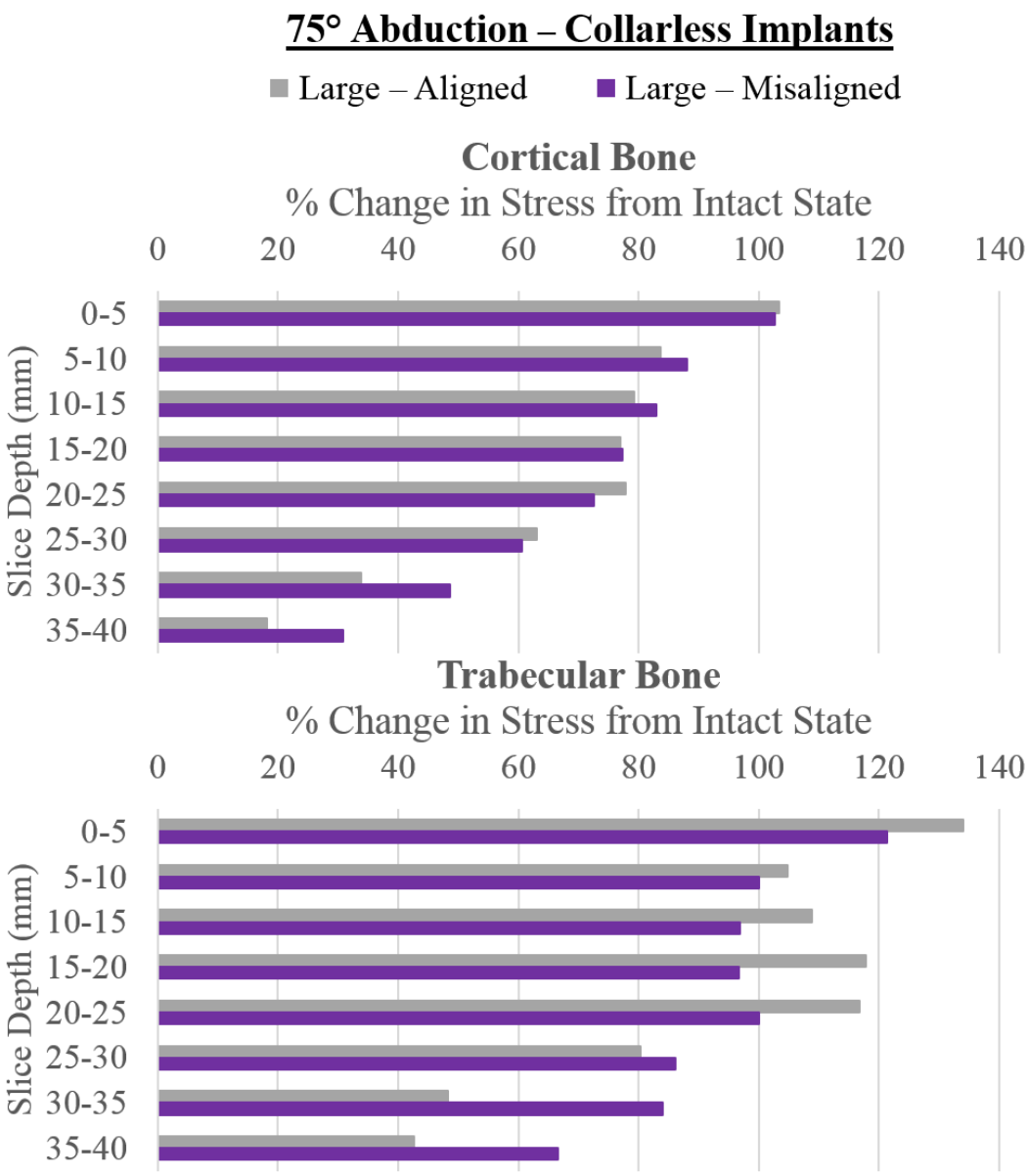

Figure E-3: Changes in Proximal Bone Stress with a Large Collarless Implant at 75° Abduction

Percent change in cortical and trabecular bone stresses from the intact to the reconstructed state when the large collarless implant was either correctly aligned or misaligned with a medial tilt contacting the distal tip of the stem to the lateral humeral wall. Changes in bone stress were obtained in 8 equal 5 mm slices distal to the cut surface.

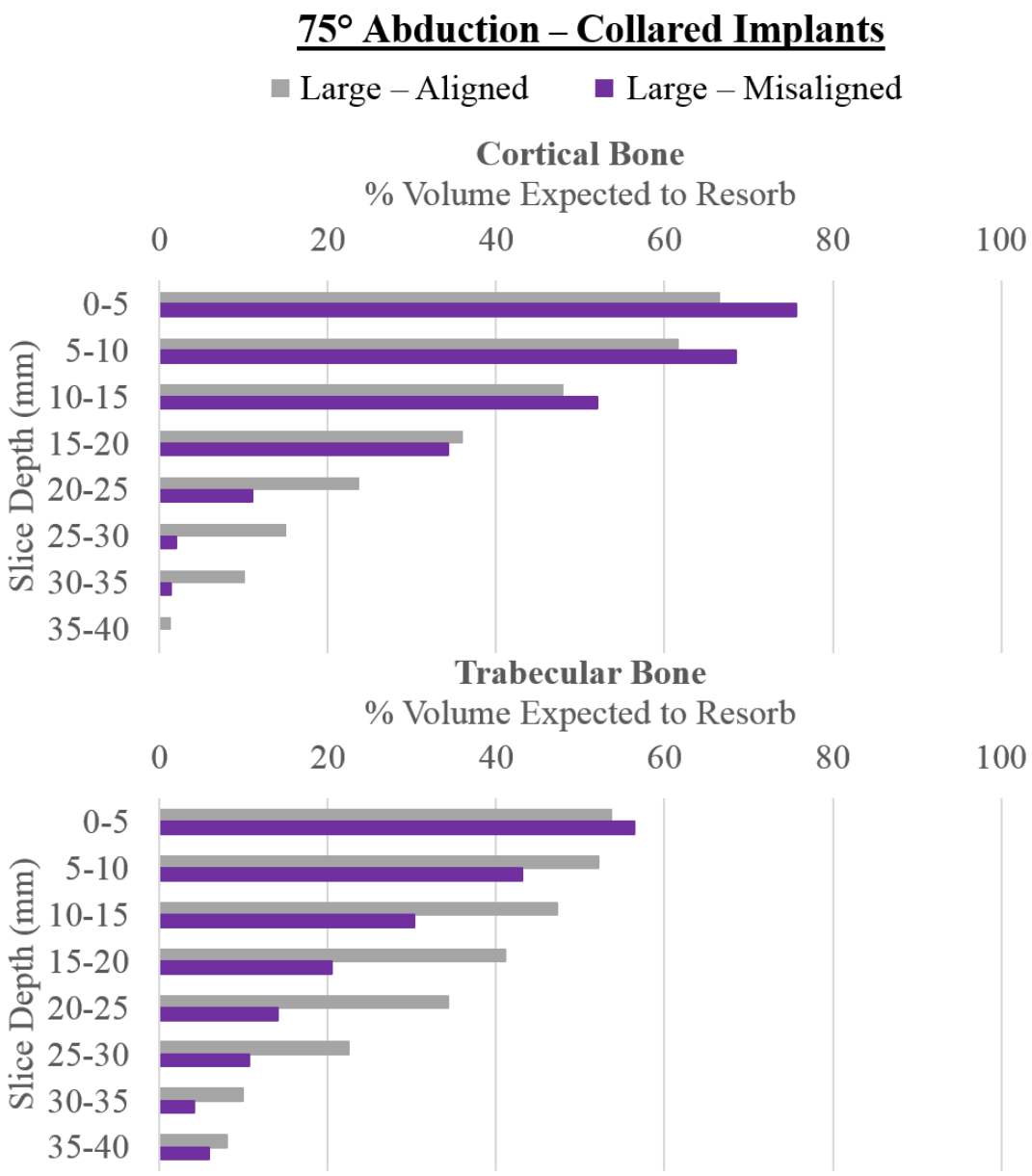

Figure E-4: Changes in Percent Volume of Bone Expected to Resorb with a Large Collared Implant at 75° Abduction

Percent change in volume of bone expected to resorb when the large collared implant was correctly aligned or misaligned with a medial tilt contacting the distal tip of the stem to the lateral humeral wall. Changes were observed in 8 equal 5 mm slices distal to the cut surface.

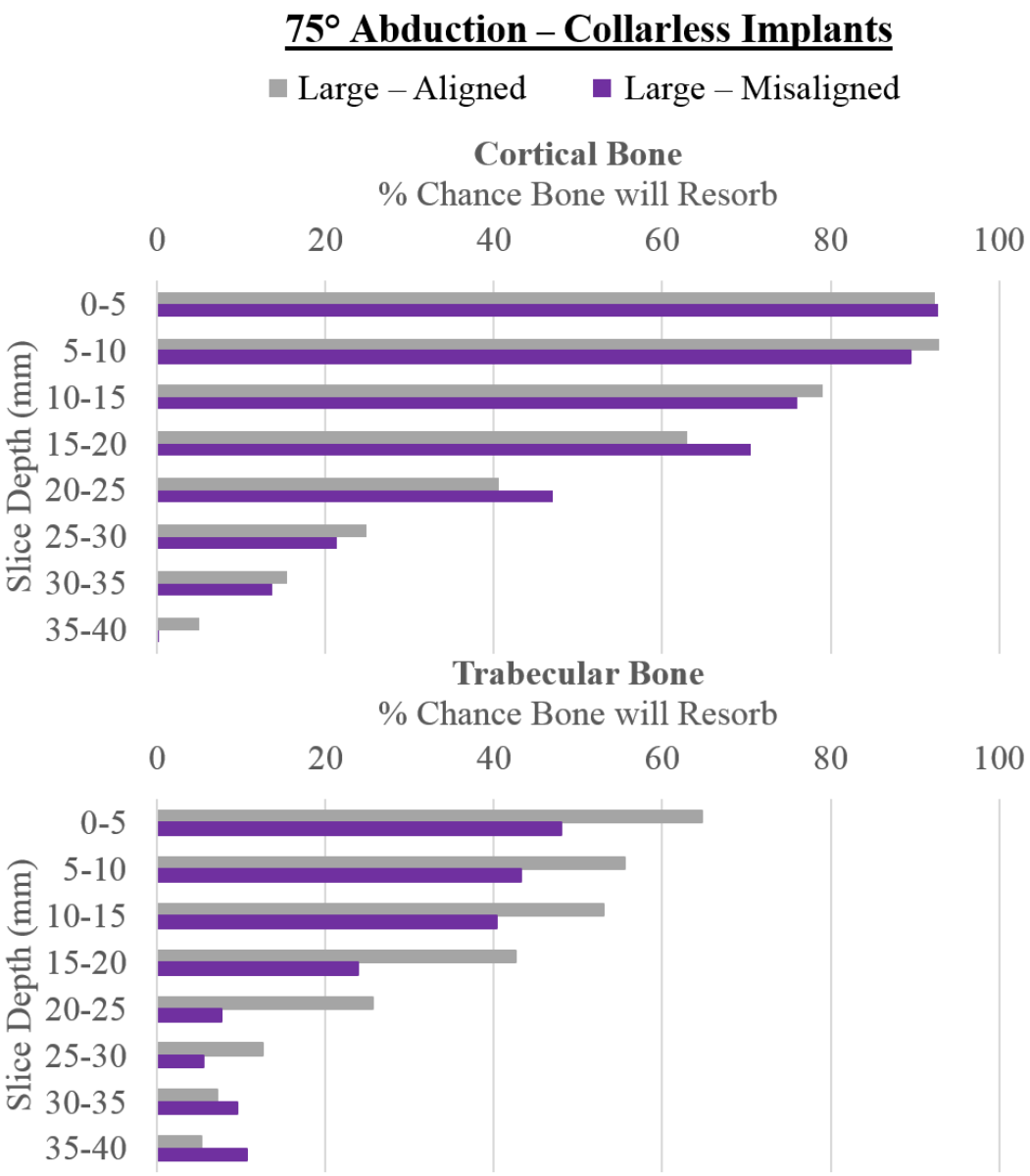

Figure E-5: Changes in Percent Volume of Bone Expected to Resorb with a Large Collarless Implant at 75° Abduction

Percent change in volume of bone expected to resorb when the large collared implant was correctly aligned or misaligned with a medial tilt contacting the distal tip of the stem to the lateral humeral wall. Changes were observed in 8 equal 5 mm slices distal to the cut surface.

Appendix F: References

Arthrex. (2018). Univers™ Apex. Retrieved from https://www.arthrex.com/shoulder/univers-apex

Duparc, F. (2013). Malunion of the proximal humerus. *Orthopaedics & Traumatology: Surgery & Research*, *99*(1 Suppl), S1–S11. https://doi.org/10.1016/j.otsr.2012.11.006

Tornier. (2013). Aequalis Ascend Flex. Retrieved from http://www.tornier.com/epaule/ascendflex-pyro/data/AN/pdf/Aequalis_AscendFlex_brochure_UDZF131.pdf

Zimmer Biomet. (2013). *Comprehensive Total Shoulder System*. Retrieved from http://www.biomet.com/patients/shoulder_replacement.cfm

Stephanie Synnott

Education

Master of Engineering Science, Biomedical Engineering 2016 – 2018
Western University, London, Ontario
Advisor: Dr. James A. Johnson

Honours Bachelor of Engineering, Biomedical 2012 – 2015
University of Guelph, Guelph, Ontario

Honours Bachelor of Science, Human Kinetics 2008 – 2012
University of Guelph, Guelph, Ontario

Awards and Scholarships

Lawson Internal Research Fund 2016
Western Graduate Research Scholarship 2016
Entrance Scholarship, University of Guelph 2008

Professional Experience

Teaching Assistant, CBE 2291: Computational Methods for Engineers Jan – Apr 2017/18
Western University
Supervisor: Lars Rehmann

- Led bi-weekly tutorial for a class of 40-50 students
- Educated students on the use of MATLAB programming to solve chemical and biochemical engineering problems

Teaching Assistant, CBE 2214: Engineering Thermodynamics Sept – Dec 2016/17
Western University
Supervisor: Sohrab Rohani

- Provided academic guidance and mentorship relating to fundamental thermodynamic laws, steam tables, and other thermodynamic concepts
- Evaluated assignments and quizzes for 70+ students
- Performed data entry into online reporting system, filed each students' work for future evaluation or meeting

Session Coordinator Sept 2016 – Apr 2017

Prep 101, London, Ontario

- Coordinated teaching sessions by preparing lecturer's and students' material
- Organized student records and managed session funds

Technical Experience

- Practice with the use of SolidWorks, Materialise Mimics, MATLAB, LabVIEW, SPSS, and Microsoft Office: Excel, Word, and PowerPoint. Able to rapidly learn and use new programs
- Experience in data collection and processing using Vicon motion capture systems and tethered EMG electrodes

Academic Projects and Designs

The Effect of Implant Girth and Implant Collar on the Degree of Bone to Implant Contact and Bone Stresses in the Proximal Humerus 2016 – 2018

Western University

- Designed three generic shoulder implant models in SolidWorks for shoulder arthroplasties
- Conducted a finite element analysis in Abaqus to analyze the changes in proximal bone stress with varying implant stem diameter and head contact configurations
- Completed statistical analysis on generated data using SPSS

Rehabilitation Vibrating Band Sept – Dec 2015

University of Guelph

- Proposed a design for rehabilitation of injured athletes; specifically targeting knee injuries
- Designed a prototype to send a therapeutic dose of vibration to the desired muscle
- Tested the effects of the device using a Biodex Isokinetic Strength Testing Machine to determine effects on peak muscle force and torque during and after use

Keg Level and Quality Sensing Device Sept – Dec 2015

University of Guelph

- Constructed a device to determine the volume and the overall quality of the contents inside a keg
- Coded sensors with an Arduino to communicate wirelessly through Bluetooth to an Android phone application
- Conducted in depth market analysis and developed a potential business plan

Fluid Flow Table Sept – Dec 2014

University of Guelph

- Collaborated with a Kindergarten Classroom at Prior Park Elementary School in Guelph Ontario to design and build an educational unit incorporating STEM
- Observed children's learning and play habits to create an engaging and educational learning system for a dynamic group of children
- Designed an open concept water table with numerous valves, funnels, and flow paths

Training Value of Squats as a Function of Squat Depth Jan – Apr 2014

University of Guelph

- Performed a biomechanical design experiment using VICON Motion Capture and electromyography by analyzing muscle activations during squatting to determine safe workout techniques
- Collected and analyzed large amounts of data using LabView and MATLAB programming

Ergonomic Assessment of Car Mechanics Jan – Apr 2012

University of Guelph

- Conducted a professional ergonomic assessment for a local car garage, providing a full safety analysis, as well as a cost analysis of possible redesigns to improve workplace safety
- Communicated professionally and effectively with the client

Analysis of Gait with Changes in Postural Stance Sept – Nov 2011

University of Guelph

- Examined variations in gait initiation with different foot positions
- Analyzed anticipatory postural adjustments and center of pressure movements
- Collected and analyzed large amounts of data using a Kistler Force plate and LabView programming